Development of Microanalysis Tools for Characterization of the Humoral Response to Infectious Diseases

by

Adebola O. Ogunniyi

M.S., Chemical Engineering Practice
Massachusetts Institute of Technology (2009)
B.S., Chemical Engineering and Economics
Rutgers University (2007)

SUBMITTED TO THE DEPARTMENT OF CHEMICAL ENGINEERING IN PARTIAL FULFILLMENT OF THE REQUIREMENTS FOR THE DEGREE OF

DOCTOR OF PHILOSOPHY
AT THE
MASSACHUSETTS INSTITUTE OF TECHNOLOGY

JUNE 2013

Signature of Author: _____

Adebola O. Ogunniyi
Department of Chemical Engineering
May 10, 2013

Certified by: _____

J. Christopher Love
Latham Family Career Development Associate Professor
Thesis Supervisor

Accepted by: _____

Patrick S. Doyle
Professor of Chemical Engineering
Chairman, Committee for Graduate Students

Development of Microanalysis Tools for Characterization of the Humoral Response to Infectious Diseases

by
Adebola O. Ogunniyi

Submitted to the Department of Chemical Engineering on May 10, 2013 in partial fulfillment of the requirements for the degree of Doctor of Philosophy (Ph.D.) in Chemical Engineering

Abstract

Antibodies are higher order protein structures produced by a subset of lymphocytes (B cells) in the immune system for protection against pathogenic species. These homodimers of heterodimers form highly specific interactions with their cognate antigens and hence have become very important for the development of prophylactic or therapeutic agents against different disease pathogens. A key step in the development of human monoclonal antibodies as therapeutics is identification of candidate antibodies either by direct screening of human antibody repertoires or by filtering through combinatorial libraries of human variable genes using display technologies. Combinatorial libraries of human variable genes afford the flexibility to pursue many targets of interest, but often result in the selection of low affinity antibodies or unnatural heavy and light chain pairings that would have been selected against *in vivo*. With direct screening of the human B cell repertoire, the challenge is how to efficiently isolate clones of interest. Presented in this thesis is a high-throughput, integrated, single-cell methodology based on microengraving that allows the rapid recovery of antigen-specific human B cells.

Microengraving is an analytical technique wherein secreted molecules from individual cells seeded into a dense array of subnanoliter wells are captured on the surface of a glass slide, generating a microarray from which desirable cells can be identified and recovered. Combined with high resolution epifluorescence microscopy and single-cell RT-PCR, we have developed assays for the simultaneous profiling of surface-expressed phenotypes of primary antibody-producing cells, as well as functional characteristics of their secreted antibodies and germline variable gene usage. Using clinical samples from HIV- and West Nile virus-infected subjects, we demonstrate that the method can identify antigen-specific neutralizing antibodies from both plasmablast/ plasma cell and memory B cell populations, and is ideal for the detailed characterization of cells from anatomical sites where sample sizes are often limited and disease pathophysiology is poorly understood (e,g. gut tissue, bone marrow).

Thesis Supervisor: J. Christopher Love
Title: Latham Family Career Development Associate Professor

ACKNOWLEDGMENTS

First, I would like to thank my advisor, Prof. J. Christopher Love, for granting me the opportunity to work as a member of his group, despite my limited background in experimental biology research when I started on this journey. I thank him for all the time and effort he put into training and teaching me how to conduct relevant research, and I greatly appreciate his patience and the plethora of ideas he provided to guide this thesis. He has been the ideal mentor, and I am honored to have worked with him all these years.

I want to thank Prof. K. Dane Wittrup and Prof. Jianzhu Chen for serving as members of my Thesis Committee. I am thankful for the time they volunteered, for the feedback and recommendations they provided to help improve the quality of my thesis, and for the advice given to help me establish a career after graduate school. I also want to express my gratitude to Dr. Eduardo Guillén, Dr. Craig Story and Dr. Jae Hyeok Choi for teaching me the basics of microengraving, and to Dr. Elizabeth Bradshaw and Dr. Sally Kent for educating me on B cell immunology and on the experimental techniques used in studying these cells.

I am extremely grateful to Dr. Douglas Kwon of the Ragon Institute for enabling the HIV mucosa study (Chapter 4) and for his unwavering faith in the project, even during the early developmental stages. Members of the Kwon lab have been very supportive, especially Kenneth Law, Melis Anathar and Alexandra Konisky, with whom I processed several biopsy samples into the early hours of the morning. I would also like to acknowledge Pascal Poignard and Elise Landis at the Scripps Institute, for their contributions to the HIV study in the form of helpful discussion and neutralization assays. Thanks also go to Dr. Ruth Mongomery and Dr. Feng Qian for samples, reagents and validation of antibodies in WNV study.

To past and present members of the Love lab: Yuan Gong, Dr. Qing Han, Dr. Qing Song, Dr. Eliseo Papa, Dr. Kerry Love, Dr. Navin Varadarajan, Yvonne Yamanaka, Vasiliki Panagiotou, Dr. Jonghoon Choi, Timothy Politano, Aaron Gawlik, Dr. Ayca Yalcin Ozkumur, Dr. Todd Gierahn, Dr. Cuong Nguyen, Viktor Adalsteinsson, Denis Loginov, Dr. Rita Contento, Dr. Alexis Torres, Dr. Sangram Bagh, Dr. Bin Jia, Sarah Schrier, Brittany Thomas, Abby Hill, Lionel Lam, Kimberly Ohn, Dr. Joe Couto, Rachel Barry, Narmin Tahirova, Thomas Douce, Dr. Konstantinos Tsioris, Dr. Li-lun Ho and Nicholas Mozdzierz, I consider myself lucky to have met each one of you, and I hope our friendship continues for many years to come. Thank you for creating a wonderful work environment, for enjoyable outings and for enlightening discussions on issues of science, culture, politics, sports and life in general. I also want to thank my UROPs: Ruby Maa, Minna and Mindy Du for their assistance with experiments and data analysis. I wish you all the best.

Finally, I would like to dedicate this work to all the friends and family who supported me throughout my graduate school experience, most of all to my mother, father and sister: Dr. Jaiyeola Ogunniyi, Dr. Adesola Ogunniyi and Dr. Adedamola Ogunniyi. I am forever indebted to you for your encouragement, provision and unconditional love, and I am excited to join you all in having earned the title of Doctor. God Bless.

TABLE OF CONTENTS

List of Figures

List of Tables

CHAPTER 1: INTRODUCTION

1.1. B cell immunology and antibody development

The immune system is a complex network of cells and proteins that interact and work in concert to protect the body from pathogenic species (e.g. bacteria, fungi, viruses, protozoa, cancerous cells, etc.) that cause disease. The innate arm of the immune system serves as the first line of defense against pathogens and is characterized by breadth – being capable of recognizing a wide range of species with limited specificity. The second arm of the immune system, the adaptive immune system, comprises both cell-mediated and humoral responses (T cell and B cell based responses, respectively) that are highly specific and able to generate immunological memory for rapid recall responses upon secondary exposure to the same antigens. Along with functioning as antigen-presenting cells (APCs), B cells are primarily responsible for the production of immunoglobulins (Igs) or antibodies [1]. Antibodies are soluble or surface-bound receptors that recognize specific structural or peptide motifs (epitopes) on the surface of antigens, allowing the neutralization, agglutination or opsonization of these targets. Antibodies are also able to induce effector functions from effector molecules and cytolytic cells by complement activation and antibody-dependent cell-mediated cytotoxicty (ADCC), respectively, initiating the destruction of infected cells.

Upon the encounter of a cognate antigen, naïve B cells undergo affinity maturation in germinal centers of lymphoid tissues, followed by clonal expansion, and finally differentiation into actively-secreting plasma cells or resting memory B cells. Plasma cells either remain in lymphoid tissues or home to the bone marrow and continuously secrete large quantities of

antibody [1, 2]. Memory B cells, on the other hand, home to other tissues awaiting subsequent encounter of the cognate antigen. Although long-lived plasma cells exist in the bone marrow, most plasma cells raised in response to an infection are short-lived [2], hence the analysis of this population only provides an instantaneous snapshot of the humoral immune response to an infection. Memory B cells persist throughout the life of an individual, documenting the evolutionary history of B cells selected for during the course of an infection. Interestingly, some evidence suggests a discrepancy in the repertoire of antibodies secreted by plasma and memory B cell populations in response to a particular antigen [3], but the extent to which these repertoires differ has yet to be explored on a cellular basis.

The sequence of amino acids in the variable regions of the heavy and light chains dictates the specificity of an antibody. The large number of V, D and J (V and J only, for light chains) gene segments in the human chromosome that can be combinatorially assembled during B cell development, and extra nucleotide additions during recombination, provide sufficient diversity to enable the generation of antibodies capable of recognizing any antigen [4, 5]. Affinity maturation by clonal selection and somatic hypermutation driven by the presence of antigen further improves the quality of antibodies produced, selecting for clones with increased affinity. During the acute phase of an infection or following vaccination, high-affinity antibodies recognizing epitopes displayed by immunogenic species are predominant. The isolation of such antibodies can be readily accomplished with existing technologies for antibody discovery [6, 7]. For chronic conditions such as type 1 diabetes or infection by the human immunodeficiency virus type 1 (HIV-1), however, the frequency of B cells producing functional antigen-specific antibodies is relatively low, making the recovery of such cells for detailed characterization a challenging

process [8, 9]. There has, therefore, been a need for new analytical tools with the sensitivity to permit access to these unique populations of cells.

1.2. Existing tools for B cell analysis

Given the successful use of antibodies in polyclonal antiserum as prophylactics and more recent success at the use of monoclonal antibodies to treat a variety of cancers, inflammatory conditions, infectious and autoimmune diseases [10-12], there is interest in understanding how the humoral immune response evolves to produce such effective antibodies, and in identifying candidate antibodies for the design of therapeutic agents or immunogens in vaccines. Traditional strategies for the discovery of B cells producing antigen-specific antibodies have relied on the use of the enzyme-linked immunosorbent assay (ELISA) [13, 14], enzyme-linked immunosorbent spot (ELISPOT) assay [15-17], flow cytometry [6, 18] or the mining of libraries of variable genes using display and expression technologies or novel bioinformatic analysis tools [4, 19-21].

In an ELISA, supernatants are incubated over a capture surface coated with antigen or a capture reagent specific for the analyte of interest. Secondary antibodies are used to detect bound analyte, which can be read and quantified by fluorescence. ELISA is sensitive but requires culturing of source cells to obtain detectable levels of Ig in supernatant. The ELISPOT assay is very similar to the ELISA. Dilutions of cells are incubated on a capture substrate, and secreted products (e.g. antibodies, cytokines) are captured then detected as "spots" of signal where antigen-specific cells were originally deposited. The technique is highly sensitive – able to detect

1 in 10^5-10^6 events – but only suitable for conveniently measuring at most two analytes per cell [22, 23]. Also, source cells are lost and cannot be recovered for subsequent analysis.

Analysis by flow cytometry has been significant in informing our current knowledge of immunology by allowing the simultaneous detection of tens of parameters [24, 25]. Fluorescence-activated cell sorting (FACS) has also made it possible to rapidly isolate unique cells from heterogeneous populations of cells, and is a cornerstone of several display technologies [6, 26-29]. A necessary feature for flow cytometric analysis is the expression of analytes of interest on the surface of source cells. This linkage between genotype and phenotype, unfortunately, has limited much of the discovery of antigen-specific B cells to searching the repertoire of memory B cells, as plasma cells only express a secreted form of Ig. The indiscriminate sorting of plasma cells or plasmablasts during acute infection or following a vaccination does provide access to native human antibodies among this population [6, 7, 30], but can be inefficient when antigen-specific cells represent a minor fraction of the population [9]. Moreover, with this technology, the lower limit for detection of rare events is on the order of 1 in 10^3-10^4 events [31, 32], therefore, more cells are required to accurately identify clones of interest. Combinatorial libraries of human variable genes afford the flexibility to pursue any target of interest, but often result in the selection of low affinity antibodies or unnatural heavy and light chain pairings that would have been selected against *in vivo* [4].

Newer technologies for the analysis of B cells and their secreted antibodies [33-35] have focused on reducing the form-factor required for culture and/or analysis, as the volumes required for analysis would be smaller and very high concentrations of Ig can be accumulated in short

periods of time. The ELISPOT-like immunospot array assay on a chip (ISAAC), for instance, has facilitated the recovery of antigen-specific actively secreting cells (ASCs) from recently vaccinated subjects [34]. In this work, the microengraving approach [36] was expanded to enable the profiling of different B cell subsets in samples from human subjects.

1.3. Microengraving

Microengraving is a high-throughput, soft lithographic technique in which an array of ~10^5 sub-nanoliter wells (nanowells) is used to partition and culture a heterogeneous population of cells as single-cell isolates. The supernatant from each nanowell, containing the secreted molecules (e.g. antibodies, cytokines, etc.) of cells confined within each nanowell, can then be transferred or "engraved" onto the surface of a functionalized glass slide (Figure 1.1), in a manner similar to intaglio printing [37]. This process generates protein microarrays detailing the secretion profile of each cell, with elements on the protein microarrays mapping directly to particular well-locations in the corresponding array of nanowells. The method is versatile, allowing the rapid profiling of different cell types (e.g. hybridomas, peripheral lymphocytes, yeast, etc.), in a compact, micrometer-scale form factor [35, 36, 38-41]. With this technique, one can simultaneously examine the phenotype and functionality of single cells, allowing the study of heterogeneous cell populations in a way unavailable in the generally accepted immunoassay formats of a 96-well microtiter plate or flow cytometer; especially when the sample-size is limited.

A distinct advantage of the microengraving approach is the ability to separate cells from the detection medium and/or surface, as baits may interact directly with the surface of cells,

increasing the number of false positives. This feature also allows for repeated analysis and multiplexing beyond what has been achieved with other techniques. In addition, cells of interest can be recovered and expanded in culture, or genetic material can be recovered for cloning, indicating that the technology would be applicable for the analysis of both memory and actively-secreting B lymphocyte populations. Plasma cells have low survivability *ex vivo*, hence studies of antigen-specific B cells to date have focused largely on the analysis of the more stable memory repertoires. With this technique, however, detailed analyses of antigen-specific plasma cells and their secreted products can be performed in a short period of time (~1-2 h), obviating the need for extended culture. Therefore, with micoengraving, it is feasible to study these terminally-differentiated ASCs essential for the observed humoral response to an infection *in vivo*.

1.4. Specific aims and outline of dissertation

Broadly, the objectives of this thesis were to establish techniques with clinical relevance that would enable comprehensive functional characterization of antibodies in a single assay, ideally from primary human B cells. The importance of such technologies in the context of infectious diseases would be to streamline the processes involved in the discovery of antibodies with desirable functionalities, and to significantly improve the efficiency with which researchers can perform the necessary analyses, in terms of cost, time and yield. Using microengraving technology, the specific goals for my doctoral thesis were as follows:

1. Establish protocols for the handling of actively-secreting cells and memory B cells *ex vivo*, along with methods for the processing of cells identified as expressing unique phenotypic traits.

2. Develop analytical tools for the detailed evaluation of multiple functionalities of antibodies produced by primary B cells, in an efficient and high throughput manner.

3. Characterize B cells of the plasma and memory cell repertoires in different lymphoid tissues, and in patients at different stages of infection, to reveal the intricacies of the humoral response to infection and to enable the construction of antibody-based disease-state profiles.

Chapter 2 of this dissertation outlines the materials and methods used in the experiments involved in establishing and validating assays for B cell analysis. A detailed description of the development and optimization of key steps in the assays is provided in Chapter 3. Chapters 4 and 5 describe studies exploring the effects of infectious diseases – HIV-1 and West Nile virus (WNV) infections, respectively – on the humoral immune repertoire, taking advantage of new improvements in the microengraving platform. Finally, a summary of all results generated in the course of this thesis, and a discussion of the significant conclusions drawn from this work are provided in Chapter 6.

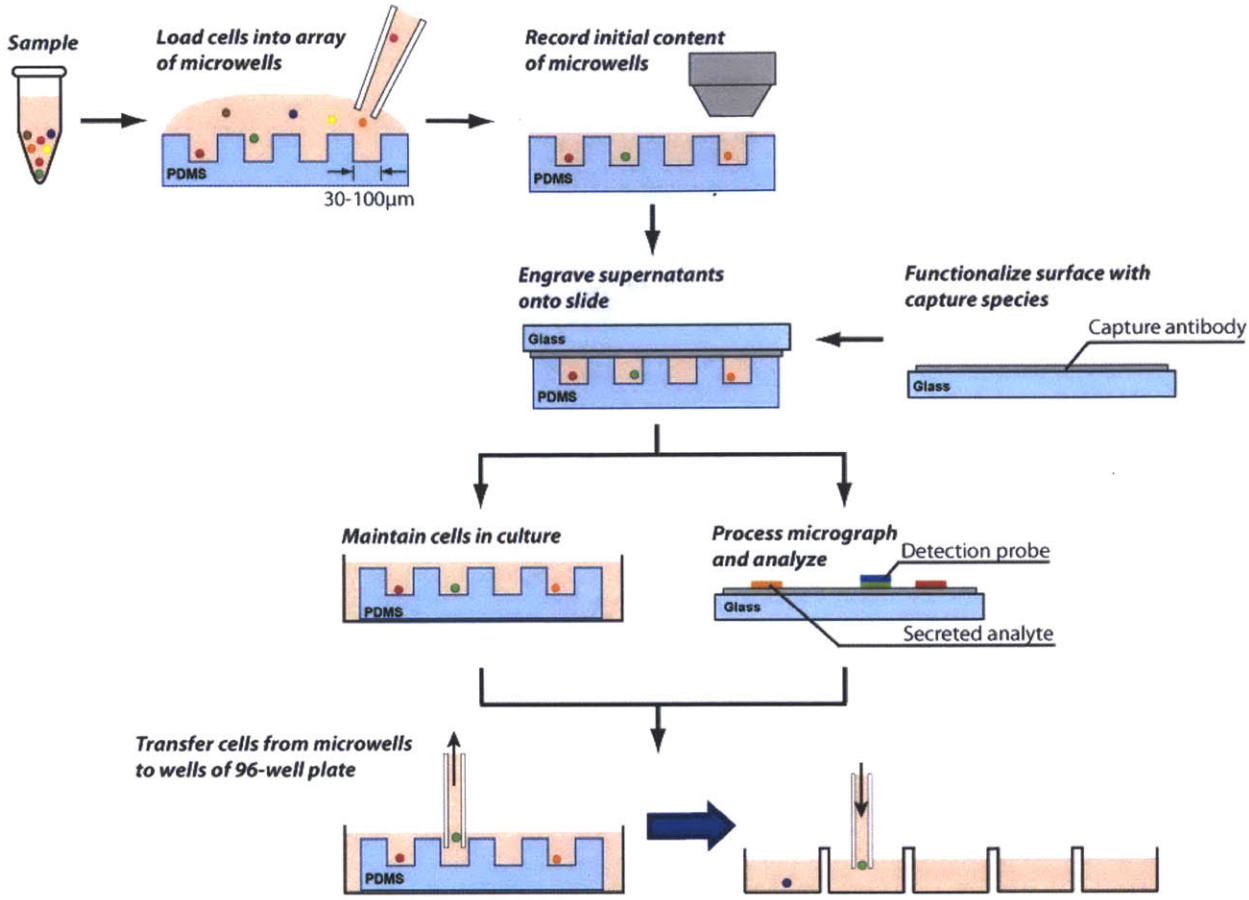

Figure 1.1: Schematic of the microengraving process for isolation of functional B cells

CHAPTER 2: MATERIALS AND METHODS

2.1. Ethics statement

Patient samples were obtained following approval by the institutional review boards at Massachusetts General Hospital (MGH), Boston; Massachusetts Institute of Technology (MIT), Cambridge; Brigham and Women's Hospital (BWH), Boston; and the Yale School of Medicine, New Haven. Written informed consent was obtained from study participants prior to enrollment in studies.

2.2. Peripheral blood and mucosal tissue samples

Blood and intestinal biopsies were collected from HIV-infected individuals from a cohort of controllers (HIV-1 viral load < 2,000 RNA copies/mL in the absence of HAART) and progressors (HIV-1 viral loads > 2,000 RNA copies/mL in the absence of HAART, or HIV-1 viral loads < 50 RNA copies/mL on fully suppressive HAART) from MGH [42]. Peripheral blood mononuclear cells (PBMCs) from blood samples were isolated using Histopaque®-1077 (Sigma-Aldrich). Cells were then either analyzed fresh or from frozen aliquots of 10^7 cells. Intestinal biopsies were obtained by upper and lower endoscopy. Tissue was disaggregated using both mechanical disruption and enzymatic digestion, based on published protocols [43]. Briefly, biopsied samples were resuspended in RPMI 1640 supplemented with 10% (v/v) fetal calf serum (FCS), L-glutamine, piperacillin/tazobactam (250 μg/ml), amphotericin B (1.25 μg/ml) and collagenase II (0.5 mg/ml; Sigma-Aldrich). Tissue was incubated for 30 min with constant agitation (37°C, 5% CO_2). The supernatant was collected and passed through a 75-μm cell strainer. The remaining tissue pieces were passed through a 16G blunt needle and then subjected to another round of collagenase digestion. This process was repeated twice. Finally, cells were

washed in media and maintained at 37°C (5% CO_2) until used. PBMCs from healthy donors were obtained from BWH or purchased from SeraCare Life Sciences Inc. (Milford, MA). Before screening populations of ASCs, PBMCs were thawed and rested for 1 h in complete media (RPMI 1640 media supplemented with 10% (v/v) fetal bovine serum (FBS), 100 U/mL penicillin and 100 μg/mL streptomycin; 37°C, 5% CO_2).

2.3. Activation of memory B cells

A mixture of stimulatory molecules based on previous reports for polyclonal activation of B cells [44-51] was used to induce antibody secretion by resting memory B cells. ~3 × 10^6 PBMCs were seeded in 5 mL round-bottom tubes (BD Falcon) and incubated for 3-7 days in 500 μL of complete media, containing combinations of antibodies, cytokines, toll-like receptor (TLR) agonists and mitogenic species. Additional information is included in Section 3.3.

2.4. Antibody-producing cell lines

12CA5 mouse hybridoma cells, secreting antibodies against hemagglutinin (HA; ATCC) were cultured in Dulbecco's Modified Eagle's Medium (DMEM; Gibco), supplemented with 10% inactivated fetal calf serum (IFS), 20 mM HEPES (Gibco), 1 mM sodium pyruvate, 0.1 mM non-essential amino acids (Gibco), 100 units/ml penicillin, 100 μg/ml streptomycin, 50 μM 2-mercaptoethanol and 5 mM L-glutamine. HYB099-01 mouse hybridoma cells, secreting antibodies against ovalbumin (OVA; Statens Serum Institut), were also cultured in the same media except that IFS was substituted with 10% fetal bovine serum (FBS; PAA). A human B cell hybridoma cell line producing the 4D20 (anti-HA) antibody [14] (courtesy of J. Crowe, Vanderbilt University) was adapted to grow in RPMI 1640 media with 15% (v/v) FBS, 2 mM L-

glutamine and 1 mM sodium pyruvate. Lastly, Chinese hamster ovary (CHO) cell lines producing b12, b6 (anti-gp120) and 2F5 (anti-gp41) antibodies (courtesy of D. Burton, Scripps Institute) were cultured in ProCHO-5 media (Lonza) with 3% FBS, 1× HT supplement (Gibco), 1× GS supplement (Sigma-Aldrich), 100 U/mL penicillin, 100 μg/mL streptomycin and 50 μM L-methionine sulfoxime (Sigma-Aldrich).

Cell lines were cultured at 37 °C (5% CO_2), and maintained at a density of 10^5-10^6 cells/mL by passaging into fresh media every 3-5 days. Cells were used in experiments when cultures were 70-80% confluent.

2.5. Microengraving

2.5.1. Fabrication of arrays of nanowells

Arrays with ~80,000-250,000 wells (50 × 50 × 50 μm^3 or 30 × 30 × 30 μm^3 in dimension, respectively) were fabricated by molding polydimethylsiloxane (PDMS; Sylgard 184) on silicon wafers patterned with SU-8 by photolithography. Arrays were designed with a dense arrangement of 7 × 7 or 12 × 12 wells (for 50- or 30-μm well dimensions, respectively) in a block of wells. Each block was equivalent in size to the field-of-view on an EM-CCD camera (Hamamatsu). Blocks were arranged in a rectangular grid of 24 columns and 72 rows to make the arrays compatible with 25 mm × 60 mm coverslips and 25 mm × 75 mm glass slides. 50 μm microchannels further partitioned the array into groups of 4 × 4 blocks to simplify subsequent analyses and facilitate drainage of media during the microengraving process [52]. PDMS prepolymer was generated by mixing elastomer base and curing agent in a 10:1 (base:curing agent) ratio by weight. Air bubbles were removed from the mixture by incubation under vacuum

at room temperature for 1 h. Degassed prepolymer was injected into custom-made molds, and then cured for 2-3 h at 80 °C. After curing, arrays were removed, covered and stored at ambient conditions until used. Arrays were treated with oxygen plasma (PDC-001, Harrick Plasma) immediately prior to use and then placed into sterile phosphate buffered saline (PBS).

2.5.2. Preparation of capture slides

3"×1" glass slides (Corning) were cleaned in a mixture of 2.5M NaOH and 60% (v/v) ethanol, washed thoroughly in deionized water, and then submerged in 0.001% (v/v) poly-L-lysine (Sigma-Aldrich) with 0.1 × PBS for 2 h. After incubation, slides were washed, dried and stored in a dessicator at room temperature until used. To generate surfaces to capture secreted antibodies, poly-L-lysine functionalized glass slides were incubated overnight with a polyclonal donkey anti-human (H+L) capture antibody (25 μg/mL, Jackson Immunoresearch) in a borate buffer solution (50 mM sodium borate, 80 mM sucrose and 50 mM NaCl, pH 9) under a LifterSlip^{TM} at 4°C. Steps for processing slides before and after capture of secreted antibodies have been previously reported [52]. Briefly, slides were placed in a solution of PBS containing nonfat milk (3% w/v) and Tween-20 (0.05% v/v) for 15 min at room temperature with mild agitation. Slides were then rinsed twice with a solution of PBS and Tween-20 (0.05% v/v), followed by PBS and water, and finally spun dry.

2.5.3. Distribution of cells into arrays of nanowells

Cells were deposited onto treated arrays of nanowells at a density of ~2 × 10^5 cells/mL and allowed to settle into wells for 5 min, under gravity. A Poisson distribution of cells was typically observed, with ~30% of wells occupied by single cells when loading 1 × 10^5 cells onto

an array with 50-μm wells. Higher loading densities were achieved by repeating this process until desired well occupancies were observed. For the analysis of primary B cells, PBMCs were deposited onto an array of nanowells to obtain a density of ~3-5 cells/well. Given that these cells constitute only ~5% of total PBMCs, each occupied well at this density holds one B cell on average. Excess cells were gently rinsed from the top of each array with complete media and then removed by aspiration. Arrays were submerged in complete media until imaging or microengraving steps.

2.5.4. Printing and interrogation of microarrays

Arrays of nanowells loaded with cells were sealed with capture slides and incubated together for 2 h (37°C, 5% CO_2). The assembly was held under compression using commercial hybridization chambers (G2534A, Agilent). The resulting microarrays of antibodies were panned with solutions of antigens diluted in PBS with 0.1% (w/v) bovine serum albumin (BSA). Bound antigen was detected with either secondary detection antibodies or direct conjugation of antigen with fluorescent species. A mixture of mouse anti-human Ig detection antibodies (anti-IgG1, clone JDC-1; anti-IgA1/2, clone G18-1; anti-IgG3, clone HP6050; and anti-IgM, clone G20-127), each at 1 μg/mL and diluted in PBS with 0.1% (w/v) BSA and 0.05% (v/v) Tween-20 was used to indicate the presence of Ig isotypes. Ig detection antibodies were purchased unconjugated from BD or Invitrogen and fluorescently labeled with Alexa Fluor® protein labeling kits (Invitrogen). Details of ideal channel combinations are given in Section 3.1. Slides were scanned on a GenePix® 4200AL microarray scanner (Molecular Devices) to register the information captured.

2.5.5. Analysis of printed microarrays

GenePix Pro 6.0 (Molecular Devices) software was used for analysis of acquired microarrays. A custom GenePix Array List (GAL) template, with blocks of spots designed to match blocks of wells within the array, was used to determine the location of cells secreting antibodies of interest. The template assigned each element a unique identifier or well ID, corresponding to the location of source cells in the array of nanowells. Alignment of the template over images was done manually. Alignments and re-orientation were performed using signal from the fluorescent channel with the highest frequency of events. After alignment, local background-corrected median fluorescent intensities (MFIs) were extracted for each element; these data were then sorted to identify elements of interest, and exported into a comma-delimited text file. Printed elements in the arrays were considered Ig^+ with % saturation ≤ 2, signal-to-noise ratio ≥ 1, $\geq 40\%$ of pixels above background + 1 standard deviation and CV ≤ 200, and after compensation for bleed-through of signal from adjacent channels. All antigen-specific events were also confirmed by visual inspection since they were typically < 10% of all Ig^+ events. More stringent criteria [52] were applied for the analysis of data from experiments with cell lines given the narrower distribution of intensities typically observed and the significantly larger fraction of elements with background-corrected MFIs $\geq 10{,}000$.

2.5.6. Spot assay

The spot assay is a cell-free assay designed to mimic the microengraving process that was used for validation of reagents and/or determination of optimal reagent concentrations for microarray analysis. Dilutions of standards or control antibodies in buffered solutions were spotted manually (~2 μL) on capture slides and incubated at 37°C in a humidified chamber for a

period of 1 h. Residual drops were aspirated, then slides were blocked and washed as previously described. Microarrays were incubated with detection species (fluorescently-labeled antigen or detection antibodies), scanned on GenePix® 4200AL and analyzed with GenePix Pro 6.0.

2.6. Cytometry

PBMCs were stained for viability and surface-expressed proteins with CellTrace™ Calcein Violet AM and a panel of mouse anti-human antibodies – anti-CD19 (clone SJ25-C1, Qdot® 605/Brilliant Violet™ 605 conjugate), anti-CD20 (clone 2H7, Alexa Fluor® 488 conjugate), anti-CD27 (clone O323, PE-Cy7 conjugate), anti-CD38 (clone HB7, PerCP-eFluor® 710 conjugate), and anti-CD138 (clone B-B4, APC conjugate), using manufacturers' recommended concentrations. Cell lines were stained with CellTrace™ Calcein Violet AM (Invitrogen), Calcein AM (Invitrogen), CellTracker™ Red (Invitrogen) or TFL4 (OncoImmunin, Inc.) viability dyes to enable capture of nanowell occupancies. Cells were labeled for 30 min at room temperature in complete media. Flow cytometry was performed on BD™ LSR II or BD LSRFortessa™ cell analyzers available at the Swanson Biotechnology Center (Koch Institute) and data was analyzed using FlowJo Version 9.6.1 (TreeStar, Inc.). For on-chip cytometry, labeled cells were loaded onto arrays of nanowells, washed with PBS containing 2% (v/v) FBS, and covered with a LifterSlip™ (EMS). Transmitted-light and fluorescent images were then acquired on an automated epifluoresence microscope (Carl Zeiss) fit with an EM-CCD camera (Hamamatsu). The images were analyzed on a block-by-block basis using custom software [39] to determine the viability and the level of expression for each marker. Data were gated first for size then mean fluorescence intensities were extracted for the different fluorescent channels.

2.7. Retrieval of cells from nanowells

Cells were recovered from arrays using an automated micromanipulator (CellCelector, ALS GmbH). Cells were retrieved for either clonal expansion or recovery of antibody genes. For clonal expansion, arrays with cells were immobilized in 4-well plates and submerged with complete media. The individual steps required for the transfer of a cell from a nanowell to a well in a 96-well plate, in order, were: (1) pre-aspiration of media from the reservoir; (2) aspiration of the cell(s) from the targeted nanowell, and (3) deposition of the picked cell(s) into the well of a 96-well plate filled with 200 μL pre-warmed complete media (37°C). Plates of cells were then returned to an incubator and maintained at 37°C (5% CO_2). For the recovery of heavy and light chain genes, arrays of nanowells were stored at 4°C in complete media until cells were to be recovered. Capillary tips used for recovery were first sterilized with RNaseZap® (Invitrogen), washed thoroughly with nuclease-free water then blocked with Salmon Sperm DNA (1 mg/ml, Ambion) to minimize spurious contamination by nucleic acid. Arrays were immobilized in 4-well plates and gently washed, then submerged in PBS to remove residual media, which can interfere with gene amplification. Target cells were picked directly and were deposited in wells of a 96-well PCR plate with 20 μL 1× First-Strand Buffer (Invitrogen) and 10 U RNasin® (Promega). After recovery, plates of cells were typically frozen and stored at -80°C until reverse transcription polymerase chain reactions (RT-PCRs) were performed.

2.8. Amplification of variable genes

Amplification of antibody genes was carried out in four steps: Cell lysis, cDNA synthesis, PCR I and PCR II. For cell lysis, 1.25% (v/v) Nonidet® P-40 (G-biosciences) and 150 ng random hexamers were added to each reaction, and then samples were heated to induce lysis

(65°C, 10 min; 25°C, 3 min). 100U Superscript® III reverse transcriptase (Invitrogen), 2 μL 5× First-Strand Buffer (Invitrogen), 2 μL 0.1 M DTT (Invitrogen) and 1 μL 2.5 mM dNTP were added for cDNA synthesis (37°C, 1 h). First PCR was then run with HotStar® Taq DNA polymerase (Qiagen) in a total reaction volume of 50 μL (~5 μL template, 5 μL 10× buffer, 2 μL 2.5 mM dNTP, 0.5 μL forward and reverse primer mixes, 0.25 μL HotStar® Taq). After activation of the polymerase at 95°C (6 min), 3 cycles of pre-amplification were carried out {94°C (45 s), 45°C (45 s), 72°C (45 s)}, followed by 30 cycles of amplification {94°C (45 s), 50°C (45 s), 72°C (1 min 45 s)}, and a final extension at 72°C (10 min). For PCR II, a nested PCR was run with cloned Pfu polymerase (Agilent), also in a total reaction volume of 50 μL (~3 μL template, 5 μL 10× buffer, 1.25 μL 2.5mM dNTP, 1 μL forward and reverse primer mixes, 0.5 μL Pfu). 30 cycles of amplification were used {94°C (45 s), 50°C (45 s), 72°C (1 min 45 s)}, with a final extension at 72°C (10 min). To improve the overall yield in amplification, restriction sites were eliminated from primers for the nested PCR. A complete list of all primers used is included in the Appendix (Table A.1)

2.9. Cloning and expression of monoclonal antibodies

Paired heavy and light chain genes were cloned into vectors for expression as human IgG1 (courtesy of M. Nussenzweig, Rockefeller University), based on a published protocol [53]. Appropriate restriction sites for expression vectors were introduced with another round of PCR using primers from Tiller *et al.* [53]. Products were purified with QIAQuick PCR Purification kit (Qiagen), digested, and ligated into Igγ1, Igκ, or Igλ vectors (50 ng) using T4 DNA ligase (NEB). Plasmids were then transformed into chemically competent NEB5α *E. coli* (NEB). Colonies were screened by PCR using 3IgVs-PCR-fwd (5'–CACTTTGCCTTTCTCTCCACAGGT–3')

and 3IgVs-PCR-rev (5'–ACAGATGGTTCTTTCCGCCTCAGA–3') primers. After sequence verification, plasmids were isolated from 2-mL overnight cultures (QIAprep Spin Miniprep Kit, Qiagen) and transiently transfected into human embryonic kidney (HEK) 293T cells (ATCC) for antibody production. HEK 293T cells were cultured in Dulbecco's Modified Eagle's Medium (DMEM) supplemented with 10% (v/v) FBS, 100 U/mL penicillin and 100 μg/mL streptomycin, but DMEM was replaced with serum-free HL-1™ media (Lonza) just before transfections were performed. Vectors were transfected into cells (1:1 ratio) using GenJet™ In Vitro DNA Transfection system (SignaGen Laboratories). After 48-72 h, supernatants were recovered, centrifuged (~450 g, 5 min), and stored with 0.02% (w/v) NaN_3, at 4°C for subsequent analyses. Despite successful recovery and sequencing, it is noteworthy that ~30% of antibodies selected either did not clone in *E.coli*, or did not express as full-length human IgG1 after transfection in the host cell line, especially with antibodies from non-IgG1 isotypes.

2.10. HIV neutralization assay

Serial dilutions of purified antibodies were made in complete DMEM and distributed in wells of a 96-well round-bottom plate (15 μL/well). 45 μL of pseudovirus (~300,000-500,000 relative luminescence units), generated by co-transfection of HEK 293T cells with an *Env*-expressing plasmid and an *Env*-deficient genomic backbone plasmid (pSG3ΔEnv), was then added to each well, and the mixture was incubated for 1 h (37°C). After incubation, the mixture was transferred onto TZM-bl cells (plated at 10,000 cell/well in a 96-well flat-bottom plate the previous day). Cells were incubated for 24 h (37°C), after which 150 μL/well of fresh complete DMEM was added and cells were again incubated for 48 h (37°C). Well contents were aspirated and cells were lysed with 60 μL of lysis buffer. 20 μL of lysates were transferred to a white 96-

well flat bottom plate and 50 μL of luciferase substrate (Promega) was added to each well. Resulting luminescence was read with a luminometer (VICTOR^{TM} *X* Light, Perkin Elmer). Dose response curves generated were fit by nonlinear regression to determine 50% inhibitory concentrations (IC_{50}) for each antibody, using signals from virus-only wells as 0% neutralization reference.

CHAPTER 3: ESTABLISHING PROTOCOLS FOR *EX VIVO* PROCESSING OF HUMAN B CELLS

3.1. Optimization of surface capture and detection of secreted antibodies

Spot assays were used to test a variety of antibody clones specific for different constant regions (isotypes) on human Igs to evaluate their suitability as secondary antibodies. Reagents were optimized to enable simultaneous capture and detection of IgG1, IgA1/2, IgG3 and IgM isotypes (Figure 3.1), all of which are known to have important effector functions in the periphery and mucosa [1]. A polyclonal donkey anti-human Ig (H+L) antibody (Jackson Immunoresearch) was determined to be optimal capture antibody when used at a concentration of $\geq$ 25 μg/mL. To determine the isotypes of captured antibodies, the following monoclonal antibodies were found to work best as a panel: mouse anti-human IgG1 clone JDC-1 (Alexa Fluor® 647 conjugate, BD Pharmigen), mouse anti-human IgA1/2 clone G18-1 (Alexa Fluor® 594 conjugate, BD Pharmigen); mouse anti-human IgG3 clone HP6050 (Alexa Fluor® 555 conjugate, Invitrogen), and mouse anti-human IgM clone G20-127 (Alexa Fluor® 488 conjugate, BD Pharmigen). Using titrations of isotype standards, it was determined that the limit of detection for this optimized panel of capture and detection antibodies is $\geq$ 10 ng/ml of Ig in the supernatant of each well (Figure 3.2) – a concentration much less than that estimated to result during microengraving for 2 h with ASCs (1-10 μg/mL) [54]. When the full panel of capture and detection species was used, apparent cross-reactivity of antibodies and/or bleed through of signal was corrected for with appropriate compensation to minimize false positives based on results from spot assays.

3.2. Optimization of on-chip image-based cytometry for immunophenotyping of human B cells

The evolution of B cells from plasmablasts to terminally differentiated plasma cells is accompanied by the increased expression and/or downregulation of CD19, CD20, CD38 and CD138 cell-surface receptors [55]. A panel of detection antibodies against these receptors was validated for the analysis of B cells in nanowells by image-based cytometry. Several clones of antibodies specific for CD19, CD20, CD27, CD38 and CD138 receptors, and conjugated to a set of fluorophores known to show minimal bleed-through into other channels on the available epifluorescence microscopes (Zeiss) were tested on PBMCs from healthy donors (Figures 3.3a and A.1, Appendix). The distributions of populations enumerated on-chip were similar to those determined by flow cytometry for the same pool of cells, stained at the same time (Figure 3.3). These results indicate that image-based cytometry can sufficiently resolve the major classes of B cells, despite the narrower dynamic range typically available on epifluoresence microscopes equipped with CCDs.

3.3. Optimization of conditions for activation of memory B cells

Antibodies secreted by plasma cells in primary samples can be captured readily with microengraving. The capture of antibodies from memory B cells, however, requires activation of this otherwise dormant population. Several stimulation conditions modified from published conditions for the polyclonal activation of B cells [44-51] were initially compared using a Luminex® isotyping kit (Millipore). After incubation of PBMCs in media containing stimulants for 7 days, the isotypes and amounts of antibodies accumulated in the recovered supernatants was measured (Figure 3.4a). The top three conditions resulting in the most secretion and the

greatest diversity of antibody isotypes (CpG + IL-15, CD40L + IL-21 and IL-2 + IL-21 + anti-human CD40 + anti-human IgM) were subjected to a time course analysis using microengraving. PBMCs from a single donor were incubated for 3, 5 and 7 days in the different cocktails of stimulants, after which samples were enriched for B cells, and antibodies secreted by individual cells were captured by microengraving, using the optimized panel of antibodies for determining isotype. From this experiment, it was determined that stimulation for 7 days was optimal (Figure 3.4b). After repeating chip-based analysis on multiple PBMC samples stimulated for 7 days, it was found that stimulation with CD40L + IL-21 was best, inducing secretion from ~20% of $CD20^+$ cells (Figure 3.4c). Naïve B cells ($CD20^+$, $CD27^-$, IgM^+, IgD^+) represent 50-70% of this population [55, 56], hence, we are able to activate 40-60% of total memory B cells with this protocol. A 100× dilution of purified Epstein-Barr virus (EBV, Advanced Biotechnologies Inc.) was included in the mixture to improve the yield of activated cells, and take advantage of potential synergistic effects from the combination of EBV and polyclonal B cell activators [19, 57, 58]. Although EBV is capable of selective immortalization of human B cells, which may skew the observed response from the memory B cell population, it was reasoned that the 1 week timeframe used for activation was too short to significantly alter the repertoire, as immortalization is typically performed over 2-4 weeks [19, 57-59].

3.4. Optimization of single-cell recovery from nanowells

In order to establish stable cell lines producing antibodies with desired functionalities, it was imperative that clones of interest could be transferred routinely from wells in an array of nanowells to larger vessels for clonal expansion or gene amplification. The AVISO CellCelector automated micromanipulation system (ALS GmbH) was used to rapidly transfer cells from

nanowells to 96-well microtiter plates. The system comprises a robotic arm carrying a module for single-cell retrieval (single-cell module, ALS GmbH); an inverted microscope (CKX41, Olympus) with an imaging CCD (CC12, Soft Imaging Systems GmbH) and an automated translation stage on which arrays of nanowells were mounted; reservoirs for both media and sterilizing solution (e.g. 70% v/v ethanol); and docks for mounting 96-well receiving plates. The single-cell module mounted on the robotic arm includes a glass capillary (50-μm diameter) connected to a 50 μL syringe via plastic tubing and a series of connectors (Figure 3.5). The hose, syringe and capillary tip were filled with mineral oil (Sigma), and air bubbles excluded to allow for precise aspiration of specified volumes. The arm was designed for a repetitive accuracy of at least 10 μm, and movement of the microscope stage was designed to be accurate to within 1 μm. Microscope images on this system were acquired at 10× magnification with a camera resolution of 1.024 μm/pixel. The instrument was operated in both a semi-automated manner, with direct input of the location of each target nanowell by the user, and in a fully automated mode. A custom software module (ALS GmbH) was developed to calibrate the system for the arrangement of the nanowells on a given array, and to import a list of well positions of interest (encoded by block, row, and column) from the analyzed microarrays generated by the microengraving process (comma-delimited text file generated from GenePix Pro). Images were recorded both before and after micromanipulation to validate the retrieval of targeted cell(s).

3.4.1. Optimization of parameters affecting the transfer of viable cells

While the micromanipulator used in these experiments is designed to allow fully automated recovery of cells, it was useful to operate the instrument in a semi-automated mode to optimize the system for reliable recovery of single cells. In this mode, cells of interest in

nanowells were positioned manually for recovery and then retrieved by initiating a programmed routine for retrieval by the micromanipulator. We used this mode to minimize the time required to transfer a single cell from a given nanowell to the well of a 96-well microtiter plate, while maximizing the accuracy of the transfer. Four parameters were considered: (1) the volume of media aspirated into the glass capillary from a reservoir of media (0.5 μL, 1.0 μL, 2.0 μL) prior to retrieving a cell, (2) the volume of media aspirated upon positioning the tip of the capillary within the targeted nanowell (0.5 μL, 1.0 μL, 2.0 μL), (3) the time allowed to elapse immediately after aspiration (0 s, 5 s, 10 s), and (4) the inclusion of a rinse cycle in the destination well of the microtiter plate immediately after deposition of the retrieved cell (Yes/No).

Liquid uptake for buffer-layer and cell retrieval

We found that pre-aspiration of media was necessary to minimize the likelihood of trapping the retrieved cell at the interface between the mineral oil in the capillary and the aspirated media. Pre-aspiration of 0.5 μL of media from the reservoir of media followed by aspiration of 1.0 μL upon positioning the tip at the nanowell was sufficient to recover single cells from a targeted well in the array without disturbing cells in adjacent wells (Table 3.1). These volumes greatly exceed the nominal volume of each nanowell (125 pL), but we did not observe any non-specific aspiration of cells from adjacent nanowells under these conditions. Volumes smaller than 1.0 μL, however, were unreliable at removing cells from the targeted wells. The rate of aspiration was fixed at the lowest setting possible on the instrument (~0.2 μL/s) in an effort to minimize the possible effects of shear stresses on the retrieved cells. At this rate of aspiration, it was estimated that the maximum stress on the surface of a cell at any instant would be ~100 dynes/cm^2, when modeling a cell as a rigid structure in a flow channel. Mammalian cells have

been exposed to this shear stress without significantly altering expressed phenotypes or damaging cellular integrity [60].

The distance set between the glass capillary tip and the surface of the PDMS chip during the calibration of the instrument also impacted the recovery of viable cells. Positioning the tip ~20 μm from the bottom surface of the nanowells allowed sufficient clearance between the tip and the surface of the PDMS for aspiration, and avoided direct contact with the cell in a well. The flexibility of the PDMS substrate was useful for preventing damage to the tip during calibration, and thus, accurate and reproducible positioning of the tip in nanowells was possible.

Inclusion of rinse cycle in transfer process

To ensure recovered cells were transferred consistently to the receiving plate, it was critical to rinse the capillary inside the targeted well of the microtiter plate after dispensing the aspirated volume. Mock transfers were performed immediately after depositing retrieved HYB099-01 hybridoma cells in the desired destination wells of a microtiter plate, to determine whether or not all recovered cells had been successfully ejected from the tip. After the initial transfer of targeted HYB099-01cells to a well of the 96-well collection plate, the tip was moved over to an empty nanowell, and the media in the nanowell was aspirated. The aspirated content was then dispensed and rinsed in media in an unused well of the 96-well collection plate. The plate of recovered cells was incubated to allow for the expansion of any transferred cells. Colonies of cells grew only in those targeted wells of the microtiter plate where cells were intentionally deposited; 17 of the 23 wells in which cells were specifically deposited yielded expanded populations of cells after incubation. These experiments confirmed that recovered cells

were transferred to targeted wells with high fidelity; that is, recovered cells were not left in the capillary to contaminate subsequent wells on the 96-well plate.

System delay following aspiration

Using this optimized set of parameters for retrieving cells from nanowells and depositing into the wells of a target receiving plate, we studied the effect of adding a short delay between aspiration of cells from wells, and subsequently moving the capillary to the receiving plate. We reasoned that the delay would allow the volume in the tip to equilibrate after the aspiration, and improve the reproducibility of the transfer. We tested the accuracy and subsequent viability associated with transferring single cells using two different cell lines (12CA5 and HYB099-01 hybridomas) and programmed delays of 0, 5, or 10 s. These values were selected to be similar in duration to the time required to aspirate 1 μL (5 s). Delays of both 5 s and 10 s yielded better accuracy of transfer and improved viability of the retrieved cells than no delay (0 s) (Table 3.2). The variability in accuracy and survival rate also decreased with increased delays. Although the delay extended the minimum time required per transfer, we concluded that a programmed delay of 10 s immediately after aspiration was optimal among the conditions tested. The duration for the entire optimized process for retrieval and transfer of cells from a nanowell to a 96-well plate, therefore, requires about 67 s, including the time for translation of the microcapillary tip from its starting position to the various stations. A Student's t-test comparison of the measured accuracies and survival rates for both the 12CA5 and HYB099-01 cell lines indicated that the observed differences in these quantities were not statistically significant ($p > 0.05$). This analysis suggests that the optimal settings identified could be used successfully for the accurate transfer of other hybridoma cell lines, with minimal effect on viability. It was also found that the optimized

parameters determined in these experiments were suitable for the recovery of both primary lymphocytes (~75% efficiency) and yeast cells [39, 61]. With these settings, ~50-60 transfers could be made in 1 h in fully automated operation.

3.4.2. Reproducibility of Recovering Discrete Numbers of Cells

An array of wells containing cells can be cultured for several days after microengraving [36, 52]. We reasoned that delaying the recovery of hybridomas to allow one to two cellular divisions may improve the yield of clones that successfully expand after transfer to the 96-well plate. Using the optimized parameters described above, we tested the accuracy of recovering defined numbers of cells from nanowells (1, 2, 3, or 4) (Figure 3.6). The numbers of recovered cells in each well of the 96-well receiving plates were counted manually 1 h after transfer. These experiments demonstrated that the recovery of single cells was highly reproducible (n = 63 transfers). When more than one cell was recovered from a given nanowell, the number of cells transferred was typically equal to or less than the targeted number. There was, however, greater variability in these data than that for the transfer of single cells, and the number of cells present in the receiving plate occasionally exceeded the targeted number. Comparing the measured accuracies, retrieval of single cells was ~95% accurate, whereas the retrieval of 4 cells was ~50% accurate. For all of these experiments, the transferred cells expanded successfully in culture (Figure 3.6b). Together, these data suggest that expanding the number of cells in each nanowell prior to their recovery is not critical for successful and accurate recovery. The ability to correctly transfer cells was further demonstrated by alternating between the transfer of 12CA5 and HYB099-01 cells identified by microengraving for 100 consecutive picks [62].

3.5. Optimization of protocol for variable gene amplification

To allow for the recovery of genes coding for the heavy and light chain variable regions of antibodies, cell retrieval was interfaced with RT-PCR steps to amplify genes from mRNA synthesized within cells. Optimized settings described in Section 3.3 were changed slightly to accommodate this linkage. Intact cells were deposited into wells of a 96-well PCR plate containing $\leq$ 30 μL of 1× First strand buffer and an RNase inhibitor with no pre-aspiration or rinse steps (Figure A.2, Appendix). These steps were removed to eliminate a potential source of contamination, to avoid adding extra volume to the subsequent RT reaction, and to avoid lysing extremely fragile cells after prolonged storage (~6-24 h) at 4°C. Accurate transfer of cells with this protocol was demonstrated by the alternating transfer of isolated 4D20 cells and the contents of empty nanowells (data not shown).

The procedure for performing RT-PCR on retrieved cells was modified from the single-cell RT-PCR protocol published by Wang et al., (2000) [63]. The most significant modification to the protocol involves the use of Taq polymerase for first round of PCR despite its lower fidelity, as it is superior at successfully amplifying mRNA with low-copy numbers [53]. With this protocol, it was possible to amplify genes from $\geq$ 0.05 pg of purified mRNA (Figure 3.7). IgA-specific primers from a published protocol by Bradshaw et al. (2007) [64] (IgA-PCRI, 5'–GCTCAGCGGGAAGACCTT–3'; IgA-PCRII, 5'–GACCTTGGGGCTGGTCGGGGA–3') were also included in primer pools. Using 4D20 hybridoma cells, for which heavy and light chain gene sequences were known, it was determined that the expected error rate for nucleotide addition when amplifying with Taq polymerase then Pfu polymerase was ~5 × 10^{-5} errors/nucleotide. This error rate was comparable to the error rate observed when using the

higher fidelity Pfu polymerase for both the first and nested PCRs. Disruption of cellular membrane integrity was also enhanced by including a freeze-thaw step after recovery; freezing cells at -80°C and thawing at room temperature before running reactions. Overall, the process allows the transfer and amplification of heavy and light chain genes from single B cells with ~50% efficiency (30-70% range), with paired sequences recovered ~40% of the time (Figure 3.8). It is important to note, however, that the amplification efficiency depends largely on the quality and state of the cells at the time of recovery. We found that the more activated the cells are at the time of retrieval, the greater the likelihood of amplifying both heavy and light chain genes. Significant delays in transitioning to the recovery step also reduce the efficiency of amplification.

3.6. Discussion

We have optimized many commonly used bioanalytical processes and processing conditions to allow their use in conjunction with arrays of nanowells. By integrating these different analysis tools, it is now possible to obtain information about the immunophenotypes (or states) of cells, the functionality of secreted antibodies *in vivo*, and to determine variable gene usage for interesting cells, all within a primary screen. We are able to profile 10-15 different parameters with this integrated approach for B cell analysis – comparable with the number of parameters that can be analyzed by flow cytometry [24, 25] – but there is still significant room for improvement.

One major advantage of the microengraving approach that has not been utilized significantly is the ability to analyze secretion from cells repeatedly, with serial microengraving [35, 65]. This has not been demonstrated for primary human B cells, as the rates of Ig secretion

from primary cells appeared to be lower in subsequent rounds of analysis, necessitating longer incubation times during microengraving. With the incorporation of signal amplification strategies such as the hybridization chain reaction [66], the incubation time required for microengraving could be truncated, allowing the generation of multiple antibody microarrays from the same antibody-secreting cells. Alternatively, exploring approaches to covalently link captured Igs to the capture surface with formaldehyde and/or imidoesters such as dimethyl adipimidate (DMA) and 1-ethyl-3-(3-dimethylaminopropyl)carbodiimide (EDC) [67, 68], may allow repeated interrogation of microarrays, also increasing the number of analytes or parameters that can be detected. Additionally, multiplexing will be achieved with improvements in microscopy and technologies for the analysis of microarrays. A transition to systems with more lasers and filters should enable the use of more fluorophores simultaneously.

The gene amplification protocol described here is another area for potential improvement. Currently, the protocol results in the successful amplification of variable genes from ~50% of recovered cells. While this efficiency is comparable with the efficiencies observed with other approaches [30, 34, 53], the inconsistency observed is concerning. Reasons for this inconsistency are thought to include problems with primer design and insufficient mRNA in the cells – either due to mRNA degradation or insufficient activation of cells. Our protocol for single-cell RT-PCR was designed to be flexible so changes to the primer sets used for gene amplification can be implemented easily. To increase the amount of mRNA available for heavy and light chain gene amplification, *in vitro* transcription methods [69] could also be adapted into the protocol. To address potential problems with memory B cell activation, transfection of primary memory B cells with oncogenes [70] could convert these cells into stable antibody-producing cell lines with

large quantities of mRNA, characteristic of hybridoma cells. Lastly, faster retrieval of cells from nanowells, either by accelerating the pipeline for analysis of microarrays, or by a redesign of the micromanipulation system to eliminate extensive translation steps, may minimize any degradation of mRNA molecules.

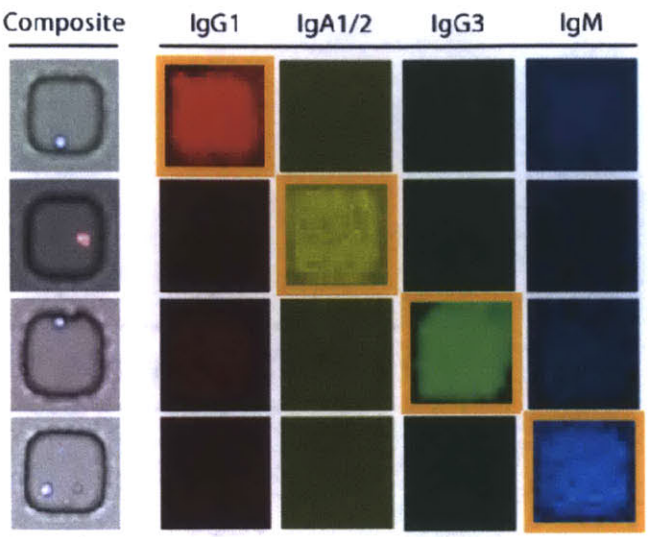

Figure 3.1: Detection of antibody isotypes secreted by human primary B cells.
ASCs were loaded into nanowells and microengraving was performed to capture secreted antibodies. Representative micrographs of the different isotypes detected are shown, with signals gated as positive for IgG1, IgA1/2, IgG3, IgM highlighted, after interrogation with optimized panel of anti-human Ig detection antibodies.

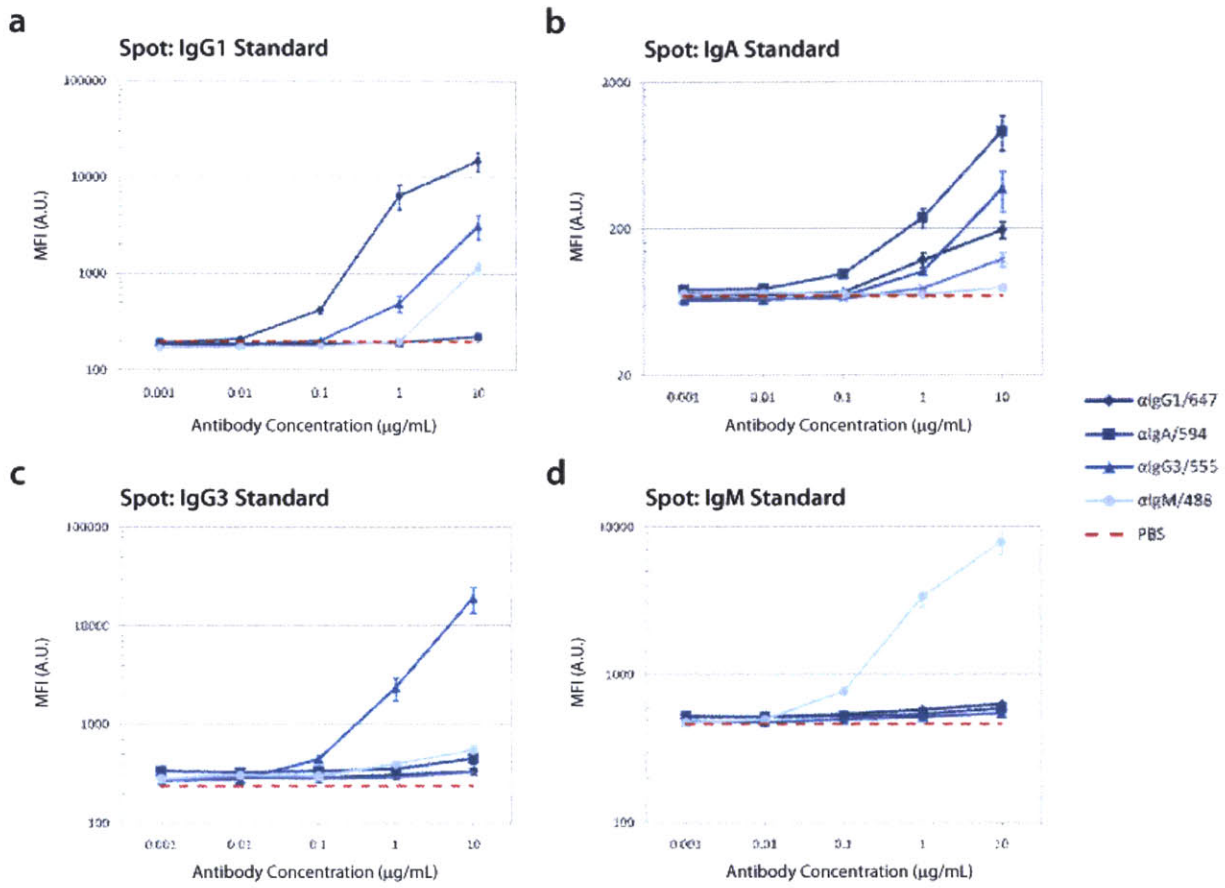

Figure 3.2: Evaluation of detection limits with optimized panel of secondary antibodies.
Titrations of isotype standards in triplicate were spotted on a uniform donkey anti-human Ig capture surface. Following incubation of spots, optimized panel of mouse anti-human IgG1-Alexa 647, IgA-Alexa 594, IgG3-Alexa 555 and IgM-Alexa 488 detection antibodies, each at 1 µg/mL, was used to evaluate the limits of detection and the amount of signal bleed-through or antibody cross-reactivity for which to compensate. Each plot shows median fluorescence intensities (MFI) in the different emission channels used for the different dilutions of a given isotype standard, spotted on a slide. MFIs from PBS control spots are indicated with red dashed line.

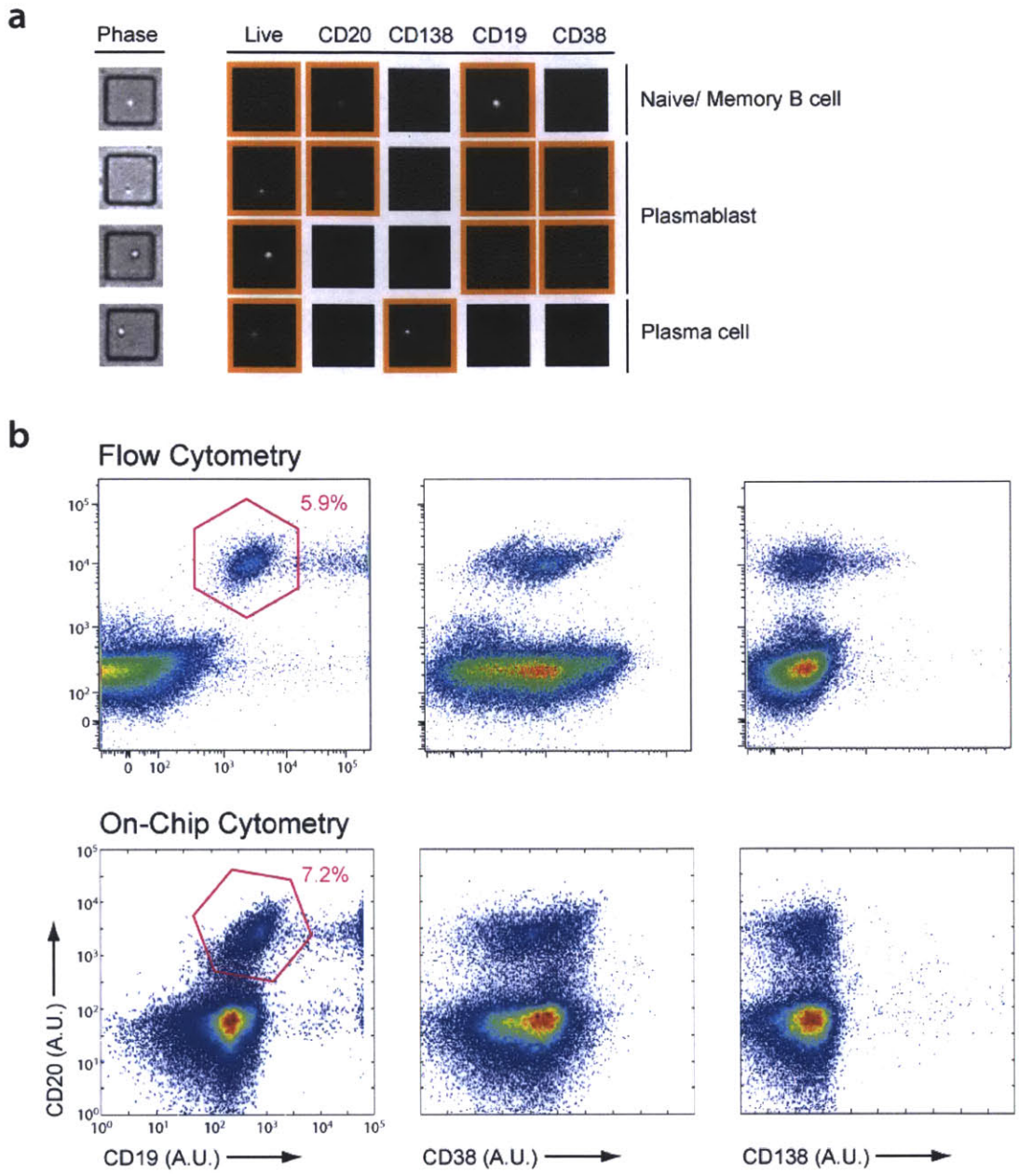

Figure 3.3: Comparison of on-chip cytometry and flow cytometry.
PBMCs from a healthy donor were stained for viability with Calcein violet AM, and for expression of CD19, CD20, CD38 and CD138. A portion of the labeled cells were loaded onto an array of nanowells and imaged by epifluoresence microscopy. The remaining cells were analyzed on a BD LSRFortessa™ cell analyzer. (**a**) Representative micrographs from wells with single cells displaying different expression patterns. Signals gated as positive with custom-built analysis script are highlighted with orange boxes for each. (**b**) Density plots of both flow cytometry (top) and on-chip cytometry (bottom) generated from the same sample.

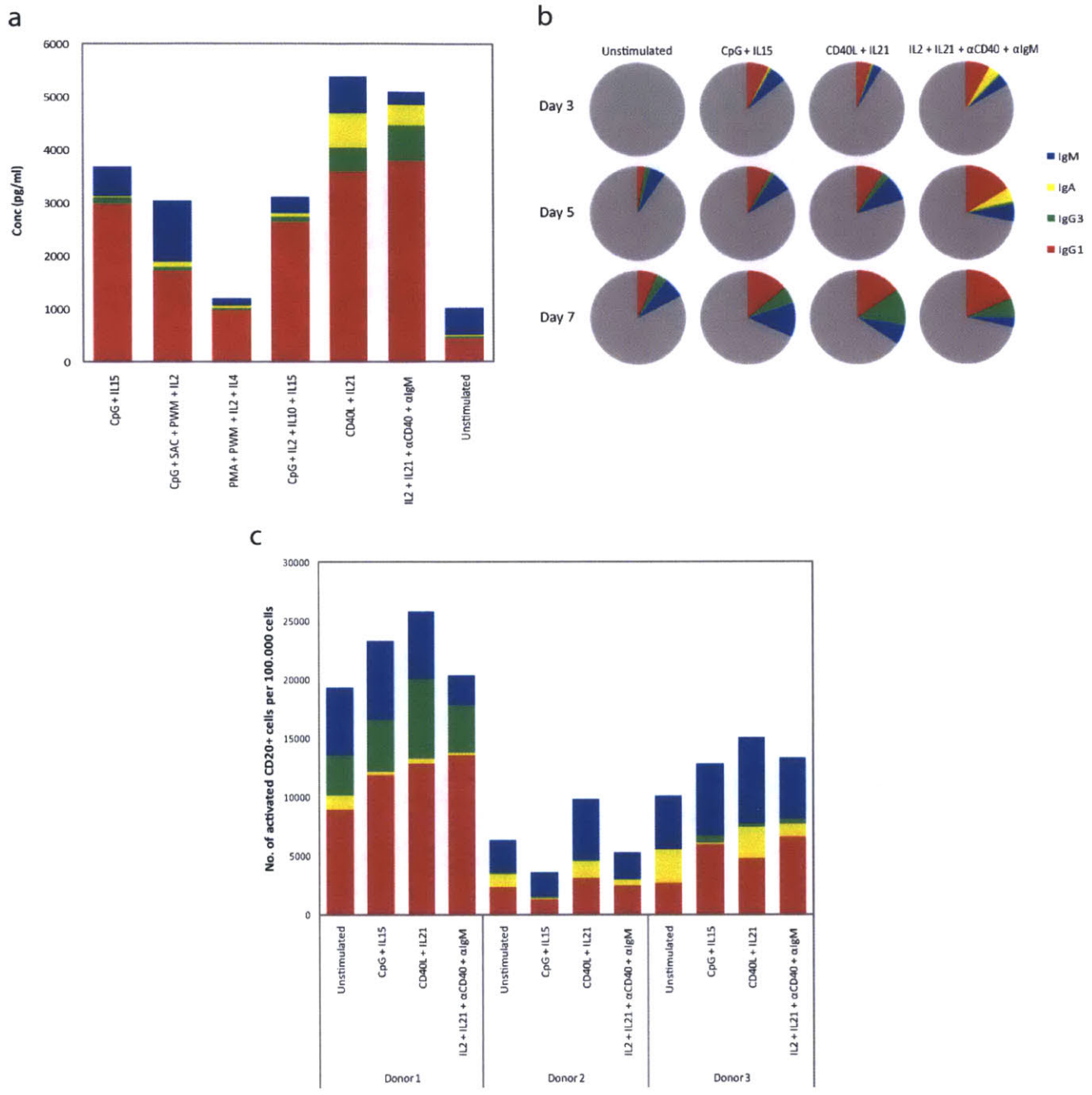

Figure 3.4: Optimization of conditions for stimulation of memory B cells *ex vivo*.
(**a**) After incubation of PBMCs with mixtures of different cytokines, mitogens and TLR agonists, supernatants were analyzed for Ig secretion with Luminex kits. (**b**) The best three conditions identified in **a** were subjected to time course analysis using microengraving to determine when to process stimulated memory cells. (**c**) Frequencies of activated $CD20^{+}$ cells following 7 days of bulk stimulation with best conditions for three donors.

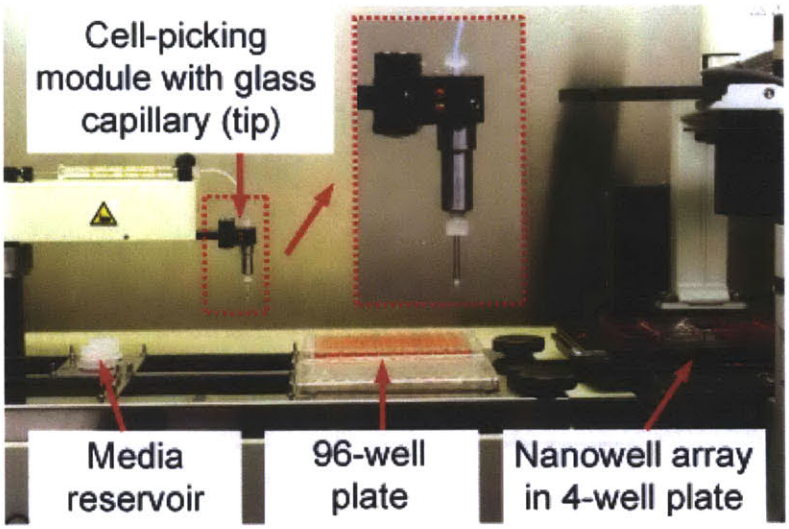

Figure 3.5: Instrument for transferring cells by automated micromanipulation
Photograph of the CellCelector showing the positioning of samples and buffers during the automated recovery of cells from an array of nanowells. (Inset) Enlarged photograph of the single-cell module fit with a 50-μm glass capillary that enables the aspiration and transfer of cells from nanowells.

Table 3.1: Optimization of liquid uptake for accurate cell retrieval

		Accuracy (%)		
		Pre-aspiration Volume (μL)		
		0.5	*1.0*	*2.0*
Aspiration Volume (μL)	*0.5*	-	85.7 (7)*	37.5 (8)*
	1.0	100.0 (8)	90.0 (10)	50.0 (10)
	2.0	-	75.0 (12)	42.9 (7)

*Values in parentheses indicate the number of picking events contributing to the calculated percent accuracy of transfer.

Table 3.2: Effect of delay on retrieval of 12CA5 and HYB099-01 cell lines

	Delay after aspiration	12CA5[a]	HYB099-01[a]
Accuracy (%)	0 s	87.4 ± 3.8	68.1 ± 21.0
	5 s	85.0 ± 3.8	83.8 ± 14.4
	10 s	92.1 ± 3.6	78.2 ± 9.2
Survival Rate (%)	0 s	92.2 ± 5.6	79.8 ± 10.1
	5 s	96.9 ± 3.6	69.3 ± 18.5
	10 s	93.6 ± 0.5	79.3 ± 6.8

[a] Minimum of 52 cells retrieved from independent wells per experiment. Experiments for each condition replicated three times. Cells only recovered from single-cell wells.

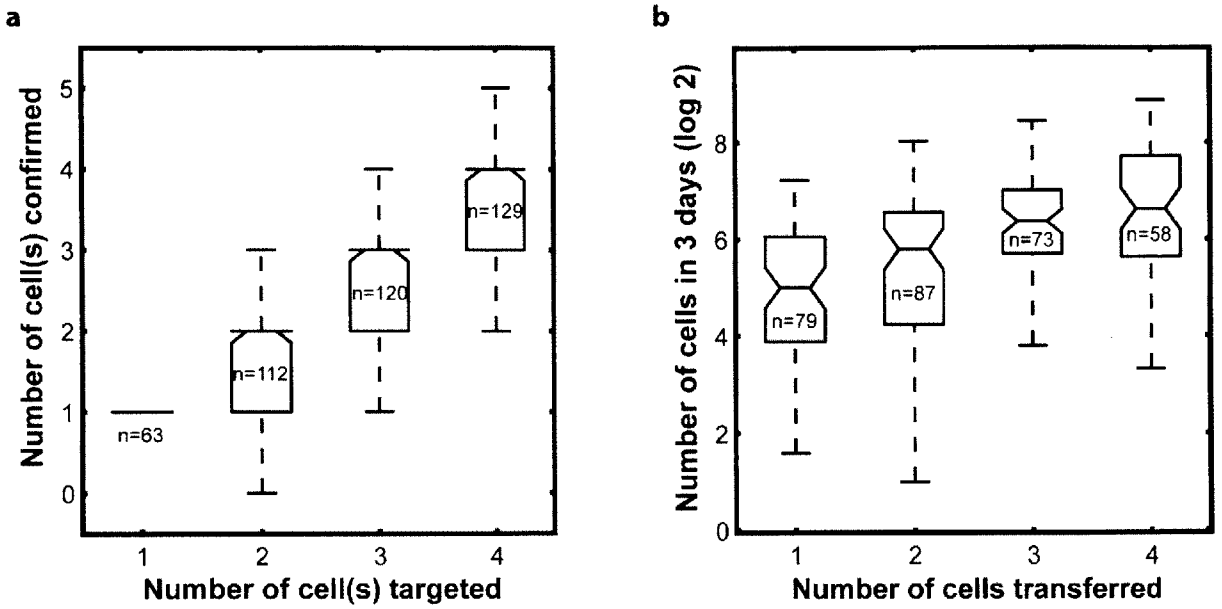

Figure 3.6: Efficiency of cell transfer with automated micromanipulation system
(a) Assessment of the accuracy of transferring HYB099-01 cells from 50-μm nanowells to 96-well plates. *(b)* Box plot of number of cells present after three days of incubation. Box plots follow Tukey's convention, with the center line representing the median and the upper and lower edges of the box representing the values of the upper and lower quartiles. Notches on the box adjacent to the median value represent the $p < 0.05$ significance interval. Bars extending from each end of a box represent the most extreme values within 1.5 times the interquartile range.

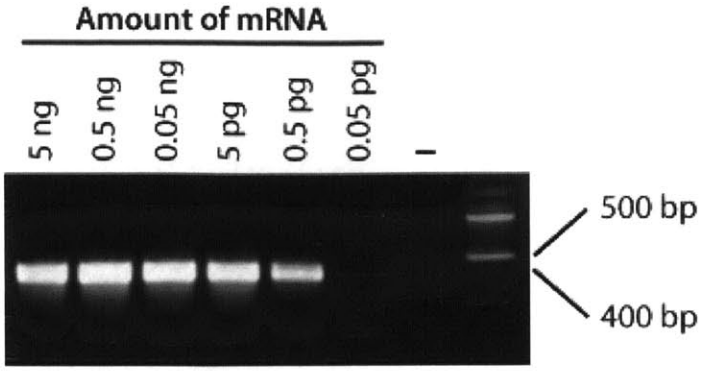

Figure 3.7: Establishing limit for amplification of antibody genes with RT-PCR protocol. Ten-fold serial dilutions of purified mRNA from 4D20 cells were amplified with optimized RT-PCR protocol. Heavy chain variable genes, 350-400 bp in size, were successfully recovered for ≥ 0.05 pg of mRNA.

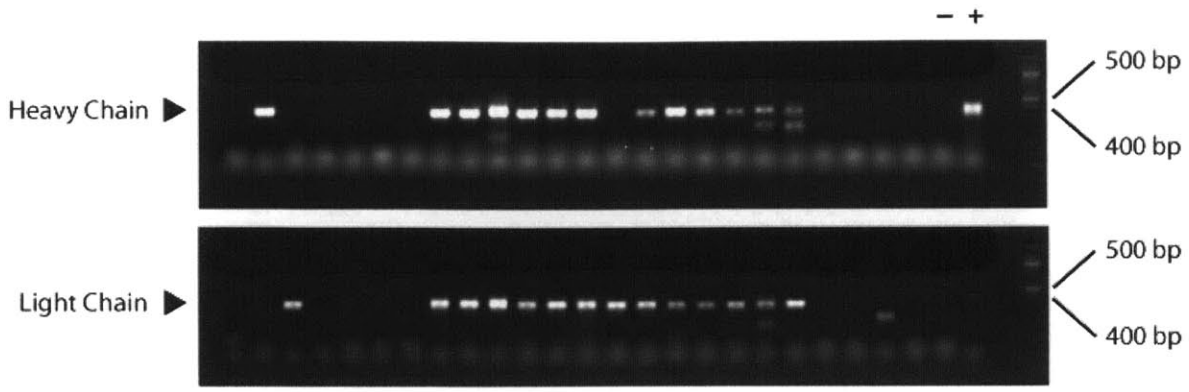

Figure 3.8: RT-PCR amplification of heavy and light chain variable genes from primary B cells.

Contents from nanowells (n = 24) matching with Ig secretion events on a printed microarray were recovered from a chip loaded with primary lymphocytes, amplified using optimized RT-PCR protocol, and resolved on a 1.5% agarose gel. Paired heavy and light chain genes were amplified in 12 of the reactions (50% efficiency). Unused wells of 96-well PCR plate served as negative controls and mRNA (~10 ng) extracted from 4D20 cells was used as positive control.

CHAPTER 4: CHARACTERIZATION OF HIV-INDUCED ANTIBODY RESPONSES IN MUCOSAL TISSUES

4.1. Background

4.1.1. Impact of HIV/AIDS pandemic

Since the identification of HIV-1 as the causative agent of the acquired immunodeficiency syndrome (AIDS) in the 1980s, the HIV/AIDS pandemic has been responsible for millions of deaths worldwide. Following the original outbreak of the disease, the spread of the epidemic globally was fairly rapid, adversely affecting the health and social well-being of individuals in different populations, and from various socioeconomic backgrounds. Current estimates indicate that over 30 million people are infected with HIV-1, and even with the availability of therapeutic drugs, HIV/AIDS remains a major cause of mortality worldwide, with increasing prevalence in some communities [71, 72]. Thus far, HIV-1 has stymied clinicians and scientists, and at present, no cure exists for HIV/AIDS, neither is there a vaccine to prevent against acquisition of the disease.

4.1.2. Overview of HIV-1 pathogenesis

HIV-1 is a lentivirus that preferentially infects the immune cells of the host, specifically the $CD4^+$ T cells, macrophages and dendritic cells, which are important for mounting an immune response to any invading pathogen. Virions exist in the blood and reproductive fluids of infected individuals; hence the virus is transmitted by intermixing of these bodily fluids between infected and uninfected persons. On entry of the virus, free-floating virus particles fuse with host cells, injecting viral genetic material into the cell, and then take advantage of cellular machinery for

viral replication and assembly [72]. Initial infection by HIV-1 is generally followed by an acute phase of infection where virus replication is exponential, resulting in a sharp increase in viral load that manifests with typical viremic symptoms in the patient. At this stage, the immune system is still able to mount a response, causing a reduction in viral load. The infection, however, is not eliminated, but progresses into a chronic phase [72]. In the chronic phase, the virus remains dormant within cells, with periodic replication to maintain the virus reservoir. This stage is accompanied by a gradual decline in the number of $CD4^+$ T cells and a steady increase in viral load, until the patient has < 200 $CD4^+$ T cells/ml of blood and $\geq 100{,}000$ copies of viral RNA/ml of plasma, at which point the individual develops AIDS [72]. Such a person is severely immunocompromised and is highly susceptible to infection by other pathogenic species, eventually ending in fatality.

4.1.3. Therapeutic strategy for controlling disease progression

Existing treatment for HIV-1 infection involves the use of HAART (highly active antiretroviral therapy), a cocktail of inhibitory molecules, designed to interfere with the function of enzymes and structural proteins at different stages in the replication-cycle of the virus. HAART has been effective in patients, enabling control of the virus in both the acute and chronic phases of infection. With HAART, there is a reduction in the viral load in infected patients, and these individuals maintain their CD4+ T cell count at a level sufficient to prevent progression to AIDS. Despite its utility as a therapeutic option, however, HAART is not the perfect solution in the global battle against HIV-1. First, HAART is largely ineffective against latent infection, and thus, unable to confer sterilizing immunity [73]. Though it reduces the risk of transmission, it does not fully eliminate the possibility of transmitting the virus to others [73, 74]. Moreover, the success of HAART greatly depends on strict adherence to a lifelong drug regimen that is

expensive. As a consequence, HAART is widely unavailable to patients in areas where the transmission rate of the disease is highest. The development of drug resistance in HIV-1 infections is also documented [72]. Therefore, if the disease is to be eradicated, it is necessary to develop a vaccine as a means of conferring protection against infection by HIV-1; a view advocated by the scientific community [72, 75-77].

4.1.4. History of HIV/AIDS vaccine development and research

Lessons from past global health crises and pandemics, such as the smallpox and polio epidemics, indicate that antibody-based vaccines represent a proven strategy for dealing with viral infectious diseases. Hence, vaccine research over the past three decades has focused principally on eliciting a humoral response to the virus, particularly neutralizing antibodies that would eliminate virus particles in the periphery, well before interaction with host cells. Traditional approaches for priming antibody production with a vaccine, however, have failed to protect against infection by HIV-1 [76-78]. Progress made in studies of vaccine strategies against viral surrogates, such as the simian immunodeficiency virus (SIV), in non-human primate models have also been difficult to replicate against HIV-1 infection in humans [79, 80]. Attempts at designing vaccines to stimulate effector functions of other immune cells have also been made, albeit without success [74, 78]. The numerous failed attempts at developing a vaccine or immunotherapeutic strategy for protection from HIV-1 infection – especially the recent failure of the MERCK vaccine [77, 81] – indicate that current knowledge of the interactions between the host immune system and the virus is inadequate.

Reevaluating the protective capability of antibodies, the characterization of the immune responses in long-term non-progressors (LTNP) or elite controllers, a cohort of individuals

capable of maintaining HIV-1 in a non-pathogenic state without the use of HAART, and highly exposed, persistently seronegative (HEPS) persons suggest that neutralization by antibodies, among other mechanisms, could be considered responsible for the regulation of viral pathogenesis [3, 72, 82, 83]. Analyses of sera from individuals with progressive disease also suggest that 20-30% of infected persons develop potent neutralizing antibody responses that unfortunately lag behind evolution of the autologous strain of HIV-1 [84, 85]. In the typical response to HIV-1, the bulk of antibodies produced recognize decoy epitopes on free-floating fragments of the *Env* spike protein. Antibodies binding highly conserved epitopes are infrequent [84, 86], and hence, have been difficult to isolate. Even with recent successes at recovering potent neutralizing antibodies [87-93], an effective vaccine strategy remains elusive. One hypothesis for why, is that there is a limited understanding of the pathophysiology of HIV-1 infection, especially in the mucosa [94-96]. Most knowledge of infection by HIV-1 comes from the analysis of blood samples from infected and healthy donors, but mucosal surfaces – through which infection is typically established – have been poorly characterized. Given the invasive nature of sample extraction from mucosal tissues, sample sizes are often insufficient for detailed analyses with existing approaches; hence, responses in these tissues are not fully understood. With microengraving technology, it is now feasible to perform multiparametric characterization of immune cells in small tissue samples, allowing the study of the humoral immune response to HIV-1 at the primary site of infection and/or in associated lymphoid tissues.

4.2. Identification of antigen-specific B cells in samples from HIV-infected subjects

4.2.1. Detection of HIV-specific antibodies

One advantage of microengraving is the flexibility to interrogate the resulting antibody microarrays with different probes to highlight specificities for different antigens. In HIV-1 infection, a major antigen encountered by lymphocytes is the *Env* spike protein [75, 78, 97, 98]. The gp140 protein (comprising gp120 and gp41 subunits) is highly immunogenic, and there is evidence from serum analysis that antibodies are raised against several of the epitopes displayed [84, 89, 90, 98]. To develop an assay suitable for highlighting cells secreting *Env*-reactive antibodies in a population, inactivated virus-like microvesicle (MV) preparations displaying gp160 [99] (HIV-1 BaL strain; courtesy of J. Lifson, Frederick National Laboratory), recombinant gp140 and gp120 proteins (HIV-1 YU2 strain; IAVI), and peptide mimetics of the gp41 membrane proximal external region (MPER; 179.4, LLELDKWASLWNWFDITNWLWY IKKKK-biotin and 57, ELLELDKWASLWNRRK-biotin; courtesy of M. Zwick, Scripps Institute) were used. Hybridoma cell lines secreting b12 (anti-HIV-1 gp120), 2F5 (anti-HIV-1 gp41) and 4D20 (anti-HA) served as control cell lines. Following the capture of secreted antibodies, the acquired microarrays were panned with a solution of antigens, then with secondary reagents to detect bound antigen. The relative affinities of captured antibodies for different antigens were obtained by comparing the ratios of background-corrected median intensities from the antigen-specific and Ig-specific channels. With thresholds set such that statistical specificities were $\geq$ 95%, statistical sensitivities were calculated to be $\geq$ 88 % for all strategies, especially with HIV-1 BaL MVs and MPER 57, where sensitivities were $\geq$ 99.9% (Figure 4.1). Specificity was also maintained when antigens were combined and used simultaneously (Figure 4.1d).

To determine the lower limit of detection for rare cells with microengraving, serial dilutions of b12-secreting cells were made in a bulk culture of 2F5-secreting cells down to a frequency of 1 b12 cell in 10,000 2F5 cells. Diluted samples were loaded onto arrays of nanowells, the original occupancy of each well was recorded with fluorescence microscopy, and microengraving was used to capture b12 and 2F5 antibodies. The resulting microarrays were probed with HIV-1 BaL MVs to pin-point locations of the less frequent b12 cells. It was estimated that rare cells at a frequency of ~0.001 % could be accurately detected (Figure 4.2). This result suggests that the limit of detection scales directly with the number of wells analyzed (~10^5 wells/chip), and cells present at lower frequencies could be identified by using multiple chips.

4.2.2. Analysis of primary B cells from an HIV-infected subject

To demonstrate the utility of this microengraving approach for the characterization of human primary B cells, PBMCs from an HIV-1 elite controller (CTR0118; courtesy of D. Kwon, Ragon Institute) were analyzed, enumerating responses from both plasmablasts/plasma cells and memory B cell populations. The immunophenotypes of B cells and the overall distribution of antibody isotypes in each population were determined (Figure 4.3). Microarrays generated were probed with monomeric HIV-1 YU2 gp140 to identify wells with B cells producing *Env*-specific antibodies, and a fraction of antigen-specific cells were recovered with the CellCelector. For this subject, no *Env*-specific events were found among actively-secreting cells (ASCs), but ~0.5% of Ig^+ events were *Env*-specific among memory B cells. Heavy and light chain genes were amplified then sequenced, and with this information, germline gene usage, mutation rates and complementarity determining region 3 (CDR3) lengths were determined using algorithms

available on IgBLAST and IMGT databases [100, 101]. Six antibodies (Table A.2, Appendix) for which paired heavy and light chain sequence data were available were cloned into human IgG1 and Igκ/Igλ expression vectors using *E. coli*, and then expressed transiently as full-length antibodies in HEK 293T cells. Dilutions of the supernatants containing expressed Ig, and a set of well-characterized control antibodies, were applied to custom protein microarrays comprising a cross-clade panel of HIV-1 antigens (Table A.3, Appendix) and an anti-Ig capture antibody (for normalization of the data) (Figure 4.4). Some of the antibodies exhibited breadth in binding for a number of gp120 variants across all clades (MIT 44, 45, 64, 65), and another exhibited preference for gp41 (MIT 78). Due to problems with cloning and expression of some antibodies, an accurate assessment of the overall false discovery rate could not be made. Nonetheless, these results demonstrate that microengraving can identify antigen-specific antibodies from human B cells, and can easily accommodate the comparative analyses of B cells from different cellular compartments.

4.3. Multiparametric characterization and comparison of ASCs in blood and GALT

Gut-associated lymphoid tissue (GALT) represents the largest reservoir of immune cells in the body and is a site of constant interaction with commensal bacteria and exogenous pathogens ingested along with food and drink [1, 95]. In HIV-1 infection, evidence exists that GALT remains an active reservoir for viral replication, even when virus is undetectable in circulation [100, 101], but the site has yet to be examined extensively with single-cell resolution to understand the effects of HIV-1 on the local humoral immune response. The ability to isolate small numbers of cells using arrays of nanowells makes this process well-suited to characterize B cells recovered from other anatomical sites such as the colon, small bowel or reproductive tracts. To study the effects of HIV infection on the humoral response in GALT, ~10^5-10^6 ASCs in the

blood, colon and small bowel (duodenum and terminal ileum) of individuals at different stages of HIV-1 infection (progressors, controllers and negatives; Table 4.1) were profiled for immunophenotypes, distributions of secreted isotypes (Figure 4.5 and Table A.4, Appendix), specificity and relative affinity to HIV-1 BaL MVs (Figures A.3 and A.4, Appendix), and for a subset of cells, the genes encoding the heavy and light chains on antibodies produced (Table A.5, Appendix).

Limiting analysis to wells with ≤ 10 viable cells (~1 B cell/well), IgG1 was observed to be the predominant isotype detected from cells in circulation, as expected [1]. Statistical analysis of the frequencies of the different isotypes examined (IgG1, IgA1/2, IgG3 and IgM), using the non-parametric Friedman test, also revealed a significant increase in the frequency of IgA secreting cells in gut tissue, relative to blood ($p \leq 0.0002$; Table 4.2), as expected [102]. Changes in the frequency of cells producing IgA, however, were most dramatic in the colon, upon progression of disease. The average frequencies of IgA^+ events enumerated for HIV-1 negative subjects, controllers and progressors were $64 \pm 32\%$, $58 \pm 21\%$ and $29 \pm 30\%$, respectively. A one-tailed Student's t-test pairwise comparison of the average frequencies (assuming unequal variances) indicated that IgA production was comparable between negatives and controllers, but significantly lower when controllers were compared to subjects with progressive disease ($p < 0.05$). The loss of IgA production is consistent with a previous observation of notable B cell dysfunction in the colon following infection by HIV [103], and this state appears to persist even after treatment with HAART. Whether or not this is a direct effect of $CD4^+$ T cell depletion in the gut is still unclear [94-96].

Analysis of heavy chain sequences from unique clones (n = 205) identifed as *Env*-specific with the Immunoglobulin Analysis Tool (IgAT) [104] using default settings revealed prevalent use of V_H3-23, D_H6-19 and J_H4 genes (Figure 4.6). The median CDR3 length estimated was 42 nucleotides (14 amino acids) with a standard deviation of ~10 nucleotides (~3 amino acids) (Figure 4.7). There was also evidence of antigenic selection during affinity maturation in 18% of the clones (α = 0.05) (Figure 4.8). Comparing V, D and J gene usage for the heavy chains of *Env*-specfic clones across compartments, differences were observed only for the dominant V_H gene segments used (Figures A.5, A.6 and A.7, Appendix). In the blood, both V_H1-69 and V_H5-51 gene segments were found to be equally prevalent in *Env*-specific antibodies. V_H3-30 and V_H3-23 were the genes present, most frequently, in *Env*-specific antibodies found in the colons and small bowels of HIV-infected subjects, respectively. Comparing the distributions of CDR3 lengths for *Env*-specific clones across each compartment using a Student's t-test, we found that the distributions were not significantly different. The median CDR3 lengths were also similar (blood – 42 nucleotides, colon – 45 nucleotides and small bowel – 42 nucleotides; Figure A.8, Appendix).

Validation of *Env*-reactive antibodies focused mostly on class-switched antibodies (non-IgM), that had long heavy chain CDR3s ($\geq$ 17 amino acids), were heavily mutated relative to germline ($\geq$ 20 nucleotide mismatches) or showed significant binding of HIV-1 BaL MV bait (backgroud corrected MFI $\geq$ 2000) in the primary screen (Table A.3, Appendix). Supernatants from transfection cultures were panned against a cross-clade panel of HIV-1 *Env* antigens on custom microarrays, and ~60% showed specificity for at least one antigen in the panel of *Env* proteins (Figure 4.9). Two antibodies (MIT 34 and 41) were also found to neutralize a few

representative tier 1 strains of HIV-1, albeit with less potency than 2G12 – a well-characterized neutralizing antibody (Figure 4.10; Table A.6, Appendix). Hiearchical clustering of binding profiles to the set of HIV-1 *Env* antigens used suggests that other antibodies (e.g. MIT 109 and 135) may have neutralizing activity (Figure 4.9b). Furthermore, there appeared to be a limited overlap of *Env*-specific clones across anatomical sites. From a comparison of mutation rates in the variable genes of recovered antibodies (Figure 4.11), there was a higher mutation rate in gut tissue, indicative of greater turnover and more activity in these sites. These observations, however, may be due to a limited sampling of the overall B cell repertoires in these compartments. To further our knowledge of differences in the B cell repertoires in these sites, complementary analysis by deep sequencing with next-generation sequencing technology and lineage analysis of identified neutralizing clones would be informative [105-108].

4.4. Discussion

In our analysis of ASCs in blood and GALT samples, we observed that a reduction in the percentage of IgA^+ events in the gut typically follows the transition from controlled infection of HIV-1 to progressive forms of disease. This reduction is most dramatic in the colon, and is accompanied by a corresponding increase in the frequency of $IgG1^+$ events in this tissue. From examination of the raw data (Table A.4, Appendix), reductions in the percentages of IgA^+ events in the colon appear to be the result of a loss of IgA-secreting plasma cells/plasmablasts in this anatomical site. IgA-secreting cells are the predominant population of B cells found in gut tissue [102], and IgA is one of the few Ig isotypes transported across mucosal membranes, enabling the neutralization of pathogenic species before permanent, irreversible colonization and infection can be established [109]. Another hypothesized function of IgA in the gut is to facilitate the

development of immune tolerance to commensal species in the gut microflora, because this isotype does not induce a significant inflammatory response when bound to antigen [102, 109, 110]. With the loss of IgA secreting cells, the gut becomes a highly inflammatory environment, suitable for replication of HIV-1 and capable of sustaining a reservoir for the virus. Our results are, therefore, reasonable, and consistent with previous observations of persistent inflammation in the guts of patients chronically infected with HIV-1 [111]. Further analyses to determine the effects of HIV-infection on humoral responses in GALT should include the examination of patterns of homing receptor expression on B cells in GALT – specifically CCR9, CCR10 and $\alpha 4\beta 7$ receptors [102] – for HIV-1 negatives, controllers and progressors, as well as patterns of expression for exhausted B cell phenotypes [112]. Frequencies of neutralizing antibodies in this anatomical compartment should also be enumerated with the aid of deep-sequencing technologies and computational analysis, to discover any HIV-induced changes.

Although the microengraving approach described here measures binding of *Env* and not neutralization, binding is a necessary condition for neutralization, and we have found neutralizing antibodies after cloning and testing only a handful of the *Env*-specific antibodies recovered. Both MIT 34 and MIT 41 have heavy chains with long CDR3s (24 amino acids) and mutations in their V_H genes relative to germline – characteristics common to all broad and potent neutralizing antibodies found to date [87-93]. Despite this similarity, MIT 34 and MIT 41 only showed efficacy at neutralizing tier 1 strains of HIV-1, suggesting that additional structural features are necessary for broad and potent neutralization of virus. Interestingly, some of the *Env*-specific antibodies recovered with microengraving possess D_H genes (D_H3-3) recently implicated in conferring neutralizing breadth and potency [113], therefore, the validation and

characterization of these and other *Env*-reactive clones may reveal other key features required for broad and potent neutralization of HIV-1 *in vivo*.

It is worth mentioning that the neutralizing monoclonal antibodies recovered were from screens with HIV-1 BaL MVs. The two HIV-specific antibodies identified with recombinant HIV-1 YU2 gp140 monomers, and tested, were non-neutralizing, despite the breadth and high apparent affinities observed against the cross-clade panel of HIV-1 antigens used. This result implies that MVs may present adequate levels of functional *Env* proteins – which is of concern with recombinant baits [114] – and may be good baits for the identification of functional HIV-specific antibodies when no prior characterization of neutralizing potency is available. We believe that most of the antibodies identified as Ig^+ MV^+ in the primary screen, but showing no specificity for any of the *Env* antigens used in secondary validation, may be specific for other membrane associated proteins incorporated during the preparation of these virus-like particles [99]. The presence of self-reactive and polyreactive antibodies in the gut [115] could also explain the levels of MV-specific responses identified in gut samples from HIV-negative individuals. Future iterations of secondary validation should include panels of self-antigens to exclusively highlight HIV-specific responses. Interrogating with combinations of wild-type and mutant HIV-1 baits, engineered to highlight conserved epitopes, should also improve the yield of functional antibodies isolated from HIV-1-infected patients.

Finally, in this study we have recovered *Env*-specific and neutralizaing antibodies in samples from HIV elite controllers. Control of HIV-1 infection is typically associated with improved T-cell functionality, and analyses of sera from such individuals suggest that humoral

immunity is not a key component for control [116]. These bulk analyses may, however, have marginalized functional responses present at low frequencies in these individuals. With the integrated approach for single B cell analysis presented here, lingering questions about the contributions of the humoral immune system to the control of HIV-infection may be answered, by allowing the direct examination of this population of cells.

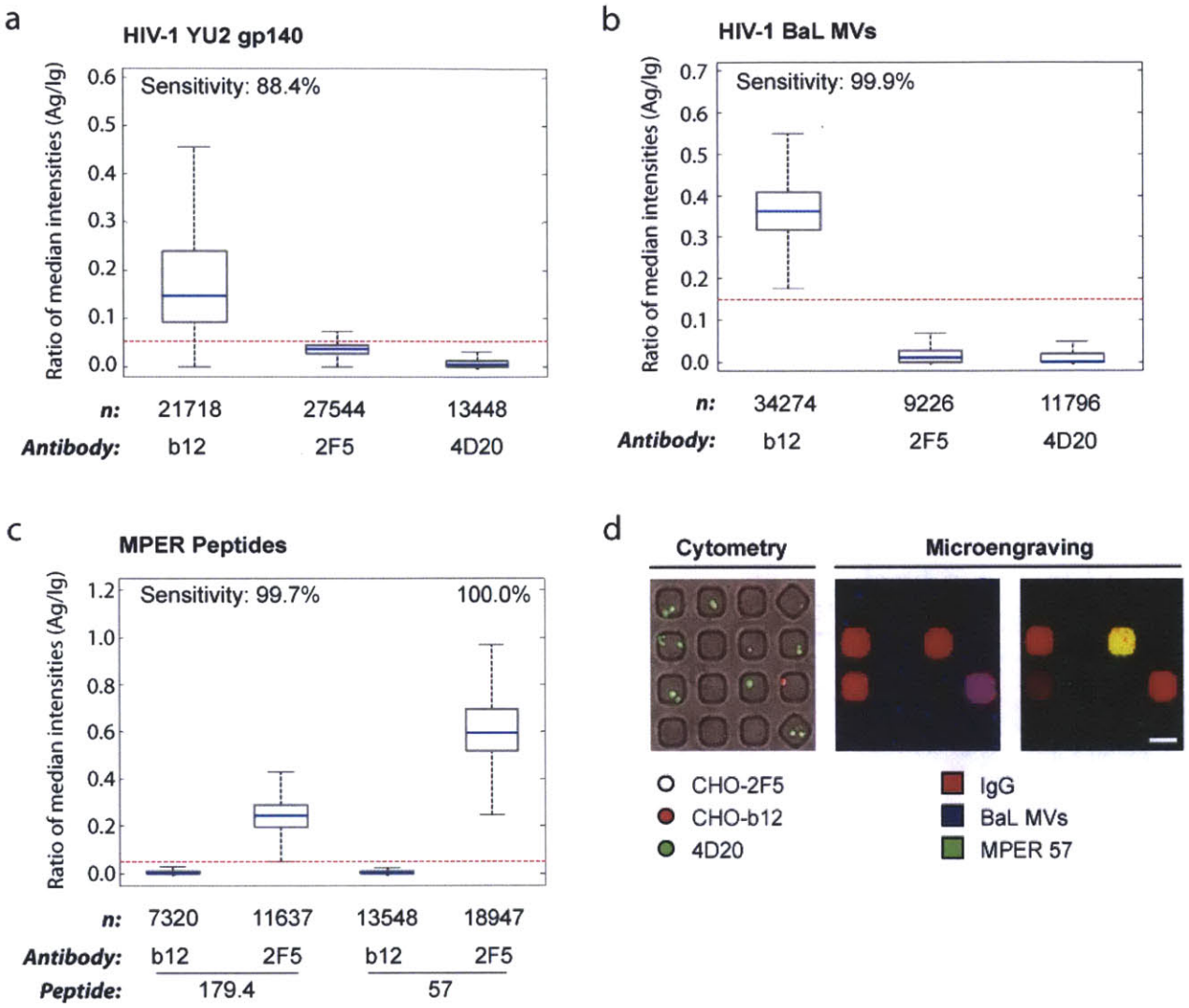

Figure 4.1: Statistical assessment of the microengraving assay with different baits.
b12-, 2F5- and 4D20-secreting cell lines were seeded into independent arrays of nanowells for microengraving, and the secreted antibodies captured on slides were probed for presence of IgG and reactivity with (a) recombinant monomeric HIV-1 YU2 gp140, (b) gp160-expressing HIV-1 BaL MVs or (c) MPER peptides (179.4 and 57). Ratios of the median intensities for antigen-specific to Ig-specific signals (Ag/Ig) for each cell line and antigen are shown as box plots. Red dashed lines represent the thresholds for evaluating sensitivities of the assay; thresholds were set such that the false positive rates were no greater than 5% for any modality. (d) Control cell lines (b12, red; 2F5, unlabeled; 4D20, green) were mixed and analyzed by microengraving. The resulting microarray was panned simultaneously with a combination of MVs (blue) and MPER 57 (green). Composite micrographs from microscopy and microarray analysis are displayed in the panel. Scale bar, 50 μm.

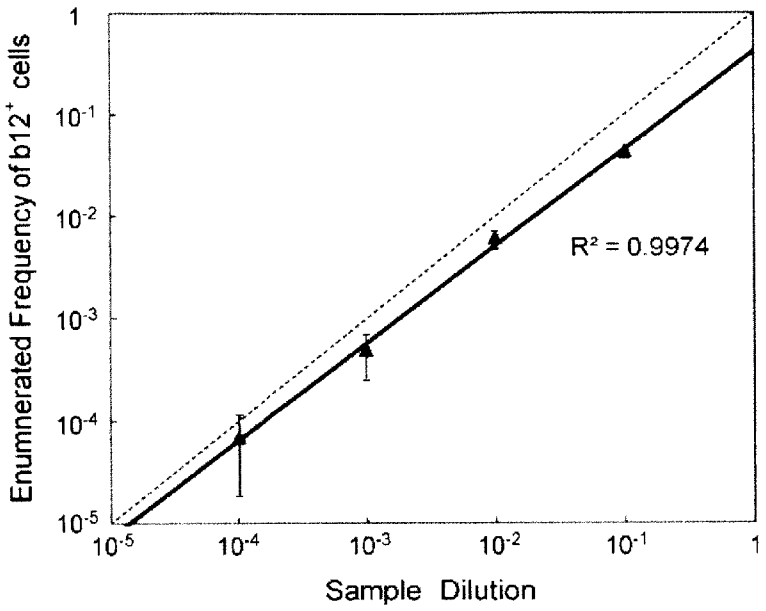

Figure 4.2: Sensitivity of the microengraving approach.
Samples with known concentrations of b12- and 2F5-secreting cells were loaded onto chips and analyzed by microengraving for binding of HIV-1 BaL MVs. Frequencies of b12 cells in the samples were calculated as the ratio of the number of Ig^+MV^+ spots with b12 cells present in the wells, and the total number of Ig^+ events.

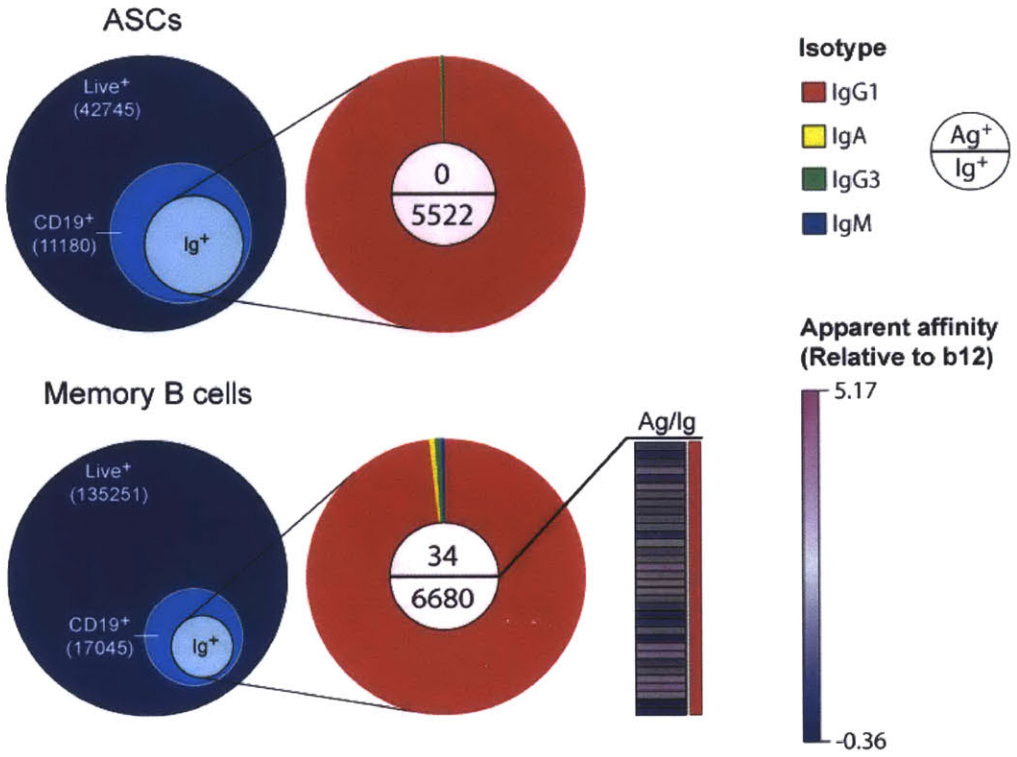

Figure 4.3: Integrated analysis of humoral responses from ASCs and memory B cells of an HIV-infected patient.

Bulk mononuclear cells from the blood were profiled for viability, surface-expressed phenotypes, isotype distribution and specificity of secreted antibodies for recombinant monomeric HIV-1 YU2 gp140. Values in Venn diagrams represent the total numbers of cells on each array of nanowells. Distributions in pie-charts include events from wells with ≤ 5 live cells (~1 B cell/well). Apparent relative affinities are presented compared to median values observed from binding of b12 from CHO cells to HIV-1 YU2 gp140.

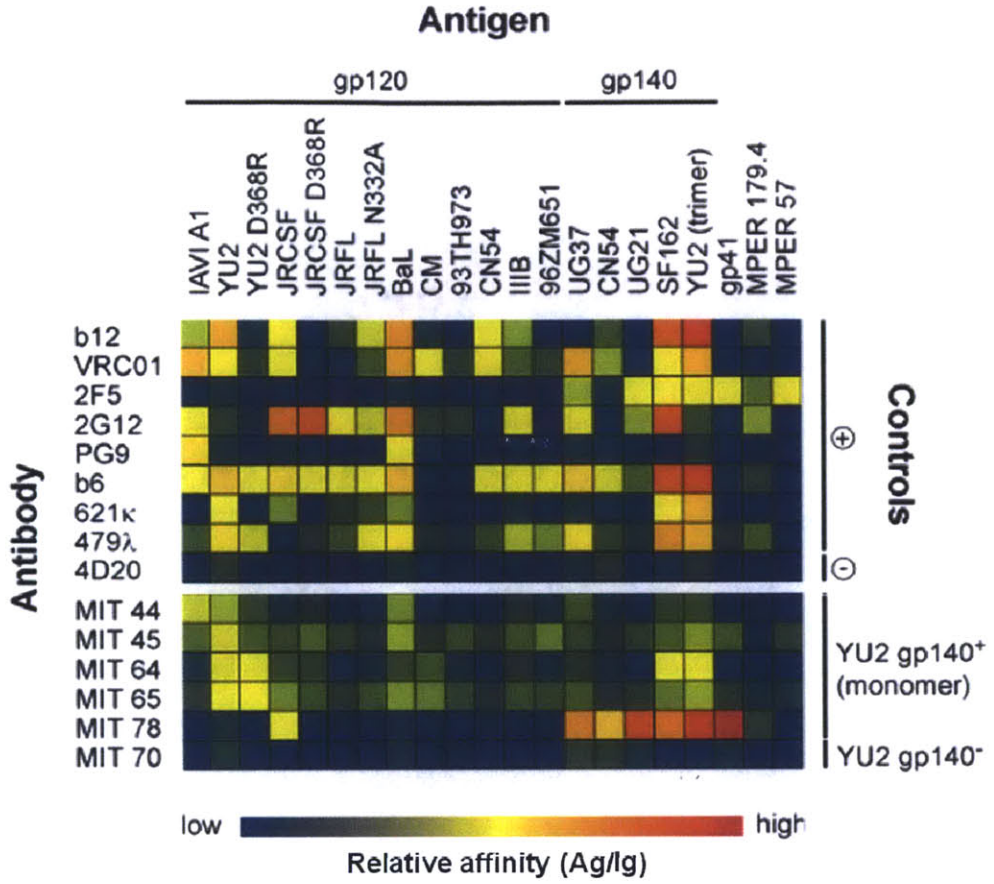

Figure 4.4: Validation of antibodies identified as HIV-1 *Env*-specific.
Supernatants from cultures of HEK 293T cells expressing recombinant antibodies from screens were collected and incubated over custom antigen microarrays, along with dilutions of control antibodies (gp120-specific: b12, VRC01, b6, PG9, 2G12, 621κ and 479λ; gp41-specific 2F5; and HA-specific 4D20). Binding to spotted antigens and anti-Ig capture species was detected with a fluorescently labeled goat anti-human Fcγ antibody (1 μg/mL, Jackson Immunoresearch). Relative affinities (Ag/Ig) of the different antibodies tested are presented as a heatmap.

Table 4.1: Clinical presentation of HIV-infected study participants

Patient ID	Gender	HIV Classification	ARV Status	Average Circulating Viral Load (copies/mL)	Average CD4+ T cell count (cells/µl)
013646A	Male	Elite Controller	Untreated	Undetectable*	785
CTR0090	Male	Elite Controller	Untreated	Undetectable	607
CR0555W	Female	Chronic Progressor	Untreated	5085	874
CTR0865	Male	Elite Controller	Untreated	Undetectable	1322
CTR0147	Male	Elite Controller	Untreated	Undetectable	1294
330183	Male	Viremic Controller	Untreated	2163	869
931995	Male	Progressing Conrtoller	Untreated	Undetectable	318
614225	Male	Chronic Progressor	Treated	Undetectable	453
604772	Male	Chronic Progressor	Untreated	5500	466
629356	Male	Chronic Progressor	Treated	2542	743
473516	Male	Elite Controller	Untreated	Undetectable	755
365685	Male	Chronic Progressor	Untreated	32120	457

*Limit of detection for assay used is $\geq$ 75 copies/mL

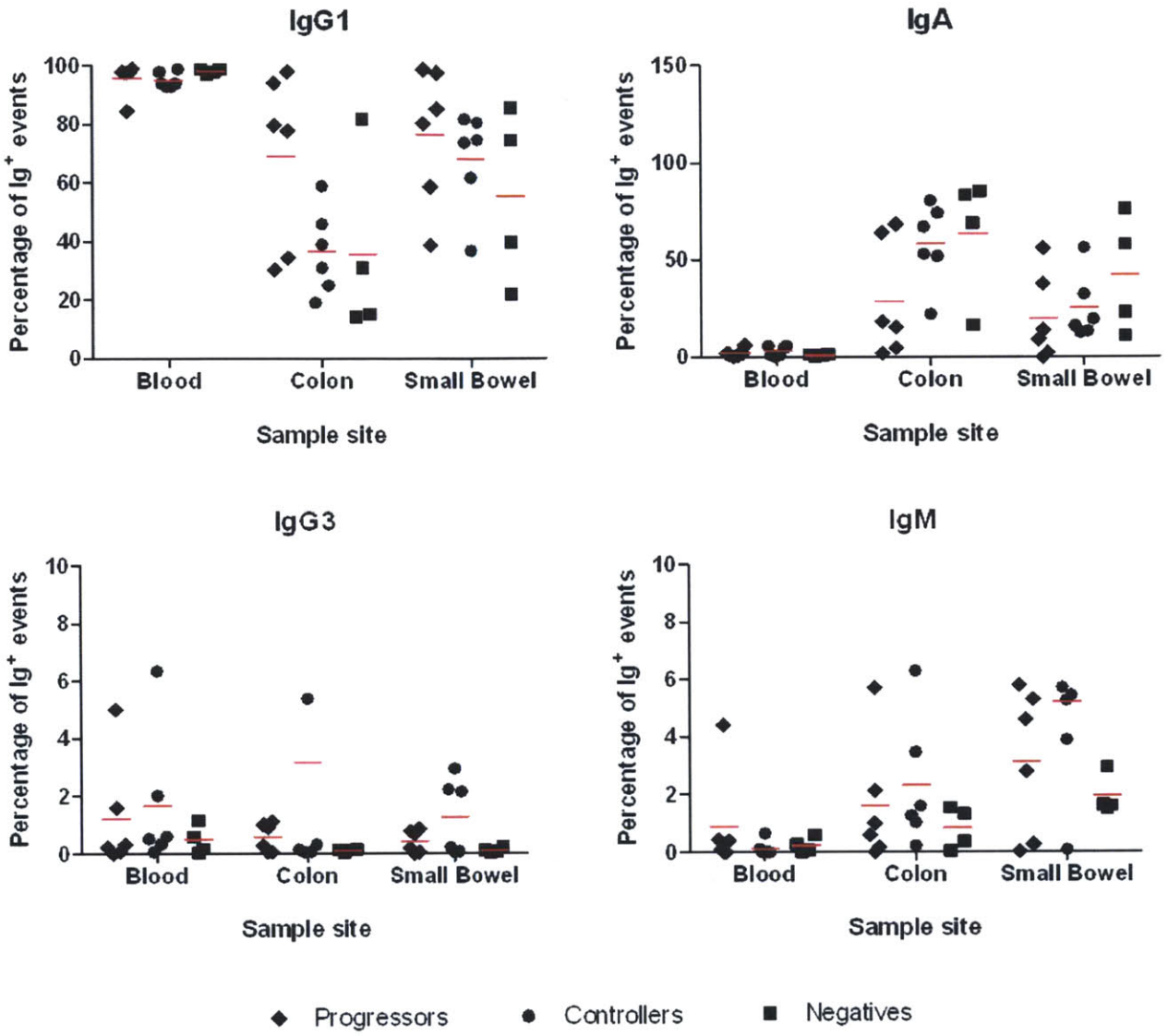

Figure 4.5: Comparison of isotype distribution of antibodies from ASCs in blood and GALT of healthy and HIV-infected patients.

ASCs in samples of PBMCs and disaggregated tissue from the colon and small bowel of HIV-1 progressors (n = 6), HIV-1 controllers (n = 6) and unifected (n = 4) individuals were processed and analyzed for secretion of IgG1, IgA, IgG3 and IgM isotypes. Analysis was limited to wells with $\leq$ 10 live (Calcein violet AM^+) cells. Comparison of responses in GALT suggests that progressor status is associated with loss of a fraction of IgA-producing population.

Table 4.2: Unadjusted comparison of isotype distributions across anatomical sites

Comparison	IgG1	IgG3	IgA	IgM
Overall	*<0.0001*	*0.7072*[†]	*<0.0001*	*0.0002*
Blood vs. Colon	<0.0001*	N.D.	<0.0001*	0.0009*
Blood vs. Bowel	0.0003*	N.D.	0.0002*	0.0004*
Colon vs. Bowel	0.0731	N.D.	0.0596	0.1129

*Significant after Bonferroni correction for multiple testing (correction within each Ig Abs)

[†] No need for pairwise comparison when the overall p-value is not significant

N.D. – Not done as overall p-value was not significant

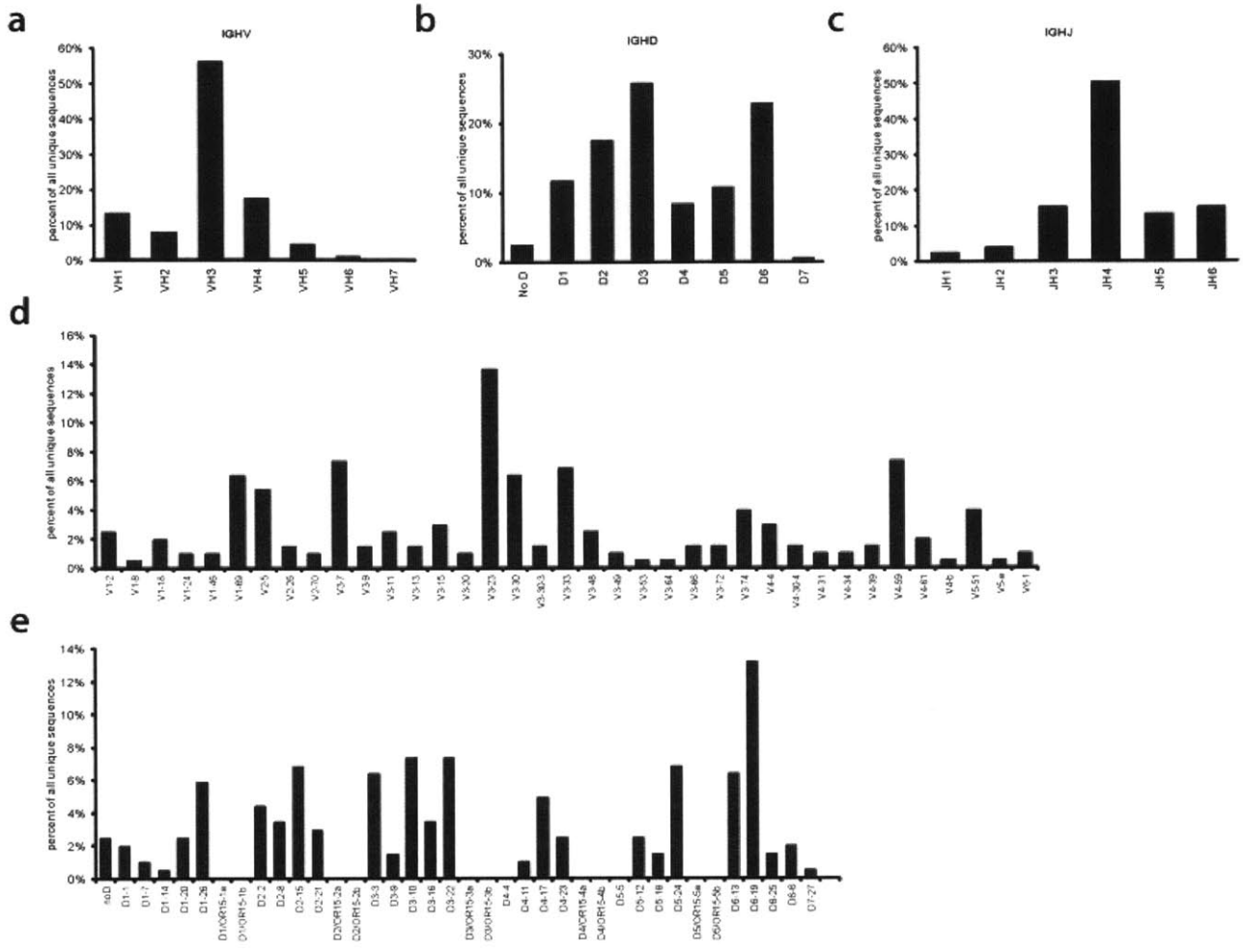

Figure 4.6: VDJ gene usage in HIV-1 *Env*-specific clones recovered from blood and GALT
Following the analysis of *Env*-specific clones with opensource software on IMGT/HighV-quest database, frequencies of the different human V (**a**,**d**), D (**b**, **e**) and J (**c**) genes rearranged into antigen-specific clones were enumerated.

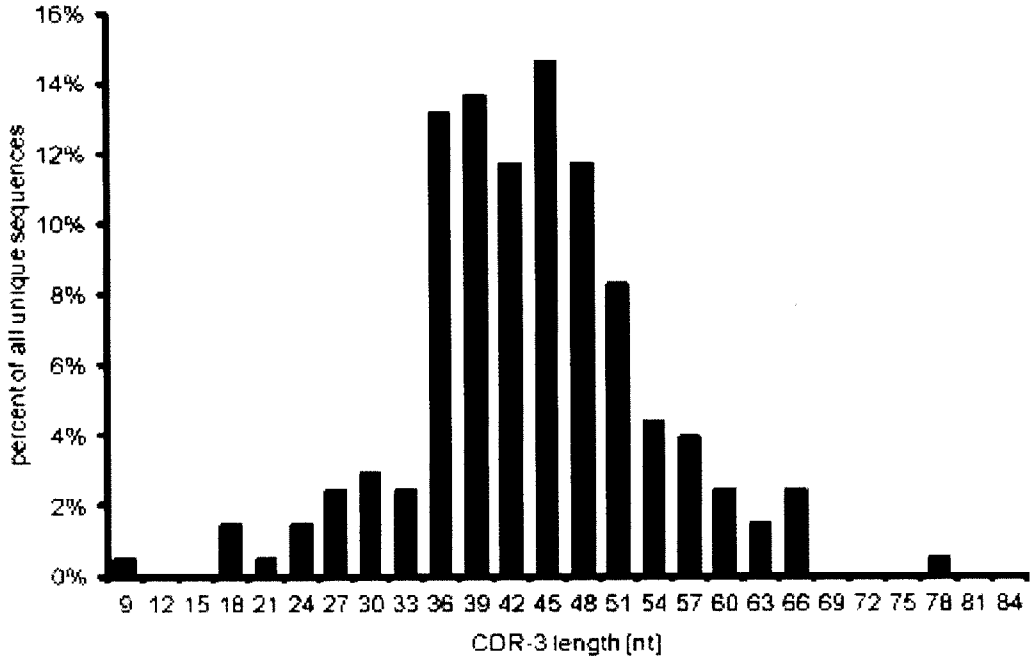

Figure 4.7: Distribution of CDR3 lengths for heavy chains of HIV-1 *Env*-specific antibodies CDR3 lengths of heavy chain sequences were compared for unique clones recovered from the blood and GALT of HIV-infected subjects analyzed. Median length was determined to be 42 nucleotides.

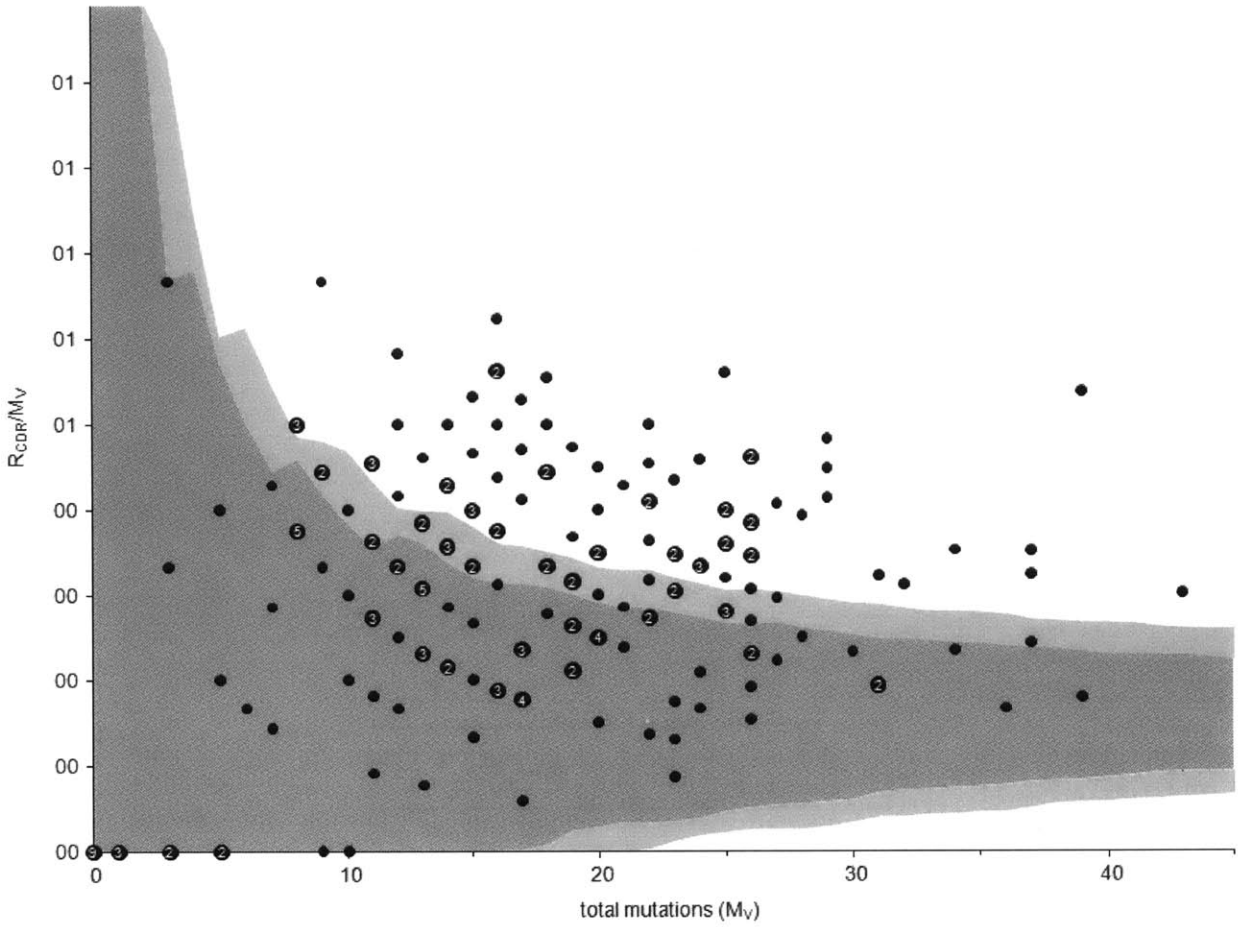

Figure 4.8: Inference of antigen selection in heavy chains of HIV-1 *Env*-specific clones
The ratio of replacement mutations in CDR-H1 and CDR-H2 (R_{CDR}) to the total number of mutations in the V region (M_V) is plotted against M_V. The light gray shaded area represents the 95% and the dark gray shaded area represents the 90% confidence limit for the probability of random mutations. A data point falling outside these confidence limits represents a sequence that has a high proportion of replacement mutations in the CDR. The probability that such a sequence has accumulated as many replacement mutations in the CDR by random mutation is $p = 0.05$. An allocation above the upper confidence limit was considered indicative of antigenic selection.

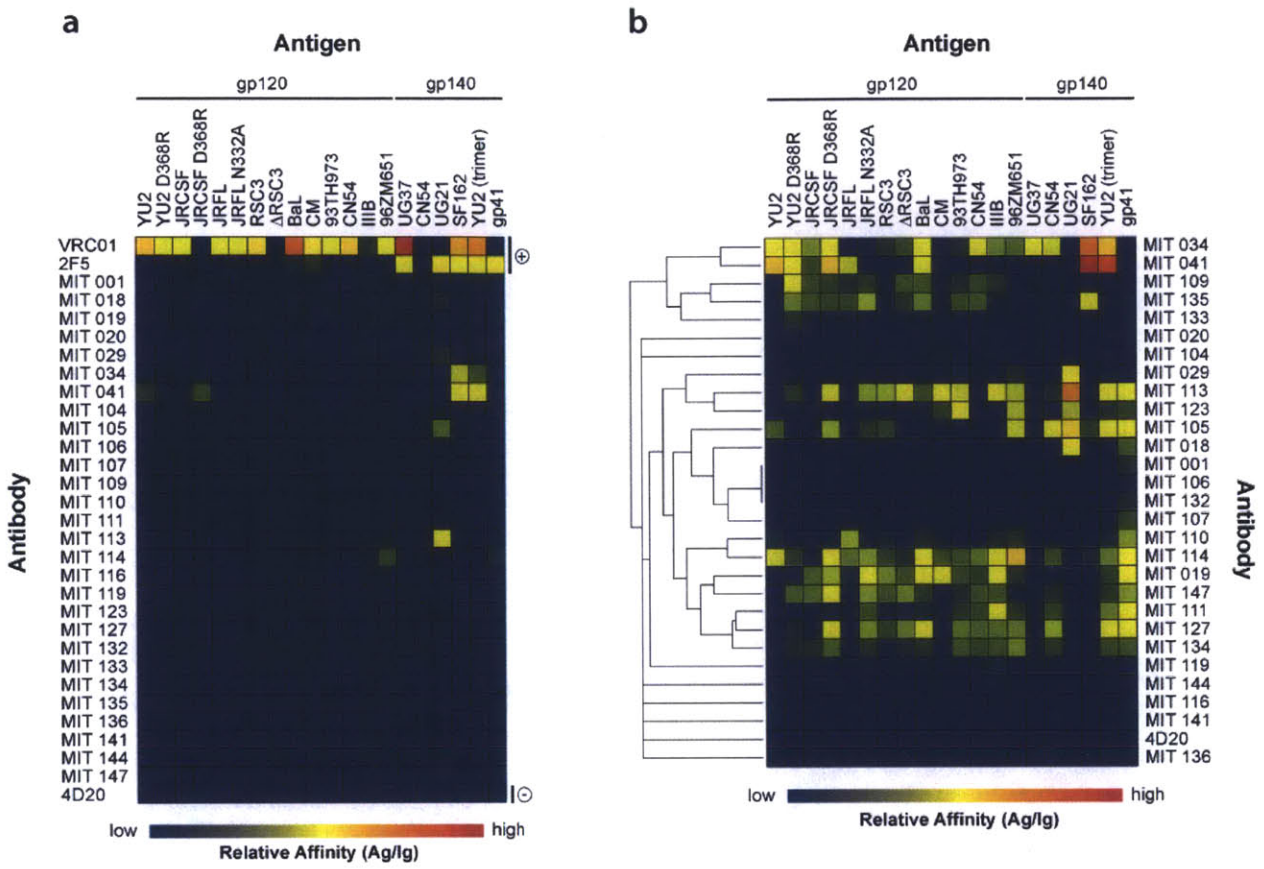

Figure 4.9: Validation of HIV-1 *Env*-specific antibodies from blood and GALT
(**a**) Supernatants from cultures of HEK 293T cells expressing antibodies recovered from screens of ASCs in blood and gut compartments with HIV-1 BaL MVs were collected and incubated over custom antigen microarrays, along with dilutions of VRC01 (gp120-specific), 2F5 (gp41-specific) and 4D20 (HA-specific). Binding to spotted antigens and anti-Ig capture species was detected with a fluorescently labeled goat anti-human Fcγ antibody. Relative affinities (Ag/Ig) of the different antibodies tested are presented as a heatmap. (**b**) Antigen binding profiles from microarray analysis were clustered using a pairwise average-linkage and Spearman's rank correlation. High affinity control antibodies were removed to highlight binding patterns of cloned antibodies. Five families of clones were identified.

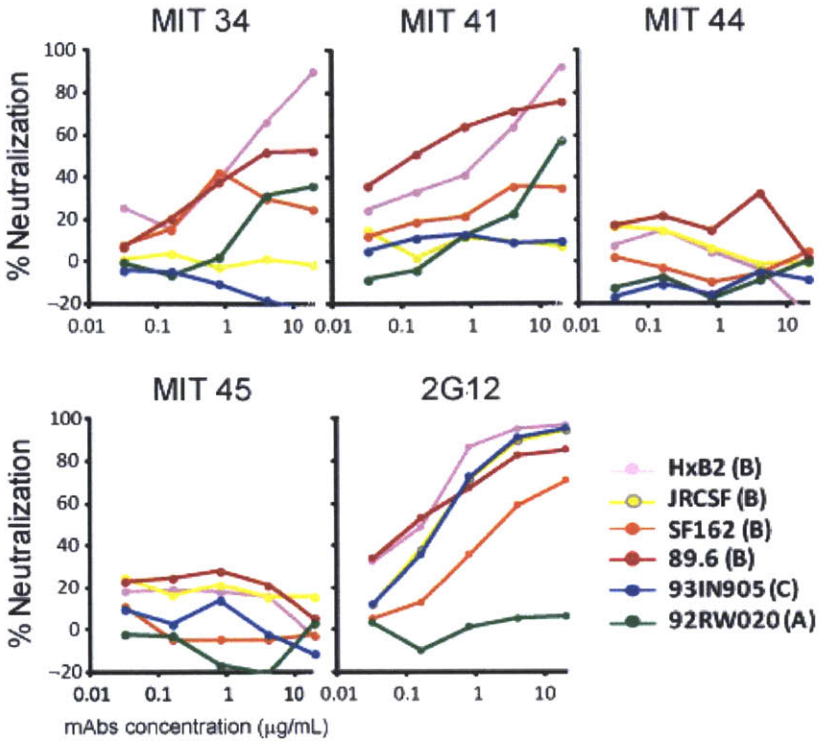

Figure 4.10: Functional characterization of validated HIV-1 *Env*-specific antibodies. Neutralizing activity was tested on a subset of validated antibodies and a known neutralizing antibody (2G12), against a panel of tier 1 and tier 2 HIV-1 strains.

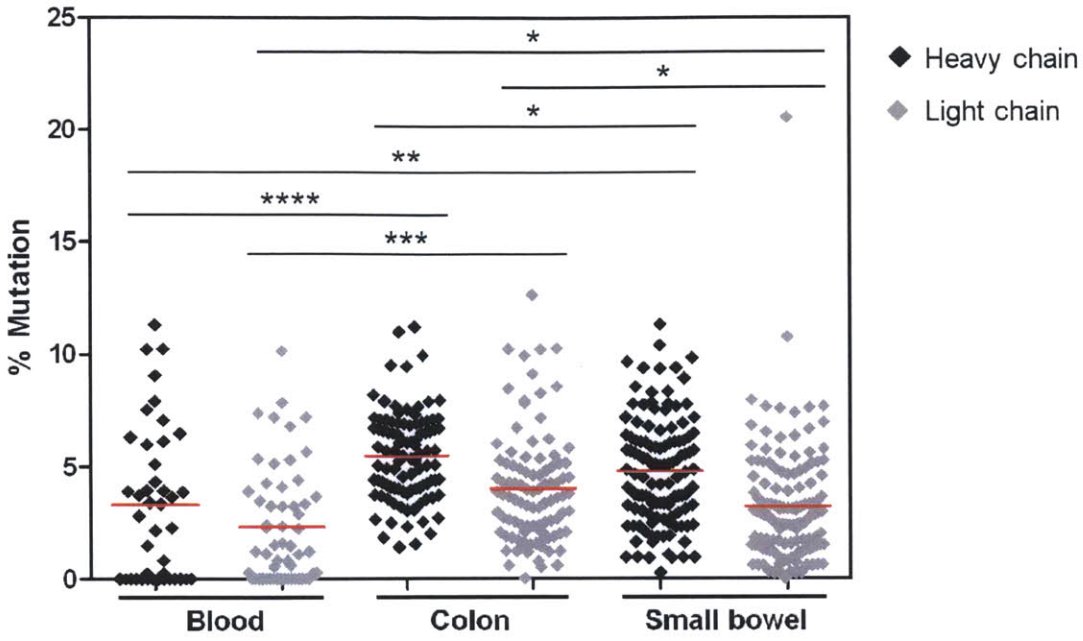

Figure 4.11: Comparison of *Env*-specifc responses in blood and GALT based on variable gene sequences.

Mutation rates in *Env*-specific antibodies recovered from HIV-infected subjects were evaluated, relative to germline gene segments, from framework region 1 (FWR1) to the end of framework region 3 (FWR3). Two-tailed Student's t-tests were used for pairwise comaparisons of mutation rates across the different sites. Statistical significance is indicated with (*) for $p > 0.05$, (**) for $p > 0.01$, (***) for $p > 0.001$ and (****) for $p > 0.0001$.

CHAPTER 5: ISOLATION OF CIRCULATING WNV-SPECIFIC B CELLS WITH MICROENGRAVING

5.1. Background

5.1.1. Overview of WNV pathogenesis

WNV is a single-stranded RNA virus in the family *Flaviviridae*, genus *Flavivirus* along with viruses such as the Yellow fever and Dengue virus. Originally identified in Uganda in the late 1930s, the virus has since spread to areas of Europe, Asia, Australia, The Middle East, North, Central and South America, reaching endemic status in some of these regions in the 2000's [117]. The virus is fairly promiscuous as it infects primarily birds, but also infects amphibians, reptiles and mammals, including humans [117]. Transmission to humans is predominantly through mosquitoes of the *Culex* species, after ingestion of a blood meal from an infected source. Other modes of transmission include through blood transfusion, organ transplantation and breast milk [118]. Symptoms of WNV infection are typically observable after 2-14 days, and range from mild flu-like symptoms to neurological disease in the form of meningitis, encephalitis or acute flaccid paralysis, and in the most severe cases, death [118]. Fortunately, however, most cases of infection are asymptomatic. The highest risk of symptomatic infection is found among elderly and immunocompromised individuals [119].

Positive sense RNA, ~11,000 bp in size, encased in an icosahedral arrangement of capsid protein is transmitted by a WNV virion. The viral genome codes for structural proteins (capsid, C; premembrane, prM; and envelope, E) and nonstructural proteins (NS1, NS2A, NS2B, NS3, NS4A, NS4B and NS5) which are required for replication and immune evasion [120]. The capsid

is entirely coated with prM, membrane (M) and E glycoproteins, which are responsible for viral diversity and tropism. As with HIV-1, the envelope protein facilitates entry of the virus into host cells. The exact populations of cells infected by WNV have not been fully established, but targets appear to include dendritic cells, macrophages, neutrophils, and neural cells [120-124]. The cell surface receptors required for viral entry are also unknown, but some C-type lectins and integrins have been implicated in mediating infection in *in vitro* studies [125-127]. Entry of WNV into host cells is by receptor-mediated endocytosis. Within the acidic environment of an endosome, conformational changes in the envelope protein result in the fusion of virions with the endosomal membrane, allowing injection of RNA into the cells. It is hypothesized that there are three stages of WNV pathogenesis: infection, amplification and neuroinvasion [120]. Following infection and spread of the virus, replication occurs in peripheral lymphoid tissues [119]. The exact mechanism of neuroinvasion is still unknown, but entry into the central nervous system allows infection of neural cells, causing neurological disease. With treatment or a vaccine, it should be possible to limit the spread and effects of WNV infection.

5.1.2. Treatment and control of WNV infection

At present, neither a cure nor treatment for WNV infection exists. Cases of symptomatic disease are typically managed with supportive care. Strategies to stem the spread of infection have focused on increasing public awareness and education, and control of mosquito vectors. Studies of the immune system following infection in humans and non-human disease models of WNV infection have revealed innate and adaptive (both cellular and humoral) immune responses that could potentially limit and/or eliminate viral replication in vivo [120, 124, 128]. Of these, the antibody response is of particular interest, given the significance of neutralizing antibodies in conferring immunity to viral pathogens. Immunization of mice and rabbits with recombinant

forms of the E protein has given rise to protective anti-WNV antibodies in these animals [129-131]. Passive immunization with antisera has also been shown to be effective at protecting against more severe manifestations of disease in animal models of infection [118, 129, 131, 132].

The E, prM and M proteins of WNV are immunogenic, with a majority of the humoral response targeting the E protein [129-131]. WNV E protein exists as a homodimer on mature viral particles [133]. There are three domains (D) of WNV E: DI, DII and DIII. Highly conserved epitopes – conserved even among other *flavivirus* species – are found in DI and DII, along with the fusion loop, required for fusion of the viral and cell membranes [133, 134]. Conserved residues are thought to remain hidden until fusion is initiated in endosomes. DIII of WNV E is relatively accessible and is involved in receptor binding that precedes endocytosis. Most WNV-specific neutralizing antibodies that have been discovered from mice and humans recognize epitopes in this domain [132, 135, 136]. The human monoclonal anti-WNV E neutralizing antibodies discovered in these studies were identified from combinatorial libraries of variable genes from convalescent individuals using phage display, raising questions about whether or not such antibodies could be generated naturally during infection. In this study, microengraving technology was used to identify WNV E-specific antibodies and to guide lineage analysis in studying the evolution of the humoral response to WNV infection.

5.2. Discovery of WNV-specific antibodies in samples from infected patients

In preliminary experiments, it was determined with polyclonal sera that direct conjugation of a recombinant, soluble, monomeric WNV E protein [131] (courtesy of R. Montgomery) to fluorophores (Alexa Fluor® dyes) blocked epitopes required for binding.

Compatible secondary antibodies for detection of bound E were also not found, hence, solution-phase presentation of antigen to captured antibodies was not ideal. Instead, poly-L-lysine slides were coated directly with E protein (50 μg/mL) diluted in borate buffer (pH 9), to mimic the direct format of an ELISA (Figure 5.1). In theory, with this approach, signal for the presence of Ig will only be detected in locations mapping to antigen-specific cells, but non-specific adsorption to protein on slides is also of concern. The false discovery rate due to non-specific adsorption was estimated to be 0.0048% of B cells ($CD19^+/CD20^+$ cells) analyzed, based on the analysis of 4D20 cells (Figure 5.2). Registration of elements on microarrays was facilitated by concurrent microcontact printing [137] of fluorescently-labeled BSA used in blocking the surface of each array of nanowells.

Samples of PBMCs from convalescent and asymptomatic individuals, ≥ 2 years post-infection, were obtained from an area where epidemic levels of disease had been experienced (Table 5.1). The presence of a WNV E-specific humoral response was first determined for each sample by immunoblot analysis of recovered patient sera [138]. Titers of neutralizing antibodies in serum were also quantified with a quantitative plaque reduction neutralization test (PRNT) to document that the humoral immune response in these patients was functional [138]. Plasma cell and memory B cell populations were screened for WNV E specificity in each sample, and cells producing functional antibodies were recovered for genetic analysis (Figure 5.2; Table A.7, Appendix). IgAT analysis of somatic hypermutations in heavy chains of E-specific clones estimated that 6.25% of unique clones recovered were selected for in the presence of antigen (Figure 5.3). Sequences from amplified genes were made available to collaborators in Kleinstein lab (Yale Medical School) to assist with lineage analysis, which may help identify families of

functionally related clones. Antibodies for which there were paired heavy and light chain variable genes were cloned and expressed in HEK293T cells (Table A.8, Appendix). Expressed monoclonal antibodies were validated for binding of WNV E on custom protein microarrays. 8 out of 11 successfully expressed antibodies showed some specificity for WNV E in this secondary validation assay (MIT 87, 89, 90, 91, 92, 93, 94, and 95) (Figure 5.4). These monoclonals were sent to the Montgomery lab (Yale Medical School) to evaluate their abilities to neutralize WNV.

5.3. Discussion

Consistent with our expectations, WNV E-specific responses were effectively absent from the circulating B cell repertoire, except in the sample from one individual. Since PBMCs were recovered from convalescent patients $\geq$ 2 years post-infection, and infection by WNV does not result in chronic disease, all antigen-specific plasma cells or plasmablast in circulation should have disappeared. Among memory B cells, the average frequency of antigen-specific memory B cells in the samples analyzed was ~0.1% of $CD19^+/CD20^+$ cells. Comparing the enumerated frequencies of E-specific antibodies in the memory B cell compartment for each patient, and the measured titers of neutralizing antibodies in their serum, we find that both variables are correlated for this limited data set ($r = 0.926$, $p = 0.037$; Pearson's correlation, one-tailed test). Interestingly, the patient with the highest titer of neutralizing antibodies and frequency of antigen-specific memory B cells was asymptomatic. It is known, however, that the presence and potency of a WNV-specific humoral immune response is uncorrelated with the severity of disease (unpublished results, Montgomery lab), hence, further attempts at finding B cells

secreting potent neutralizing antibodies for the development of vaccines must still include the analysis of samples from individuals with severe manifestations of infection by WNV.

Along with the enumeration of WNV-specific cells in different B cell repertoires, a parallel objective for this study was to facilitate the development of a pipeline for genome-wide analysis of antigen-specific B cell repertoires in infected patients. Given that < 5% of clones in the memory B cell repertoire show any significant expansion (i.e. > 0.4% of the repertoire) [56], and considering that ~10^4-10^5 useful reads are typically generated with current next-generation sequencing techniques, lineage mapping for the purpose of comprehensive repertoire analysis and the identification of functionally-related antibodies could be challenging for the set of samples collected in this pilot study. For convalescent individuals ≥ 2 years post-infection, it is likely that the frequencies of unique WNV E-specific clones in the memory B cell repertoire are < 0.1%. It is, therefore, recommended that future studies of this sort focus on the analysis of immune responses during acute stages of infections, when WNV E-specific responses would be dominant.

Overall, we have successfully demonstrated that the microengraving approach can be readily adapted for the identification of WNV E-specific antibodies. Importantly, the lessons learned from this course of investigation should inform any endeavors targeted at the discovery of novel antibodies generated naturally against WNV and other *Flaviviridae*, such as Yellow fever and Dengue.

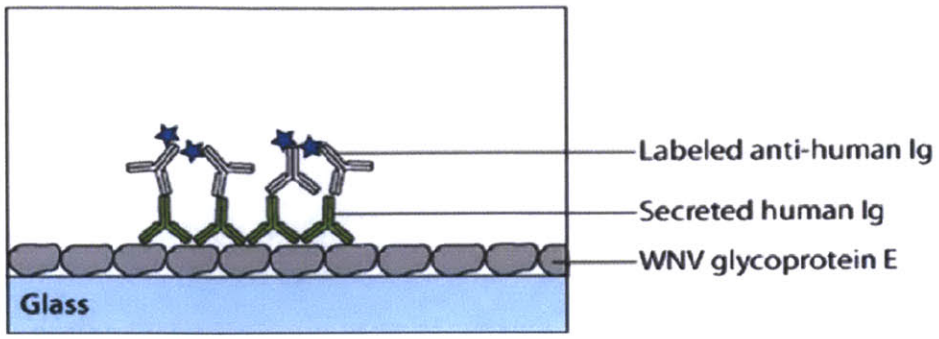

Figure 5.1: Schematic of direct format of microengraving

Table 5.1: Clinical presentation of WNV study subjects

U19_ID	Recruitment Source	Diagnosis[†]	WNV E IgG immunoblot	Serum Neutralizing titer*
100041	Texas	WNF	++	1:40
110038	Texas	WNF	++++	1:40
100032	Texas	WNM	++++	1:80
100038	Texas	Asymp	++++	1:160

[†] WNF – febrile illness, WNM – meningitis, Asymp – asymptomatic infection

* Highest dilution for which 100% neutralization was observed in PRNT

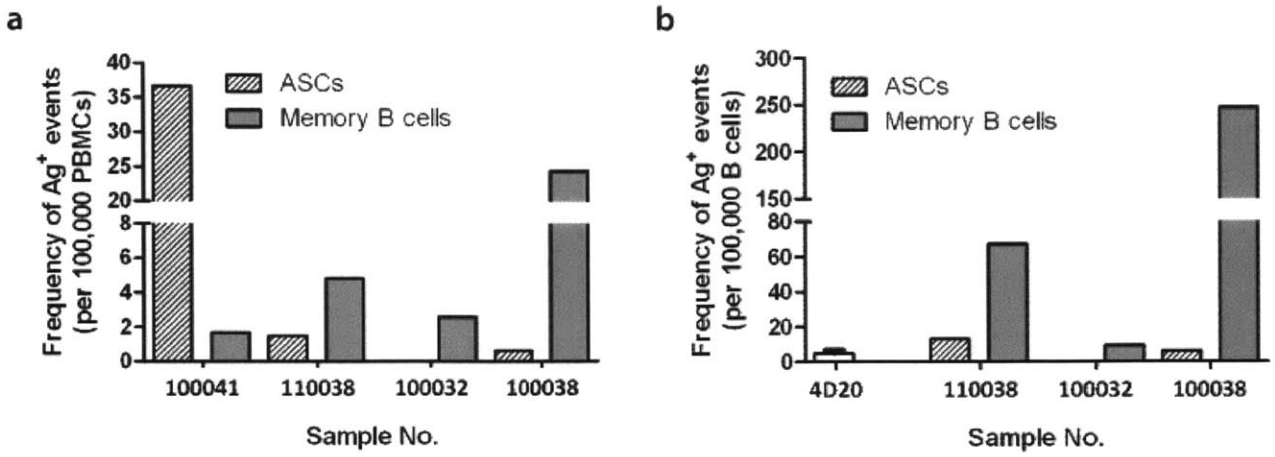

Figure 5.2: Frequencies of enumerated WNV-specific antibodies in circulation.
ASCs and activated memory cells were screened by microengraving to identify naturally selected E-specific antibodies. The data above represents the frequency of Ag^+ events (detected as bound Ig on microarrays with anti-human κ and λ secondary antibodies, each at 1 μg/mL) from wells with cells, normalized by the total number of (**a**) live (Calcein Violet AM^+) cells or (**b**) live B cells (Calcein Violet AM^+, $CD19^+/CD20^+$) screened. Additional criteria ($CV \leq 70$ and background corrected $MFI \geq 1500$) were included in analysis of microarrays with GenePix® 6.0 to reduce the number of false positives identified. Error bar represents standard error of measurement from triplicate experiments.

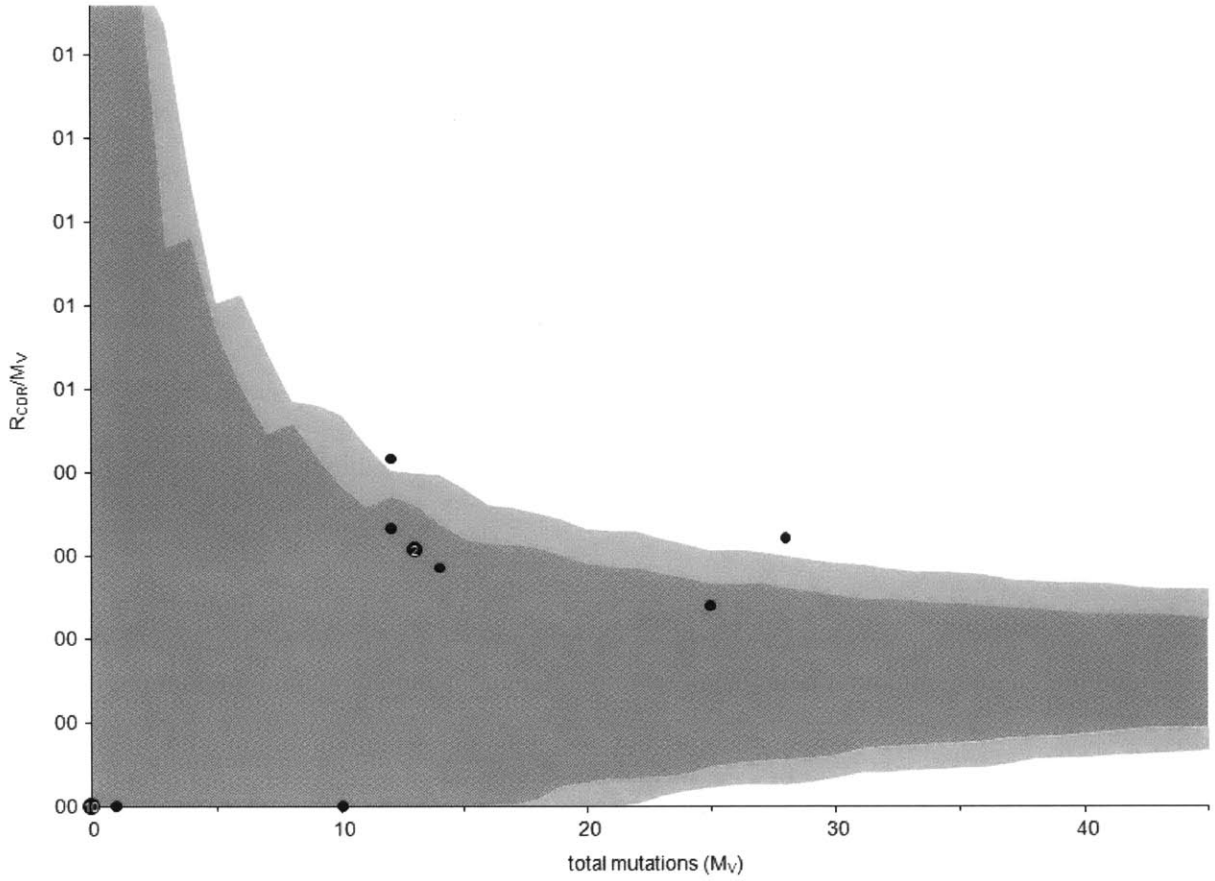

Figure 5.3: Inference of antigen selection in heavy chains of WNV E-specific clones
The ratio of replacement mutations in CDR-H1 and CDR-H2 (R_{CDR}) to the total number of mutations in the V region (M_v) is plotted against M_v. The light gray shaded area represents the 95% and the dark gray shaded area represents the 90% confidence limit for the probability of random mutations. A data point falling outside these confidence limits represents a sequence that has a high proportion of replacement mutations in the CDR. The probability that such a sequence has accumulated as many replacement mutations in the CDR by random mutation is $p = 0.05$. An allocation above the upper confidence limit was considered indicative of antigenic selection.

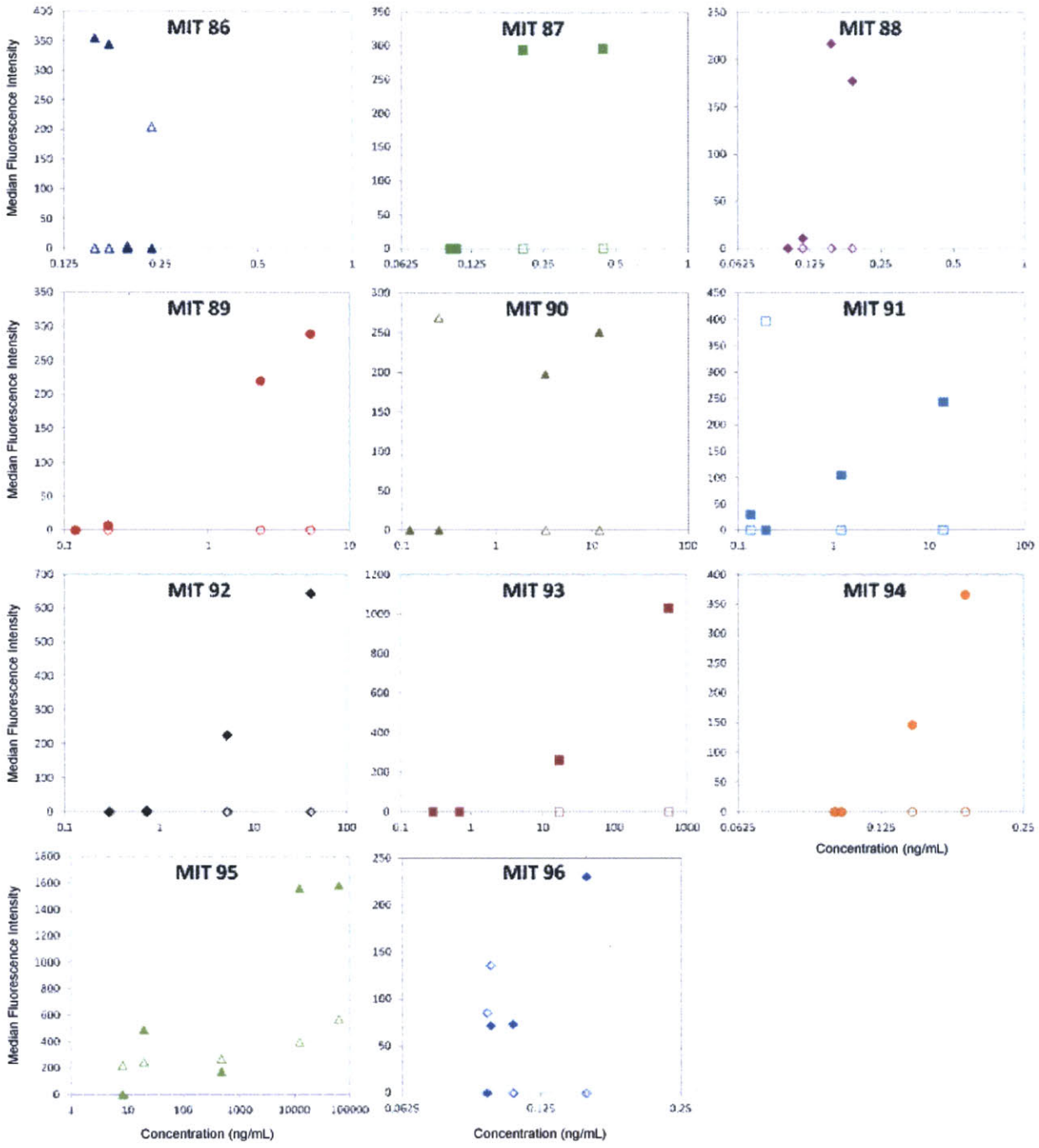

Figure 5.4: Validation of WNV E-specific monoclonal antibodies.
Microarrays with four replicate spots of anti-human Ig (H+L) (300 ng/mL), WNV E (100 µg/mL) and IAVI A1 (100 µg/mL; negative control) were used to test for WNV E specificity. Dilutions of supernatant from transfections were incubated over microarrays, and binding was detected with labeled anti-human Fcγ, κ and λ antibodies. The concentration of bound Ig in each dilution was estimated from a standard curve generated with titrations of a control human monoclonal antibody. Filled markers are for binding to WNV E. Open markers are from binding to IAVI A1.

CHAPTER 6: CONCLUSIONS

Presented in this dissertation is an integrated process for generating detailed profiles of human humoral responses that highlight characteristics of both antigen-specific B cells and their antibodies. The approach extends the capabilities of the nanowell platform beyond the characterization of mouse B cells and hybridomas [35, 36], and incorporates the ability to recover the genes encoding human antibodies of interest by single-cell RT-PCR. The combination of on-chip cytometry, microengraving, and RT-PCR yields comprehensive data on the immunophenotypes of B cells, the isotypes and relative affinities of their antibodies for particular antigens, as well as the genes of the variable regions of the antibodies. It was shown that this approach produced detailed profiles of the diversity of HIV *Env*-specific B cells present in blood and mucosal tissue, and yielded new antibodies with neutralizing activity. The technique is also adaptable and was easily modified to enable the recovery of circulating B cells producing WNV E-specific antibodies in convalescent patient samples.

The integrated process for profiling the breadth of antigen-specific human B cells has three advantages over methods relying on FACS and other microtechnologies. First, the method is well-suited to characterize primary B cells from any anatomical site from which a biopsy can be obtained. The examples shown here with cells from intestinal biopsies underscores the ability to isolate and interrogate single cells from samples when the total numbers of cells are limited ($\sim 10^5$ cells). This capability should enable detailed profiling of the cells contributing to humoral responses at sites of infection such as the reproductive tract and other lymphoid tissues. Second, compared to flow cytometry, microengraving has better sensitivity for rare cells (1-2 orders of

magnitude) and allows characterization of the specificity of antibodies from plasmablasts/plasma cells without compulsory recombinant expression. The larger surface area available for the presentation of antibodies in microengraving, also suggests that there is greater opportunity for high avidity interactions with antigen, hence, both low and high affinity antibodies are easier to detect. Third, compared to other microtechnologies demonstrated for antibody screening [33, 34], the ability to separate secreted antibodies physically from the cells producing them allows for easy multiplexed characterization and repeated analysis of the antibodies without potential damage or loss of source cells. Here it was shown that antibody microarrays produced by microengraving can be probed by inactivated virions, but other modalities of screening that use intact pathogens (e.g., fungi or bacteria) are also possible (unpublished results, J. Christopher Love), highlighting the applicability of the method for identifying antibodies of interest in other disease models.

In spite of the many advantages of the integrated approach for B cell analysis presented, there are still areas for further technical development. The prolonged period of time between the analysis of acquired microarrays and the recovery of cells of interest often results in the degradation or loss of mRNA coding for antibody genes. This delay is hypothesized as one of the reasons for the reduced amplification efficiency in certain samples. Bead-based approaches for capturing nucleic acids from cells in micron-scale confinements [139, 140] represent potential solutions to the problem, if such methods can be implemented immediately after microengraving. Additionally, the incorporation of technologies with faster rates of single-cell recovery from arrays of nanowells [141] could enable deeper analysis of antigen-specific B cell repertoires. Along with improvements in mechanistic aspects of the process, expanding on the technique to

allow the assessment of other effector functions of antibodies such as ADCC would be valuable in determining the efficacy of an immune response.

In summary, the microengraving-based approach described in this thesis provides an efficient and flexible means of assessing global and localized humoral responses to immunogenic species – which is currently a challenge with existing technology – and also provides a consistent basis for the analysis and comparison of different B cell subsets. The use of this technique for the integrated analysis of ASCs and memory B cells from primary human clinical samples should facilitate the discovery of cells producing antigen-reactive antibodies against targets such as HIV-1, WNV, autoantigens in autoimmune responses [5, 142] or immunogens used in vaccination. The routine application of this technology in the analysis of tissue and blood samples would provide, at the single-cell level, a snapshot of the antigen-specific humoral response elicited following infection or vaccination. Finally, combined with data from repertoire analysis by deep sequencing, important connections between function and prevalence of monoclonal antibodies would help further our understanding of B cell immunology in diseases like HIV/AIDS, informing the design of therapeutic and/or vaccine strategies against such elusive targets.

REFERENCES

1. Kindt, T.J., R.A. Goldsby, and B.A. Osbourne, *Kuby's Immunology.* 6 ed. 2007, New York: W.H. Freeman and Company.
2. Slifka, M.K., et al., *Humoral Immunity Due to Long-Lived Plasma Cells.* Immunity, 1998. **8**(3): p. 363-372.
3. Guan, Y., et al., *Discordant memory B cell and circulating anti-Env antibody responses in HIV-1 infection.* Proceedings of the National Academy of Sciences, 2009. **106**(10): p. 3952-3957.
4. Beerli, R.R. and C. Rader, *Mining human antibody repertoires.* MAbs, 2010. **2**(4).
5. Foreman, A.L., et al., *B cells in autoimmune diseases: Insights from analyses of immunoglobulin variable (Ig V) gene usage.* Autoimmunity Reviews, 2007. **6**(6): p. 387-401.
6. Wrammert, J., et al., *Rapid cloning of high-affinity human monoclonal antibodies against influenza virus.* Nature, 2008. **453**(7195): p. 667-671.
7. Corti, D., et al., *A Neutralizing Antibody Selected from Plasma Cells That Binds to Group 1 and Group 2 Influenza A Hemagglutinins.* Science, 2011. **333**(6044): p. 850-856.
8. Madec, A.M., et al., *Four IgG anti-islet human monoclonal antibodies isolated from a type 1 diabetes patient recognize distinct epitopes of glutamic acid decarboxylase 65 and are somatically mutated.* The Journal of Immunology, 1996. **156**(9): p. 3541-9.
9. Zwick, M.B., J.S. Gach, and D.R. Burton, *A welcome burst of human antibodies.* Nature Biotechnology, 2008. **26**(8): p. 886-887.
10. Lachmann, P.J., *The use of antibodies in the prophylaxis and treatment of infections.* Emerging Microbes and Infections, 2012. **1**: p. e11.
11. Nelson, A.L., E. Dhimolea, and J.M. Reichert, *Development trends for human monoclonal antibody therapeutics.* Nature Reviews Drug Discovery, 2010. **9**(10): p. 767-774.
12. Both, L., et al., *Monoclonal antibodies for prophylactic and therapeutic use against viral infections.* Vaccine, 2013. **31**(12): p. 1553-1559.
13. Engvall, E. and P. Perlmann, *Enzyme-linked immunosorbent assay (ELISA) quantitative assay of immunoglobulin G.* Immunochemistry, 1971. **8**(9): p. 871-874.
14. Yu, X., et al., *Neutralizing antibodies derived from the B cells of 1918 influenza pandemic survivors.* Nature, 2008. **455**(7212): p. 532-536.
15. Cao, Y., et al., *An optimized assay for the enumeration of antigen-specific memory B cells in different compartments of the human body.* Journal of Immunological Methods, 2010. **358**(1-2): p. 56-65.
16. Kyu, S.Y., et al., *Frequencies of human influenza-specific antibody secreting cells or plasmablasts post vaccination from fresh and frozen peripheral blood mononuclear cells.* Journal of Immunological Methods, 2009. **340**(1): p. 42-47.
17. Henn, A.D., et al., *Modulation of Single-Cell IgG Secretion Frequency and Rates in Human Memory B Cells by CpG DNA, CD40L, IL-21, and Cell Division.* The Journal of Immunology, 2009. **183**(5): p. 3177-3187.

18. Scheid, J.F., et al., *A method for identification of HIV gp140 binding memory B cells in human blood.* Journal of Immunological Methods, 2009. **343**(2): p. 65-67.
19. Traggiai, E., et al., *An efficient method to make human monoclonal antibodies from memory B cells: potent neutralization of SARS coronavirus.* Nature Medicine, 2004. **10**(8): p. 871-875.
20. Reddy, S.T., et al., *Monoclonal antibodies isolated without screening by analyzing the variable-gene repertoire of plasma cells.* Nature Biotechnology, 2010. **28**(9): p. 965-969.
21. Liao, H.-X., et al., *High-throughput isolation of immunoglobulin genes from single human B cells and expression as monoclonal antibodies.* Journal of Virological Methods, 2009. **158**(1-2): p. 171-179.
22. Czerkinsky, C., et al., *A novel two colour ELISPOT assay: I. Simultaneous detection of distinct types of antibody-secreting cells.* Journal of Immunological Methods, 1988. **115**(1): p. 31-37.
23. Kesa, G., et al., *Comparison of ELISpot and FluoroSpot in the Analysis of Swine Flu-Specific IgG and IgA Secretion by in Vivo Activated Human B Cells.* Cells, 2012. **1**(2): p. 27-34.
24. De Rosa, S.C., J.M. Brenchley, and M. Roederer, *Beyond six colors: A new era in flow cytometry.* Nature Medicine, 2003. **9**(1): p. 112-117.
25. Perfetto, S.P., P.K. Chattopadhyay, and M. Roederer, *Seventeen-colour flow cytometry: unravelling the immune system.* Nature Reviews Immunology, 2004. **4**(8): p. 648-655.
26. Feldhaus, M.J., et al., *Flow-cytometric isolation of human antibodies from a nonimmune Saccharomyces cerevisiae surface display library.* Nature Biotechnology, 2003. **21**(2): p. 163-170.
27. Mazor, Y., et al., *Isolation of engineered, full-length antibodies from libraries expressed in Escherichia coli.* Nature Biotechnology, 2007. **25**(5): p. 563-565.
28. Bowers, P.M., et al., *Coupling mammalian cell surface display with somatic hypermutation for the discovery and maturation of human antibodies.* Proceedings of the National Academy of Sciences, 2011. **108**(51): p. 20455-20460.
29. Beerli, R.R., et al., *Isolation of human monoclonal antibodies by mammalian cell display.* Proceedings of the National Academy of Sciences, 2008. **105**(38): p. 14336-14341.
30. Smith, K., et al., *Rapid generation of fully human monoclonal antibodies specific to a vaccinating antigen.* Nature Protocols, 2009. **4**(3): p. 372-384.
31. Vollers, S.S. and L.J. Stern, *Class II major histocompatibility complex tetramer staining: progress, problems, and prospects.* Immunology, 2008. **123**(3): p. 305-313.
32. de Tute, R.M., et al., *A single-tube six-colour flow cytometry screening assay for the detection of minimal residual disease in myeloma.* Leukemia, 2007. **21**(9): p. 2046-2049.
33. Debs, B.E., et al., *Functional single-cell hybridoma screening using droplet-based microfluidics.* Proceedings of the National Academy of Sciences, 2012. **109**(29): p. 11570-11575.
34. Jin, A., et al., *A rapid and efficient single-cell manipulation method for screening antigen-specific antibody-secreting cells from human peripheral blood.* Nature Medicine, 2009. **15**(9): p. 1088-1092.
35. Story, C.M., et al., *Profiling antibody responses by multiparametric analysis of primary B cells.* Proceedings of the National Academy of Sciences, 2008. **105**(46): p. 17902-17907.

36. Love, J.C., et al., *A microengraving method for rapid selection of single cells producing antigen-specific antibodies.* Nature Biotechnology, 2006. **24**(6): p. 703-707.
37. Saff, D. and D. Sacilotto, *Printmaking: History and Process*. 1978, New York: Holt, Rinehart and Winston.
38. Han, Q., et al., *Multidimensional analysis of the frequencies and rates of cytokine secretion from single cells by quantitative microengraving.* Lab on a Chip, 2010. **10**(11): p. 1391-400.
39. Love, K.R., et al., *Integrated single-cell analysis shows Pichia pastoris secretes protein stochastically.* Biotechnology and Bioengineering, 2010. **106**(2): p. 319-325.
40. Love, K.R., et al., *Systematic Single-Cell Analysis of Pichia pastoris Reveals Secretory Capacity Limits Productivity.* PLoS ONE, 2012. 7(6): p. e37915.
41. Bradshaw, E.M., et al., *Concurrent detection of secreted products from human lymphocytes by microengraving: antigen-reactive antibodies and cytokines.* Clinical Immunology, 2008. **129**: p. 10-18.
42. The International HIV Controllers Study, *The Major Genetic Determinants of HIV-1 Control Affect HLA Class I Peptide Presentation.* Science, 2010. **330**(6010): p. 1551-1557.
43. Shacklett, B.L., J.W. Critchfield, and D. Lemongello, *Isolating mucosal lymphocytes from biopsy tissue for cellular immunology assays.* Methods in Molecular Biology, 2009. **485**: p. 347-356.
44. Galli, G., et al., *Adjuvanted H5N1 vaccine induces early CD4+ T cell response that predicts long-term persistence of protective antibody levels.* Proceedings of the National Academy of Sciences, 2009. **106**(10): p. 3877-3882.
45. Bryant, V.L., et al., *Cytokine-Mediated Regulation of Human B Cell Differentiation into Ig-Secreting Cells: Predominant Role of IL-21 Produced by CXCR5+ T Follicular Helper Cells.* The Journal of Immunology, 2007. **179**(12): p. 8180-8190.
46. Mora, J.R., et al., *Generation of Gut-Homing IgA-Secreting B Cells by Intestinal Dendritic Cells.* Science, 2006. **314**(5802): p. 1157-1160.
47. Weitkamp, J.-H., et al., *Generation of recombinant human monoclonal antibodies to rotavirus from single antigen-specific B cells selected with fluorescent virus-like particles.* Journal of Immunological Methods, 2003. **275**(1-2): p. 223-237.
48. Ettinger, R., et al., *IL-21 Induces Differentiation of Human Naive and Memory B Cells into Antibody-Secreting Plasma Cells.* The Journal of Immunology, 2005. **175**(12): p. 7867-7879.
49. Bernasconi, N.L., E. Traggiai, and A. Lanzavecchia, *Maintenance of Serological Memory by Polyclonal Activation of Human Memory B Cells.* Science, 2002. **298**(5601): p. 2199-2202.
50. Pinna, D., et al., *Clonal dissection of the human memory B-cell repertoire following infection and vaccination.* European Journal of Immunology, 2009. **39**(5): p. 1260-1270.
51. Huggins, J., et al., *CpG DNA activation and plasma-cell differentiation of CD27- naive human B cells.* Blood, 2007. **109**(4): p. 1611-1619.
52. Ogunniyi, A.O., et al., *Screening individual hybridomas by microengraving to discover monoclonal antibodies.* Nature Protocols, 2009. **4**(5): p. 767-782.
53. Tiller, T., et al., *Efficient generation of monoclonal antibodies from single human B cells by single cell RT-PCR and expression vector cloning.* Journal of Immunological Methods, 2008. **329**(1-2): p. 112-124.

54. Hendershot, L.M. and R. Sitia, *Molecular Biology of B Cells*, ed. T. Honjo, F. Alt, and M. Neuberger. 2003, London: Elsevier Science Ltd.
55. Perez-Andres, M., et al., *Human peripheral blood B-cell compartments: A crossroad in B-cell traffic.* Cytometry Part B: Clinical Cytometry, 2010. **78B**(S1): p. S47-S60.
56. Wu, Y.-C., et al., *High-throughput immunoglobulin repertoire analysis distinguishes between human IgM memory and switched memory B-cell populations.* Blood, 2010. **116**(7): p. 1070-1078.
57. Levesque, M.C., et al., *Polyclonal B Cell Differentiation and Loss of Gastrointestinal Tract Germinal Centers in the Earliest Stages of HIV-1 Infection.* PLoS Medicine, 2009. **6**(7): p. e1000107.
58. Simmons, C.P., et al., *Prophylactic and therapeutic efficacy of human monoclonal antibodies against H5N1 influenza.* PLoS Medicine, 2007. **4**(5): p. e178.
59. Tosato, G. and J.I. Cohen, *Generation of Epstein-Barr Virus (EBV)–Immortalized B Cell Lines*, in *Current Protocols in Immunology*. 2001, John Wiley & Sons, Inc.
60. Srivastava, N., et al., *Fully Integrated Microfluidic Platform Enabling Automated Phosphoprofiling of Macrophage Response.* Analytical Chemistry, 2009. **81**(9): p. 3261-3269.
61. Varadarajan, N., et al., *Rapid, efficient functional characterization and recovery of HIV-specific human CD8+ T cells using microengraving.* Proceedings of the National Academy of Sciences, 2012.
62. Choi, J.H., et al., *Development and optimization of a process for automated recovery of single cells identified by microengraving.* Biotechnology Progress, 2010. **26**(3): p. 888-895.
63. Wang, X. and B.D. Stollar, *Human immunoglobulin variable region gene analysis by single cell RT-PCR.* Journal of Immunological Methods, 2000. **244**(1-2): p. 217-225.
64. Bradshaw, E.M., et al., *A Local Antigen-Driven Humoral Response Is Present in the Inflammatory Myopathies.* The Journal of Immunology, 2007. **178**(1): p. 547-556.
65. Han, Q., et al., *Polyfunctional responses by human T cells result from sequential release of cytokines.* Proceedings of the National Academy of Sciences, 2012. **109**(5): p. 1607-1612.
66. Choi, J., et al., *Immuno-Hybridization Chain Reaction for Enhancing Detection of Individual Cytokine-Secreting Human Peripheral Mononuclear Cells.* Analytical Chemistry, 2011. **83**(17): p. 6890-6895.
67. Kurdistani, S.K. and M. Grunstein, *In vivo protein-protein and protein-DNA crosslinking for genomewide binding microarray.* Methods, 2003. **31**(1): p. 90-95.
68. Zeng, P.Y., et al., *In vivo dual cross-linking for identification of indirect DNA-associated proteins by chromatin immunoprecipitation.* Biotechniques, 2006. **41**(6): p. 694, 696, 698.
69. Franz, B., et al., *Ex vivo characterization and isolation of rare memory B cells with antigen tetramers.* Blood, 2011.
70. Kwakkenbos, M.J., et al., *Generation of stable monoclonal antibody-producing B cell receptor-positive human memory B cells by genetic programming.* Nature Medicine, 2010. **16**(1): p. 123-128.
71. in *AIDS epidemic update: December 2007*. 2007, Joint United Nations Programme on HIV/AIDS and World Health Organization.
72. Simon, V., D.D. Ho, and Q. Abdool Karim, *HIV/AIDS epidemiology, pathogenesis, prevention, and treatment.* The Lancet, 2006. **368**(9534): p. 489-504.

73. Richman, D.D., et al., *The Challenge of Finding a Cure for HIV Infection.* Science, 2009. **323**(5919): p. 1304-1307.
74. Huber, M., W.C. Olson, and A. Trkola, *Antibodies for HIV Treatment and Prevention: Window of Opportunity?*, in *Human Antibody Therapeutics for Viral Disease* D. S.K., Editor. 2008, Springer Berlin Heidelberg.
75. Karlsson Hedestam, G.B., et al., *The challenges of eliciting neutralizing antibodies to HIV-1 and to influenza virus.* Nature Reviews Microbiology, 2008. **6**(2): p. 143-155.
76. Fauci, A.S., *HIV and AIDS: 20 years of science.* Nat Med, 2003. **9**(7): p. 839-43.
77. Barouch, D.H., *Challenges in the development of an HIV-1 vaccine.* Nature, 2008. **455**(7213): p. 613-619.
78. Walker, B.D. and D.R. Burton, *Toward an AIDS vaccine.* Science, 2008. **320**(5877): p. 760-764.
79. Shedlock, D.J., G. Silvestri, and D.B. Weiner, *Monkeying around with HIV vaccines: using rhesus macaques to define 'gatekeepers' for clinical trials.* Nature Reviews Immunology, 2009. **9**(10): p. 717-728.
80. Genesca , M. and C. Miller, *Use of Nonhuman Primate Models to Develop Mucosal AIDS Vaccines.* Current HIV/AIDS Reports, 2010. **7**(1): p. 19-27.
81. Steinbrook, R., *One Step Forward, Two Steps Back - Will There Ever Be an AIDS Vaccine?* New England Journal of Medicine, 2007. **357**(26): p. 2653-2655.
82. Scheid, J.F., et al., *Broad diversity of neutralizing antibodies isolated from memory B cells in HIV-infected individuals.* Nature, 2009.
83. Devito, C., et al., *Mucosal and Plasma IgA from HIV-1-Exposed Uninfected Individuals Inhibit HIV-1 Transcytosis Across Human Epithelial Cells.* The Journal of Immunology, 2000. **165**(9): p. 5170-5176.
84. McMichael, A.J., et al., *The immune response during acute HIV-1 infection: clues for vaccine development.* Nature Reviews Immunology, 2010. **10**(1): p. 11-23.
85. Euler, Z., et al., *Cross-Reactive Neutralizing Humoral Immunity Does Not Protect from HIV Type 1 Disease Progression.* Journal of Infectious Diseases, 2010. **201**(7): p. 1045-1053.
86. Burton, D.R., R.L. Stanfield, and I.A. Wilson, *Antibody vs. HIV in a clash of evolutionary titans.* Proceedings of the National Academy of Sciences, 2005. **102**(42): p. 14943-14948.
87. Walker, L.M., et al., *Broad and Potent Neutralizing Antibodies from an African Donor Reveal a New HIV-1 Vaccine Target.* Science, 2009. **326**(5950): p. 285-289.
88. Scheid, J.F., et al., *Broad diversity of neutralizing antibodies isolated from memory B cells in HIV-infected individuals.* Nature, 2009. **458**(7238): p. 636-640.
89. Walker, L.M., et al., *Broad neutralization coverage of HIV by multiple highly potent antibodies.* Nature, 2011. **477**(7365): p. 466-470.
90. Walker, L.M., et al., *A Limited Number of Antibody Specificities Mediate Broad and Potent Serum Neutralization in Selected HIV-1 Infected Individuals.* PLoS Pathogens, 2010. **6**(8): p. e1001028.
91. Zhou, T., et al., *Structural Basis for Broad and Potent Neutralization of HIV-1 by Antibody VRC01.* Science, 2010. **329**(5993): p. 811-817.
92. Burton, D.R., et al., *HIV vaccine design and the neutralizing antibody problem.* Nature Immunology, 2004. **5**(3): p. 233-236.

93. Burton, D.R., et al., *Broadly Neutralizing Antibodies Present New Prospects to Counter Highly Antigenically Diverse Viruses.* Science, 2012. **337**(6091): p. 183-186.
94. Brenchley, J.M. and D.C. Douek, *HIV infection and the gastrointestinal immune system.* Mucosal Immunology, 2008. **1**(1): p. 23-30.
95. Mehandru, S., *The Gastrointestinal Tract in HIV-1 Infection: Questions, Answers, and More Questions!* The PRN Notebook, 2007. **12**: p. 1-10.
96. Veazey, R.S. and A.A. Lackner, *Impact of Antiretroviral Therapy on Intestinal Lymphoid Tissues in HIV Infection.* PLoS Medicine, 2006. **3**(12): p. e515.
97. Pancera, M. and R. Wyatt, *Selective recognition of oligomeric HIV-1 primary isolate envelope glycoproteins by potently neutralizing ligands requires efficient precursor cleavage.* Virology, 2005. **332**(1): p. 145-156.
98. Koefoed, K., et al., *Molecular characterization of the circulating anti-HIV-1 gp120-specific B cell repertoire using antibody phage display libraries generated from pre-selected HIV-1 gp120 binding PBLs.* Journal of Immunological Methods, 2005. **297**(1-2): p. 187-201.
99. Chertova, E., et al., *Envelope Glycoprotein Incorporation, Not Shedding of Surface Envelope Glycoprotein (gp120/SU), Is the Primary Determinant of SU Content of Purified Human Immunodeficiency Virus Type 1 and Simian Immunodeficiency Virus.* Journal of Virology, 2002. **76**(11): p. 5315-5325.
100. Altschul, S.F., et al., *Gapped BLAST and PSI-BLAST: a new generation of protein database search programs.* Nucleic Acids Research, 1997. **25**(17): p. 3389-3402.
101. Brochet, X., M.-P. Lefranc, and V.r. Giudicelli, *IMGT/V-QUEST: the highly customized and integrated system for IG and TR standardized V-J and V-D-J sequence analysis.* Nucleic Acids Research, 2008. **36**(suppl 2): p. W503-W508.
102. Cerutti, A. and M. Rescigno, *The Biology of Intestinal Immunoglobulin A Responses.* Immunity, 2008. **28**(6): p. 740-750.
103. Scamurra, R.W., et al., *Mucosal Plasma Cell Repertoire During HIV-1 Infection.* The Journal of Immunology, 2002. **169**(7): p. 4008-4016.
104. Rogosch, T., et al., *IgAT (Immunoglobulin Analysis Tool): A novel tool for the analysis of human and mouse heavy and light chain transcripts.* Frontiers in Immunology, 2012. **3**.
105. Wu, X., et al., *Focused Evolution of HIV-1 Neutralizing Antibodies Revealed by Structures and Deep Sequencing.* Science, 2011. **333**(6049): p. 1593-1602.
106. Hershberg, U., et al., *Improved methods for detecting selection by mutation analysis of Ig V region sequences.* International Immunology, 2008. **20**(5): p. 683-694.
107. Uduman, M., et al., *Detecting selection in immunoglobulin sequences.* Nucleic Acids Research, 2011.
108. Jiang, N., et al., *Lineage Structure of the Human Antibody Repertoire in Response to Influenza Vaccination.* Science Translational Medicine, 2013. **5**(171): p. 171ra19.
109. Hapfelmeier, S., et al., *Reversible Microbial Colonization of Germ-Free Mice Reveals the Dynamics of IgA Immune Responses.* Science, 2010. **328**(5986): p. 1705-1709.
110. Cerutti, A., *IgA Changes the Rules of Memory.* Science, 2010. **328**(5986): p. 1646-1647.
111. Sankaran, S., et al., *Gut mucosal T cell responses and gene expression correlate with protection against disease in long-term HIV-1-infected nonprogressors.* Proceedings of the National Academy of Sciences of the United States of America, 2005. **102**(28): p. 9860-9865.

112. Moir, S., et al., *Evidence for HIV-associated B cell exhaustion in a dysfunctional memory B cell compartment in HIV-infected viremic individuals.* The Journal of Experimental Medicine, 2008. **205**(8): p. 1797-1805.
113. Briney, B.S., J.R. Willis, and J.E. Crowe, Jr., *Human Peripheral Blood Antibodies with Long HCDR3s Are Established Primarily at Original Recombination Using a Limited Subset of Germline Genes.* PLoS ONE, 2012. **7**(5): p. e36750.
114. Poignard, P., et al., *Heterogeneity of Envelope Molecules Expressed on Primary Human Immunodeficiency Virus Type 1 Particles as Probed by the Binding of Neutralizing and Nonneutralizing Antibodies.* Journal of Virology, 2003. **77**(1): p. 353-365.
115. Benckert, J., et al., *The majority of intestinal IgA+ and IgG+ plasmablasts in the human gut are antigen-specific.* The Journal of Clinical Investigation, 2011. **121**(5): p. 1946-1955.
116. Deeks, S.G. and B.D. Walker, *Human Immunodeficiency Virus Controllers: Mechanisms of Durable Virus Control in the Absence of Antiretroviral Therapy.* Immunity, 2007. **27**(3): p. 406-416.
117. Kramer, L.D., L.M. Styer, and G.D. Ebel, *A Global Perspective on the Epidemiology of West Nile Virus.* Annual Review of Entomology, 2008. **53**(1): p. 61-81.
118. Kramer, L.D., J. Li, and P.-Y. Shi, *West Nile virus.* The Lancet Neurology, 2007. **6**(2): p. 171-181.
119. Campbell, G.L., et al., *West Nile virus.* The Lancet Infectious Diseases, 2002. **2**(9): p. 519-529.
120. Suthar, M.S., M.S. Diamond, and M. Gale Jr, *West Nile virus infection and immunity.* Nature Reviews Microbiology, 2013. **11**(2): p. 115-128.
121. Ye, C., et al., *Silencing Early Viral Replication in Macrophages and Dendritic Cells Effectively Suppresses Flavivirus Encephalitis.* PLoS ONE, 2011. **6**(3): p. e17889.
122. Bai, F., et al., *A Paradoxical Role for Neutrophils in the Pathogenesis of West Nile Virus.* Journal of Infectious Diseases, 2010. **202**(12): p. 1804-1812.
123. Diniz, J.A., et al., *West Nile virus infection of primary mouse neuronal and neuroglial cells: the role of astrocytes in chronic infection.* The American Journal of Tropical Medicine and Hygiene, 2006. **75**(4): p. 691-6.
124. Suthar, M.S., et al., *IPS-1 Is Essential for the Control of West Nile Virus Infection and Immunity.* PLoS Pathogens, 2010. **6**(2): p. e1000757.
125. Chu, J.J.-h. and M.-L. Ng, *Interaction of West Nile Virus with alpha-v-beta-3 Integrin Mediates Virus Entry into Cells.* Journal of Biological Chemistry, 2004. **279**(52): p. 54533-54541.
126. Davis, C.W., et al., *West Nile Virus Discriminates between DC-SIGN and DC-SIGNR for Cellular Attachment and Infection.* Journal of Virology, 2006. **80**(3): p. 1290-1301.
127. Martina, B.E.E., et al., *DC-SIGN enhances infection of cells with glycosylated West Nile virus in vitro and virus replication in human dendritic cells induces production of IFN-alpha and TNF-alpha.* Virus Research, 2008. **135**(1): p. 64-71.
128. Diamond, M.S., *Virus and Host Determinants of West Nile Virus Pathogenesis.* PLoS Pathogens, 2009. **5**(6): p. e1000452.
129. Wang, T., et al., *Immunization of mice against West Nile virus with recombinant envelope protein.* Journal of Immunological Methods, 2001. **167**(9): p. 5273-7.
130. Wang, T., et al., *West Nile virus envelope protein: role in diagnosis and immunity.* Annals of the New York Academy of Sciences, 2001. **951**: p. 325-7.

131. Ledizet, M., et al., *A recombinant envelope protein vaccine against West Nile virus.* Vaccine, 2005. **23**(30): p. 3915-3924.
132. Gould, L.H., et al., *Protective and Therapeutic Capacity of Human Single-Chain Fv-Fc Fusion Proteins against West Nile Virus.* Journal of Virology, 2005. **79**(23): p. 14606-14613.
133. Nybakken, G.E., et al., *Crystal Structure of the West Nile Virus Envelope Glycoprotein.* Journal of Virology, 2006. **80**(23): p. 11467-11474.
134. Kanai, R., et al., *Crystal Structure of West Nile Virus Envelope Glycoprotein Reveals Viral Surface Epitopes.* Journal of Virology, 2006. **80**(22): p. 11000-11008.
135. Oliphant, T., et al., *Development of a humanized monoclonal antibody with therapeutic potential against West Nile virus.* Nature Medicine, 2005. **11**(5): p. 522-530.
136. Vogt, M.R., et al., *Human Monoclonal Antibodies against West Nile Virus Induced by Natural Infection Neutralize at a Postattachment Step.* Journal of Virology, 2009. **83**(13): p. 6494-6507.
137. Kaufmann, T. and B.J. Ravoo, *Stamps, inks and substrates: polymers in microcontact printing.* Polymer Chemistry, 2010. **1**(4): p. 371-387.
138. Sultana, H., et al., *Fusion Loop Peptide of the West Nile Virus Envelope Protein Is Essential for Pathogenesis and Is Recognized by a Therapeutic Cross-Reactive Human Monoclonal Antibody.* The Journal of Immunology, 2009. **183**(1): p. 650-660.
139. DeKosky, B.J., et al., *High-throughput sequencing of the paired human immunoglobulin heavy and light chain repertoire.* Nature Biotechnology, 2013. **31**(2): p. 166-169.
140. Zeng, Y., et al., *High-Performance Single Cell Genetic Analysis Using Microfluidic Emulsion Generator Arrays.* Analytical Chemistry, 2010. **82**(8): p. 3183-3190.
141. Kovac, J.R. and J. Voldman, *Intuitive, image-based cell sorting using optofluidic cell sorting.* Analytical Chemistry, 2007. **79**(24): p. 9321-9330.
142. Yanaba, K., et al., *B-lymphocyte contributions to human autoimmune disease.* Immunological Reviews, 2008. **223**(1): p. 284-299.

APPENDIX

Table A.1: Primers for amplification and cloning of heavy and light chain variable genes

Primer Name	5'-3' Sequence	Direction	Chain	Use
VHL-1	TCACCATGGACTGSACCTGGA	Forward	Heavy	PCR I
VHL-2	CCATGGACACACTTTGYTCCAC	Forward	Heavy	PCR I
VHL-3	TCACCATGGAGTTTGGGCTGAGC	Forward	Heavy	PCR I
VHL-4	AGAACATGAAACAYCTGTGGTTCTT	Forward	Heavy	PCR I
VHL-5	ATGGGGTCAACCGCCATCCT	Forward	Heavy	PCR I
VHL-6	ACAATGTCTGTCTCCTTCCTCAT	Forward	Heavy	PCR I
VkappaL-1	GCTCAGCTCCTGGGGCTCCTG	Forward	Light	PCR I
VkappaL-2	CTGGGGCTGCTAATGCTCTGG	Forward	Light	PCR I
VkappaL-3	TTCCTCCTGCTACTCTGGCTC	Forward	Light	PCR I
VkappaL-4	CAGACCCAGGTCTTCATTTCT	Forward	Light	PCR I
VlambdaL-1	CCTCTCCTCCTCACCCTCCT	Forward	Light	PCR I
VlambdaL-2	CTCCTCACTCAGGGCACA	Forward	Light	PCR I
VlambdaL-3	ATGGCCTGGAYCSCTCTCC	Forward	Light	PCR I
C-mu II	CAGGAGACGAGGGGGAAAAG	Reverse	Heavy	PCR I
C-gammaII	GCCAGGGGGAAGACSGATG	Reverse	Heavy	PCR I
IgA-PCRI	GCTCAGCGGGAAGACCTT	Reverse	Heavy	PCR I
C-kappaII	TTTCAACTGCTCATCAGATGGCGG	Reverse	Light	PCR I
C-lambdaII	AGCTCCTCAGAGGAGGGYGG	Reverse	Light	PCR I
VH-1	CAGGTSCAGCTGGTRCAGTC	Forward	Heavy	PCR II, Sequencing
VH-2	CAGRTCACCTTGAAGGAGTC	Forward	Heavy	PCR II, Sequencing
VH-3	SAGGTGCAGCTGGTGGAGTC	Forward	Heavy	PCR II, Sequencing
VH-4	CAGGTGCAGCTGCAGGAGTC	Forward	Heavy	PCR II, Sequencing
VH-5	GARGTGCAGCTGGTGCAGTC	Forward	Heavy	PCR II, Sequencing
VH-6	CAGGTACAGCTGCAGCAGTC	Forward	Heavy	PCR II, Sequencing
Vkappa-1	CGMCATCCRGWTGACCCAGT	Forward	Light	PCR II, Sequencing
Vkappa-2	CGATRTTGTGATGACYCAG	Forward	Light	PCR II, Sequencing
Vkappa-3	CGAAATWGTGWTGACRCAGTCT	Forward	Light	PCR II, Sequencing
Vkappa-4	CGACATCGTGATGACCCAGT	Forward	Light	PCR II, Sequencing
Vlambda-1	CCAGTCTGTGCTGACTCAGC	Forward	Light	PCR II, Sequencing
Vlambda-2	CCAGTCTGCCCTGACTCAGC	Forward	Light	PCR II, Sequencing
Vlambda-3	CTCCTATGAGCTGACWCAGC	Forward	Light	PCR II, Sequencing
C-mu III	GAAAAGGGTTGGGGCGGATGC	Reverse	Heavy	PCR II, Sequencing
C-gammaIII	GACSGATGGGCCCTTGGTGGA	Reverse	Heavy	PCR II, Sequencing
IgA-PCRII	GACCTTGGGGCTGGTCGGGGA	Reverse	Heavy	PCR II, Sequencing
C-kappaIII	AAGATGAAGACAGATGGTGC	Reverse	Light	PCR II, Sequencing
C-lambdaIII	GGGAACAGAGTGACCG	Reverse	Light	PCR II, Sequencing
5' AgeI VH1	CTGCAACCGGTGTACATTCCCAGGTGCAGCTGGTGCAG	Forward	Heavy	Cloning
5' AgeI VH1/5	CTGCAACCGGTGTACATTCCGAGGTGCAGCTGGTGCAG	Forward	Heavy	Cloning
5' AgeI VH3	CTGCAACCGGTGTACATTCTGAGGTGCAGCTGGTGGAG	Forward	Heavy	Cloning
5' AgeI VH3–23	CTGCAACCGGTGTACATTCTGAGGTGCAGCTGTTGGAG	Forward	Heavy	Cloning
5' AgeI VH4	CTGCAACCGGTGTACATTCCCAGGTGCAGCTGCAGGAG	Forward	Heavy	Cloning
5' AgeI VH 4–34	CTGCAACCGGTGTACATTCCCAGGTGCAGCTACAGCAGTG	Forward	Heavy	Cloning
5' AgeI VH 1–18	CTGCAACCGGTGTACATTCCCAGGTTCAGCTGGTGCAG	Forward	Heavy	Cloning
5' AgeI VH 1–24	CTGCAACCGGTGTACATTCCCAGGTCCAGCTGGTACAG	Forward	Heavy	Cloning
5' AgeI VH3–33	CTGCAACCGGTGTACATTCTCAGGTGCAGCTGGTGGAG	Forward	Heavy	Cloning

5′ AgeI VH 3–9	CTGCAACCGGTGTACATTCTGAAGTGCAGCTGGTGGAG	Forward	Heavy	Cloning
5′ AgeI VH4–39	CTGCAACCGGTGTACATTCCCAGCTGCAGCTGCAGGAG	Forward	Heavy	Cloning
5′ AgeI VH 6–1	CTGCAACCGGTGTACATTCCCAGGTACAGCTGCAGCAG	Forward	Heavy	Cloning
5′ AgeI Vκ 1–5	CTGCAACCGGTGTACATTCTGACATCCAGATGACCCAGTC	Forward	Kappa	Cloning
5′ AgeI Vκ 1–9	TTGTGCTGCAACCGGTGTACATTCAGACATCCAGTTGACCCAGTCT	Forward	Kappa	Cloning
5′ AgeI Vκ 1D–43	CTGCAACCGGTGTACATTGTGCCATCCGGATGACCCAGTC	Forward	Kappa	Cloning
5′ AgeI Vκ 2–24	CTGCAACCGGTGTACATGGGGATATTGTGATGACCCAGAC	Forward	Kappa	Cloning
5′ AgeI Vκ 2–28	CTGCAACCGGTGTACATGGGGATATTGTGATGACTCAGTC	Forward	Kappa	Cloning
5′ AgeI Vκ 2–30	CTGCAACCGGTGTACATGGGGATGTTGTGATGACTCAGTC	Forward	Kappa	Cloning
5′ Age Vκ 3–11	TTGTGCTGCAACCGGTGTACATTCAGAAATTGTGTTGACACAGTC	Forward	Kappa	Cloning
5′ Age Vκ 3–15	CTGCAACCGGTGTACATTCAGAAATAGTGATGACGCAGTC	Forward	Kappa	Cloning
5′ Age Vκ 3–20	TTGTGCTGCAACCGGTGTACATTCAGAAATTGTGTTGACGCAGTCT	Forward	Kappa	Cloning
5′ Age Vκ 4–1	CTGCAACCGGTGTACATTCGGACATCGTGATGACCCAGTC	Forward	Kappa	Cloning
5′ AgeI Vλ 1	CTGCTACCGGTTCCTGGGCCCAGTCTGTGCTGACKCAG	Forward	Lambda	Cloning
5′ AgeI Vλ 2	CTGCTACCGGTTCCTGGGCCCAGTCTGCCCTGACTCAG	Forward	Lambda	Cloning
5′ AgeI Vλ 3	CTGCTACCGGTTCTGTGACCTCCTATGAGCTGACWCAG	Forward	Lambda	Cloning
5′ AgeI Vλ 4/5	CTGCTACCGGTTCTCTCTCSCAGCYTGTGCTGACTCA	Forward	Lambda	Cloning
5′ AgeI Vλ 6	CTGCTACCGGTTCTTGGGCCAATTTTATGCTGACTCAG	Forward	Lambda	Cloning
3′ SalI JH 1/2/4/5	TGCGAAGTCGACGCTGAGGAGACGGTGACCAG	Reverse	Heavy	Cloning
3′ SalI JH 3	TGCGAAGTCGACGCTGAAGAGACGGTGACCATTG	Reverse	Heavy	Cloning
3′ SalI JH 6	TGCGAAGTCGACGCTGAGGAGACGGTGACCGTG	Reverse	Heavy	Cloning
3′ BsiWI Jκ 1-4	GCCACCGTACGTTTGATYTCCACCTTGGTC	Reverse	Kappa	Cloning
3′ BsiWI Jκ 2	GCCACCGTACGTTTGATCTCCAGCTTGGTC	Reverse	Kappa	Cloning
3′ BsiWI Jκ 3	GCCACCGTACGTTTGATATCCACTTTGGTC	Reverse	Kappa	Cloning
3′ BsiWI Jκ 5	GCCACCGTACGTTTAATCTCCAGTCGTGTC	Reverse	Kappa	Cloning
3′ XhoI Cλ	CTCCTCACTCGAGGGYGGGAACAGAGTG	Reverse	Lambda	Cloning
3IgVs-PCR-fwd	CACTTTGCCTTTCTCTCCACAGGT	Forward	All	Colony PCR
3IgVs-PCR-rev	ACAGATGGTTCTTTCCGCCTCAGA	Reverse	All	Colony PCR

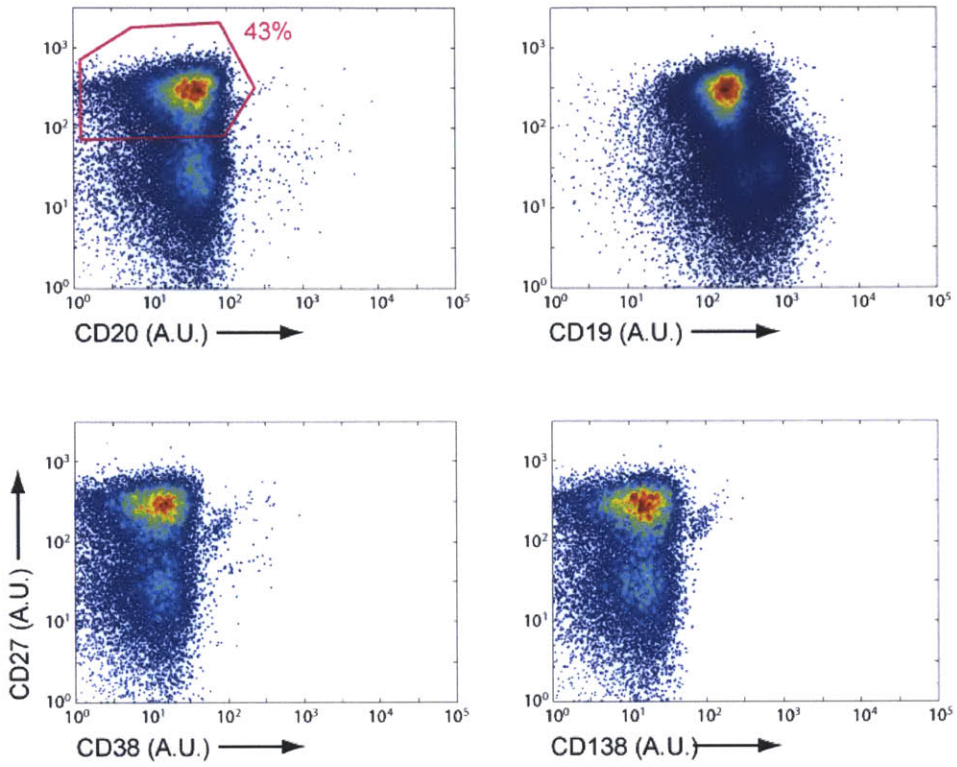

Figure A.1: Validation of anti-CD27 antibody in cytometry panel.
PBMCs from a healthy donor were stained for viability with Calcein violet AM, and for expression of CD27 only. Labeled cells were loaded onto an array of nanowells and imaged by epifluoresence microscopy in all fluorescent channels typically used for human B cell immunophenotyping. Density plots of the signal recorded in each channel after gating for viable cells are shown.

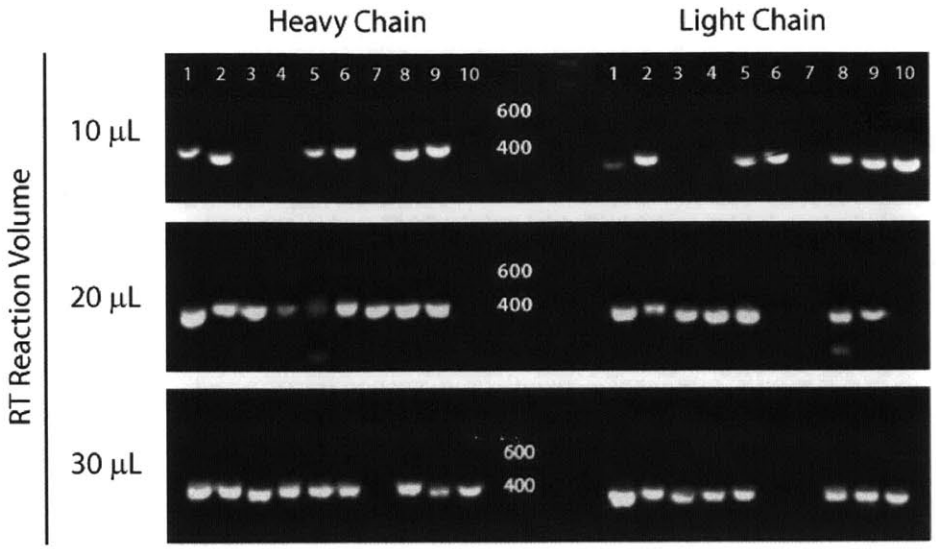

Figure A.2: Effect of buffer volume on variable gene amplification efficiency
CD19+ B cells (n = 30) sorted into 10 µL of 1× First strand buffer were obtained courtesy of Dr. Elizabeth Bradshaw, BWH. To 10 wells an additional 10 µL of 1× First strand buffer was added, and to another 10 wells, 20 µL of 1× First strand buffer was added before running RT-PCR protocol. Comparable amplification efficiency was observed even when using larger volumes of buffer for RT reaction.

Table A.2: Germline gene usage of validated HIV-1 Env-specific clones

Clone No.	Patient ID	Tissue Site	V Region	D Region	J Region	Mutation Rate (%)‡	CDR3	V Region	J Region	Mutation Rate (%)‡	CDR3
MIT 001	013646A	COLP	IGHV4-30-4*01	IGHD5-24*01	IGHJ5*02	4.1	CARDLADSYNRLDPW	IGKV1D-33*01	IGKJ3*01	0.6	CQQYDNLPRGFTF
MIT 018	CTR0147	SIP	IGHV3-15*01	IGHD5-5*01	IGHJ4*02	2.3	CLQLTYDFW	IGKV1-9*01	IGKJ4*01	3.3	CQQLNSKPSF
MIT 019	CTR0865	SIP	IGHV3-23*04	IGHD3-22*01	IGHJ4*02	3.3	CAKVEDTSRYYYGALDSW	IGKV1-5*03	IGKJ2*01	3.1	CQQYNSYPYTF
MIT 020	CTR0865	COLP	IGHV1-46*01	IGHD2-15*01	IGHJ6*02	7.2	CARDWPIVVVTTNGYYHGLDVW	IGKV1D-39*01	IGKJ3*01	6.7	CQQTYSPPRTF
MIT 029	CTR0090	BLDP	IGHV1-69*09	IGHD5-24*01	IGHJ4*02	6.3	CTTDDEPSGHW	IGKV2D-28*01	IGKJ4*01	1.5	CMQALQTPLTF
MIT 034	013646A	COLP	IGHV1-69*01	IGHD2-15*01	IGHJ6*02	3.6	CAGQDIVVVMATDADFYYYGLDDW	IGLV2-14*01	IGLJ3*02	2.7	CSSHASGDTLVF
MIT 041	013646A	COLP	IGHV1-24*01	IGHD3-22*01	IGHJ5*02	7.1	CTTTRGQKDYYDGSGVPGIYFDPW	IGKV1D-12*02	IGKJ4*01	5.0	CQQANSLLALSF
MIT 044	CTR0118	BLDP	IGHV1-69*02	IGHD2-15*01	IGHJ4*02	10.2	CARDAGLPQSFDFW	IGKV3-20*01	IGKJ1*01	3.3	CQQYGRSPRTF
MIT 045	CTR0118	BLDP	IGHV1-69*02	IGHD2-15*01	IGHJ4*02	9.6	CARDAGLPQSFDFW	IGKV3-20*01	IGKJ1*01	3.3	CQQYGRSPRTF
MIT 064	CTR0118	BLDP	IGHV1-8*01	IGHD3-3*01	IGHJ5*02	6.4	CARGRLFMQWPPQGGFDPW	IGKV3-20*01	IGKJ2*01	2.6	CQEYGRSPPYPF
MIT 065	CTR0118	BLDP	IGHV3-23*04	IGHD3-3*01	IGHJ6*03	5.1	CAKAAGHNFWSGYQAASYYYYMDVW	IGKV1-5*03	IGKJ2*02	1.4	CQQYNSYPYTF
MIT 070	CTR0118	BLDP	IGHV1-18*01	IGHD4-17*01	IGHJ4*02	0.6	CARDRNDYGVLLYW	IGKV3-11*01	IGKJ4*01	0.6	CQQRSNWRLTF
MIT 078	CTR0118	BLDP	IGHV1-58*02	IGHD6-13*01	IGHJ5*02	11.3	CSARGHSFSLPFDSW	IGKV3-20*01	IGKJ4*01	6.3	CQKYGGSLTF
MIT 104	604772	BLDP	IGHV3-7*01	IGHD6-6*01	IGHJ2*01	0.0	CARDSSSDGYFDLW	IGKV3-11*01	IGKJ3*01	0.0	CQQRSNWPPFTF
MIT 105	604772	COLP	IGHV5-a*03	IGHD5-24*01	IGHJ6*02	2.0	CASQPERRDGHNLGAGYYDMDVW	IGKV1D-33*01	IGKJ4*01	1.8	CQQYDNLPLTF
MIT 106	604772	COLP	IGHV6-1*01	IGHD5-24*01	IGHJ5*02	5.7	CARDKTAIGAGYFDSW	IGKV1-5*03	IGKJ2*01	5.1	CQHYNSYPYTF
MIT 107	604772	COLP	IGHV1-18*01	IGHD6-13*01	IGHJ4*02	6.7	CVRFNRAADYW	IGKV3-11*01	IGKJ4*01	2.1	CQHRYNWPPVTF
MIT 109	604772	SIP	IGHV1-46*01	IGHD3-10*02	IGHJ1*01	2.7	CARAVDSESRGVYFLYW	IGKV1D-39*01	IGKJ1*01	5.4	CQQSYSSPWTF
MIT 110	604772	SIP	IGHV1-2*05	IGHD3-9*01	IGHJ4*02	4.9	CARDSKPYPDWYSPFDYW	IGKV1-9*01	IGKJ2*01	1.5	CQHLNIYNTF
MIT 111	604772	SIP	IGHV1-2*02	IGHD3-9*01	IGHJ4*02	8.3	CARDFKPYPDWYSPFDYW	IGKV1-9*01	IGKJ2*01	4.6	CQHLNAYNTF
MIT 113	604772	SIP	IGHV3-13*01	IGHD6-19*01	IGHJ2*01	1.6	CARGRGYSSGWPNWYFDLW	IGKV4-1*01	IGKJ2*01	0.6	CQQYYSTPYTF
MIT 114	604772	SIP	IGHV4-59*01	IGHD3-9*01	IGHJ4*02	5.9	CARDGGNGYSQGPIDSW	IGLV2-23*03	IGLJ1*01	2.9	CCSYAGLTSYVF
MIT 116	931995	BLDP	IGHV5-51*03	IGHD6-19*01	IGHJ3*02	0.0	CARQRQWLAEGAFDIW	IGKV1D-39*01	IGKJ4*01	3.6	CQQSSRTPITF
MIT 119	CTR0090	BLDP	IGHV1-69*09	IGHD5-24*01	IGHJ4*02	7.1	CTTDDEPSGHW	IGKV3-20*01	IGKJ2*01	6.8	CQQYGDSPYTF
MIT 123	CTR0090	COLP	IGHV3-7*01	IGHD5-24*01	IGHJ4*01	6.2	CARDPDTANKIDYW	IGKV3-20*01	IGKJ4*01	2.0	CQQYANSPLTF
MIT 127	CTR0865	SIP	IGHV3-30-3*01	IGHD3-9*01	IGHJ5*02	5.7	CARDRDFYVNTGFYYNFW	IGKV1D-39*01	IGKJ3*01	7.7	CQQSFSIPPMNIF
MIT 132	629356	BLDP	IGHV1-69*12	IGHD6-6*01	IGHJ4*02	3.9	CARDPGVYGEVGLVVGADYW	IGKV4-1*01	IGKJ1*01	0.8	CHQYYTTPHWTF
MIT 133	CR0555w	COLP	IGHV3-33*05	IGHD3-22*01	IGHJ3*02	6.8	CARDFPLSRIPNPYDAIDLW	IGKV1D-39*01	IGKJ4*01	3.1	CQQSSRTPITF
MIT 134	614225	SIP	IGHV4-39*02	IGHD2-2*03	IGHJ4*02	3.5	CVRHRGYCSNASCYGYFDFW	IGKV3-11*01	IGKJ5*01	1.7	CQQRNNWPPGITF
MIT 135	CTR0865	COLP	IGHV3-30*13	IGHD3-16*02	IGHJ4*02	6.7	CARDPRFGVGTGVYIDHW	IGKV2-30*01	IGKJ2*01	4.9	CMQGTHWPHTF
MIT 136	629356	BLDP	IGHV3-30*18	IGHD5-12*01	IGHJ6*03	0.0	CAKEREVATHYYYYYMDVW	IGKV1-9*01	IGKJ3*01	0.6	CQQLNSYGFTF
MIT 141	629356	BLDP	IGHV5-51*03	IGHD1-1*01	IGHJ5*02	2.2	CVRHGFAGTHPHNWFDPW	IGKV1-5*03	IGKJ1*01	1.2	CQQYNSYTTF
MIT 144	CTR0147	COLP	IGHV3-23*04	IGHD1-26*01	IGHJ4*02	4.4	CAKDRAGVVGANWGFDYW	IGKV3-15*01	IGKJ4*01	3.8	CQQYTIWPLTF
MIT 147	CTR0865	SIP	IGHV3-23*05	IGHD3-22*01	IGHJ3*02	6.3	CAKDLYSSDWHNDACELW	IGLV2-11*01	IGLJ3*01	2.4	CCSYAGTYLMVF

‡ Refers to mismatches in FWR1, CDR1, FWR2, CDR2 and FWR3

Antibodies highlighted in green were antigen specific and those in yellow were neutralizing.

Antibody highlighted in grey was identified as negative in microengraving assay.

Table A.3: Cross-clade panel of recombinant HIV-1 proteins spotted on antigen microarrays

Strain	Protein	Clade	Source
IAVI A1	gp120	A	IAVI
YU2	gp120 and gp140*	B	IAVI
YU2 D368R	gp120	B	IAVI
JRCSF	gp120	B	IAVI
JRCSF D368R	gp120	B	IAVI
JRFL	gp120	B	IAVI
JRFL N332A	gp120	B	IAVI
BaL	gp120	B	NIH AIDS Research and Reagent Program
CM	gp120 and gp140	E	NIH AIDS Research and Reagent Program
93TH973	gp120	E	NIH AIDS Research and Reagent Program
CN54	gp120	C/B'	NIH AIDS Research and Reagent Program
IIIB	gp120	B	NIH AIDS Research and Reagent Program
96ZM651	gp120	C	NIH AIDS Research and Reagent Program
UG37	gp140	A	NIH AIDS Research and Reagent Program
UG21	gp140	D	NIH AIDS Research and Reagent Program
SF162	gp140	B	NIH AIDS Research and Reagent Program
HxB2	gp41	B	Vybion Inc.
MPER 179.4	oligopeptide	-	Scripps Institute
MPER 57	oligopeptide	-	Scripps Institute

* Protein exists as a trimeric construct.

Table A.4: Enumerated frequencies of Ig^+ events in blood and GALT samples

Patient ID	HIV Status	Tissue Site	Secreted Ig				
			IgG1	IgA	IgG3	IgM	Total
013646A	Elite controller	Blood	2147	7	146	0	**2300**
		Colon	2025	755	450	217	**3447**
		Small Bowel	1070	179	31	157	**1437**
CTR0090	Elite controller	Blood	811	8	5	0	**824**
		Colon	2037	6104	6	85	**8232**
		Small Bowel	2122	546	6	154	**2828**
CR0555W	Chronic progressor	Blood	2373	35	2	11	**2421**
		Colon	3756	852	3	100	**4711**
		Small Bowel	1918	325	1	138	**2382**
CTR0865	Elite controller	Blood	2659	29	2	3	**2693**
		Colon	3414	3978	11	95	**7498**
		Small Bowel	2414	390	2	156	**2962**
CTR0147	Elite controller	Blood	1341	83	5	0	**1429**
		Colon	2745	5902	5	141	**8793**
		Small Bowel	1475	766	1	136	**2378**
330183	Viremic controller	Blood	883	55	5	0	**943**
		Colon	3313	4400	456	294	**8463**
		Small Bowel	1844	2799	147	194	**4984**
629356	Chronic progressor	Blood	2041	38	5	0	**2084**
		Colon	1695	32	1	0	**1728**
		Small Bowel	1709	37	0	0	**1746**
614225	Chronic progressor	Blood	2521	23	0	0	**2544**
		Colon	1656	83	16	3	**1758**
		Small Bowel	1136	0	9	3	**1148**
604772	Chronic progressor	Blood	4595	89	15	4	**4703**
		Colon	2648	4925	79	45	**7697**
		Small Bowel	945	601	14	45	**1605**
931995	Progressing controller	Blood	4054	15	66	16	**4151**
		Colon	1789	352	26	131	**2298**
		Small Bowel	2725	290	6	169	**3190**
966971	Uninfected donor	Blood	5335	21	9	0	**5365**
		Colon	1850	369	3	30	**2252**
		Small Bowel	1496	188	2	51	**1737**
900158	Uninfected donor	Blood	7746	67	3	21	**7837**
		Colon	1745	9596	16	178	**11535**
		Small Bowel	5957	1820	6	119	**7902**
874612	Uninfected donor	Blood	330	5	4	2	**341**
		Colon	3757	8430	5	45	**12237**
		Small Bowel	2218	7560	2	164	**9944**
473516	Elite controller	Blood	3989	201	87	28	**4305**
		Colon	428	1806	7	5	**2246**
		Small Bowel	4307	843	117	4	**5271**
205120	Uninfected donor	Blood	6709	69	26	1	**6805**
		Colon	687	4129	5	1	**4822**
		Small Bowel	1896	2138	16	58	**4108**
365685	Chronic progressor	Blood	575	41	34	30	**680**
		Colon	1060	2395	10	35	**3500**
		Small Bowel	2009	2884	36	238	**5167**

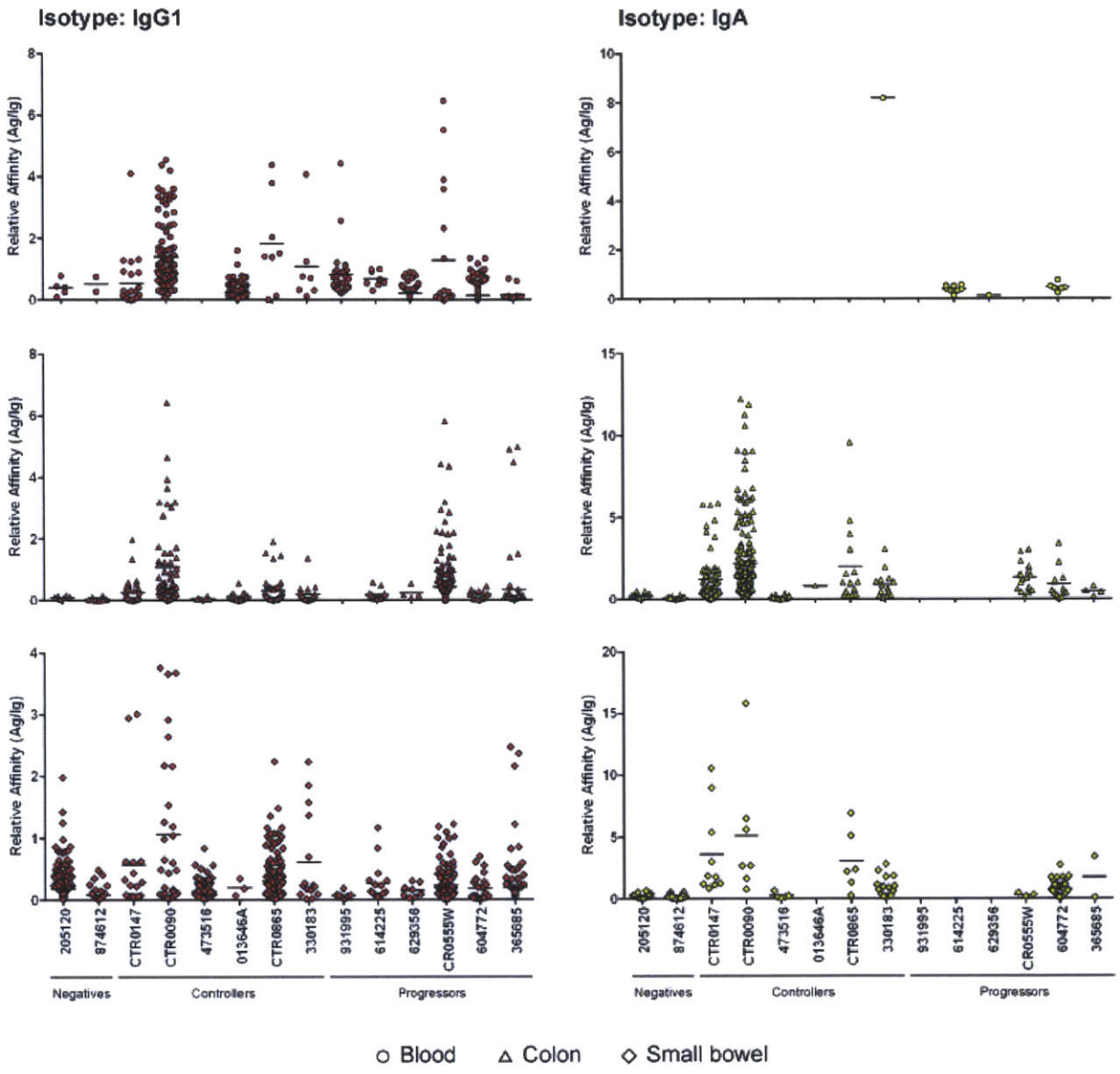

Figure A.3: Relative affinity measurements of IgG1 and IgA events enumerated in screens of blood and GALT samples.

Ratios of background corrected MFIs for captured Ig and bound antigen (Ag) in $Ig^{+}MV^{+}$ positions were used to calculate relative affinities (Ag/Ig) of HIV-1 BaL MV reactive spots identified in the analysis of blood (○), colon (Δ) and small bowel (◊) samples from HIV-1 negatives, controllers and progressors (in order).

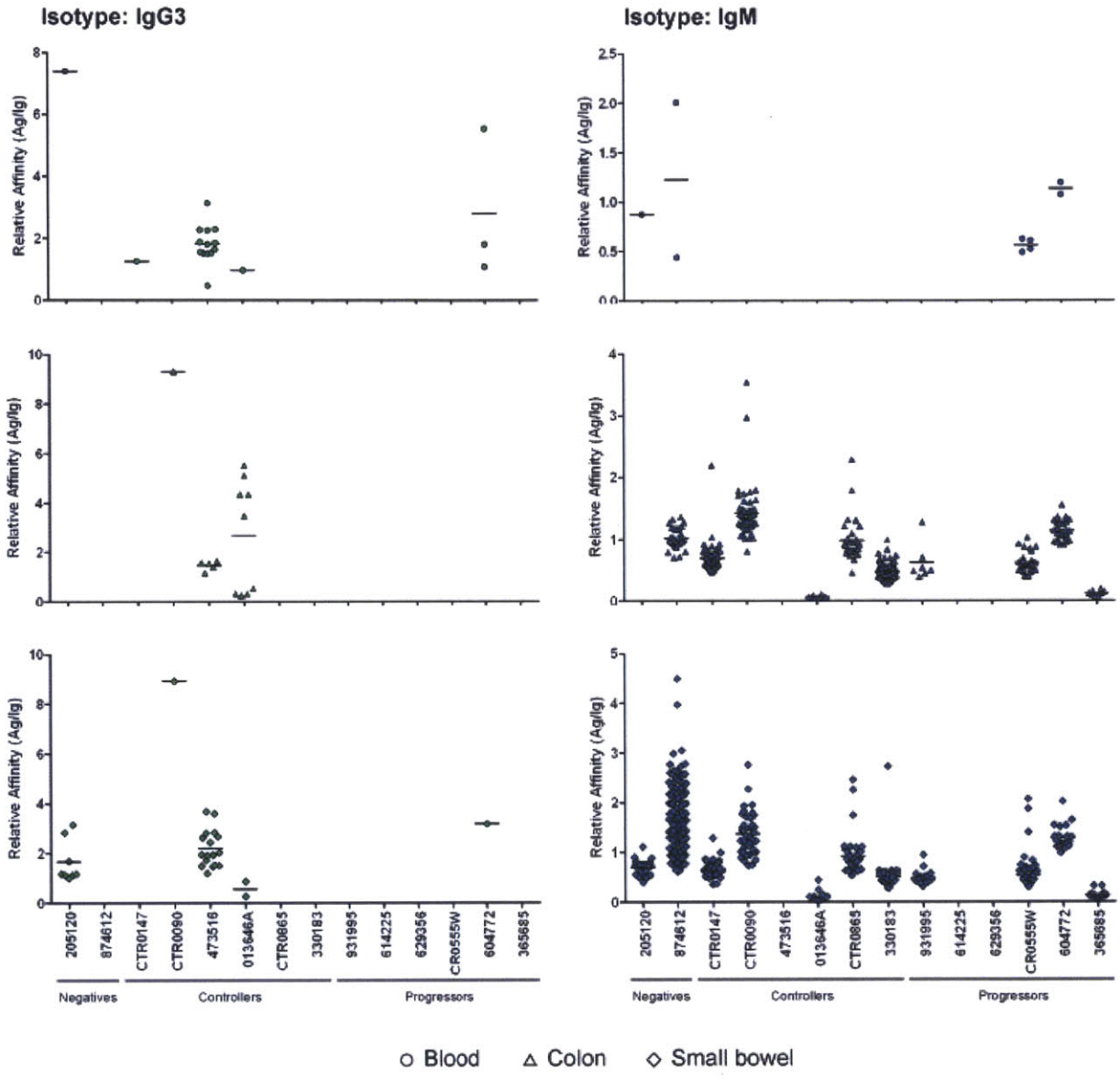

Figure A.4: Relative affinity measurements of IgG3 and IgM events enumerated in screens of blood and GALT samples.

Ratios of background corrected MFIs for captured Ig and bound antigen (Ag) in $Ig^{+}MV^{+}$ positions were used to calculate relative affinities (Ag/Ig) of HIV-1 BaL MV reactive spots identified in the analysis of blood (○), colon (Δ) and small bowel (◊) samples from HIV-1 negatives, controllers and progressors (in order).

Table A.5: Summary of heavy and light chain gene usage for HIV-1 BaL *Env*-specific clones

	total sequences	non functional sequences	functional sequences	unique sequences	clonotypes	diversity: clonotypes	diversity: unique functional
	554	18	536	427	389	0.9110	0.7966
heavy chain	264	5	259	205	192	0.9366	0.7915
lambda chain	15	1	14	12	12	1.0000	0.8571
kappa chain	275	12	263	210	185	0.8810	0.7985

no. of not imported sequences 10 (564)
(marked by IMGT as no result, or unknown)

V gene usage			D gene usage			J gene usage		
VH1	27	13.17%	No D	5	2.44%	JH1	5	2.44%
VH2	16	7.80%	D1	24	11.71%	JH2	8	3.90%
VH3	115	56.10%	D2	36	17.56%	JH3	31	15.12%
VH4	36	17.56%	D3	53	25.85%	JH4	103	50.24%
VH5	9	4.39%	D4	17	8.29%	JH5	27	13.17%
VH6	2	0.98%	D5	22	10.73%	JH6	31	15.12%
VH7	0	0.00%	D6	47	22.93%			
			D7	1	0.49%			

V gene usage			D gene usage			J gene usage		
VK1	108	51.43%	No D	210	100.00%	JK1	57	27.14%
VK2	25	11.90%				JK2	49	23.33%
VK3	70	33.33%				JK3	27	12.86%
VK4	7	3.33%				JK4	64	30.48%
VK5	0	0.00%				JK5	13	6.19%
VK6	0	0.00%						
VK7	0	0.00%						

V gene usage			D gene usage			J gene usage		
VL1	3	25.00%	No D	12	100.00%	JL1	4	33.33%
VL2	8	66.67%				JL2	4	33.33%
VL3	1	8.33%				JL3	4	33.33%
VL4	0	0.00%				JL4	0	0.00%
VL5	0	0.00%				JL5	0	0.00%
VL6	0	0.00%				JL6	0	0.00%
VL7	0	0.00%				JL7	0	0.00%
VL8	0	0.00%						
VL9	0	0.00%						
VL10	0	0.00%						
VL11	0	0.00%						

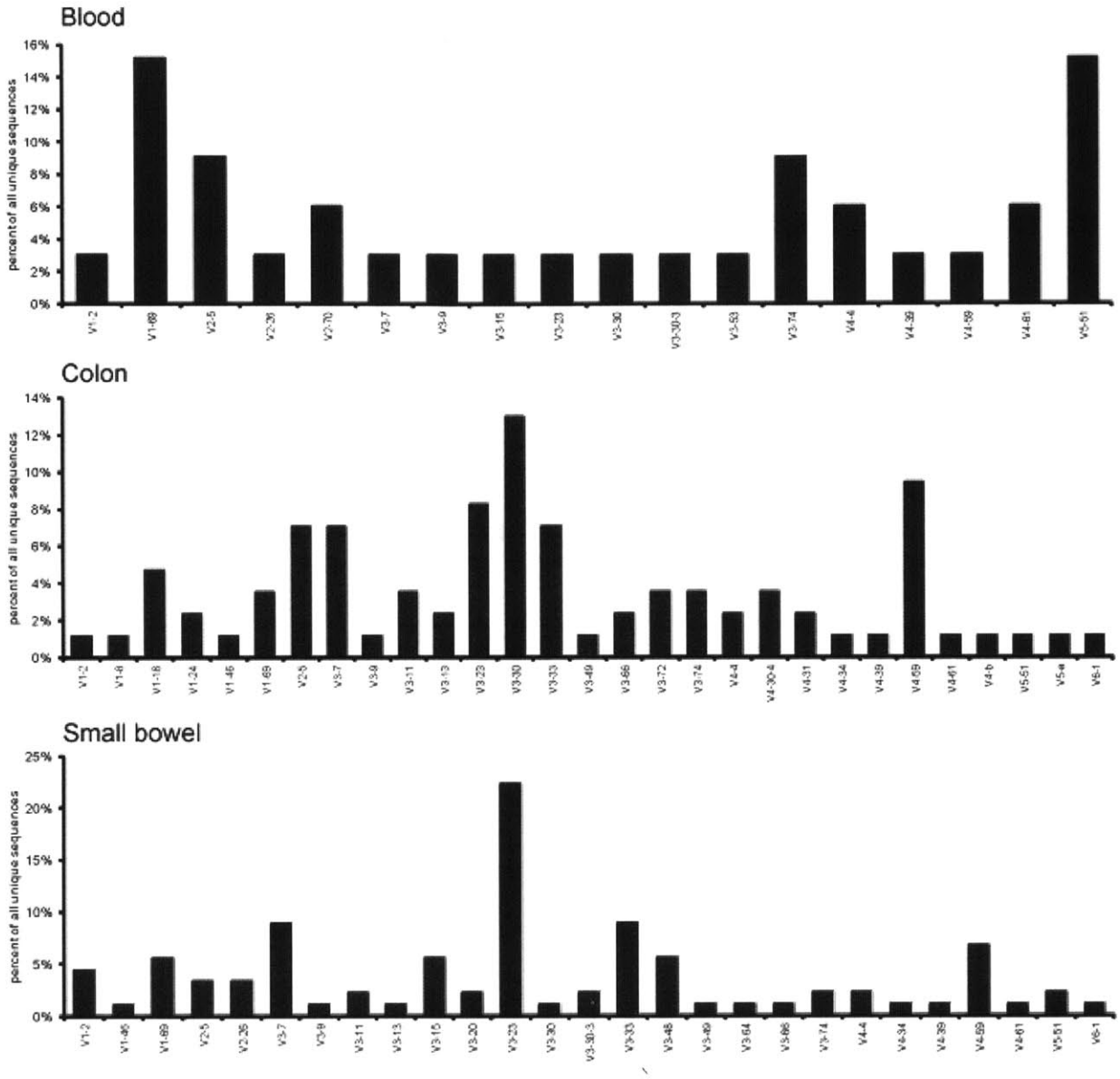

Figure A.5: Distribution of V_H genes in HIV-1 *Env*-specific clones in each compartment
Following the analysis of heavy chain sequences for *Env*-specific clones with IMGT/HighV-quest software, frequencies of the different V_H genes rearranged into antigen-specific antibodies were enumerated with IgAT software package. 33 unique clones were considered from the blood, 85 clones from the colon, and 90 clones from the small bowel.

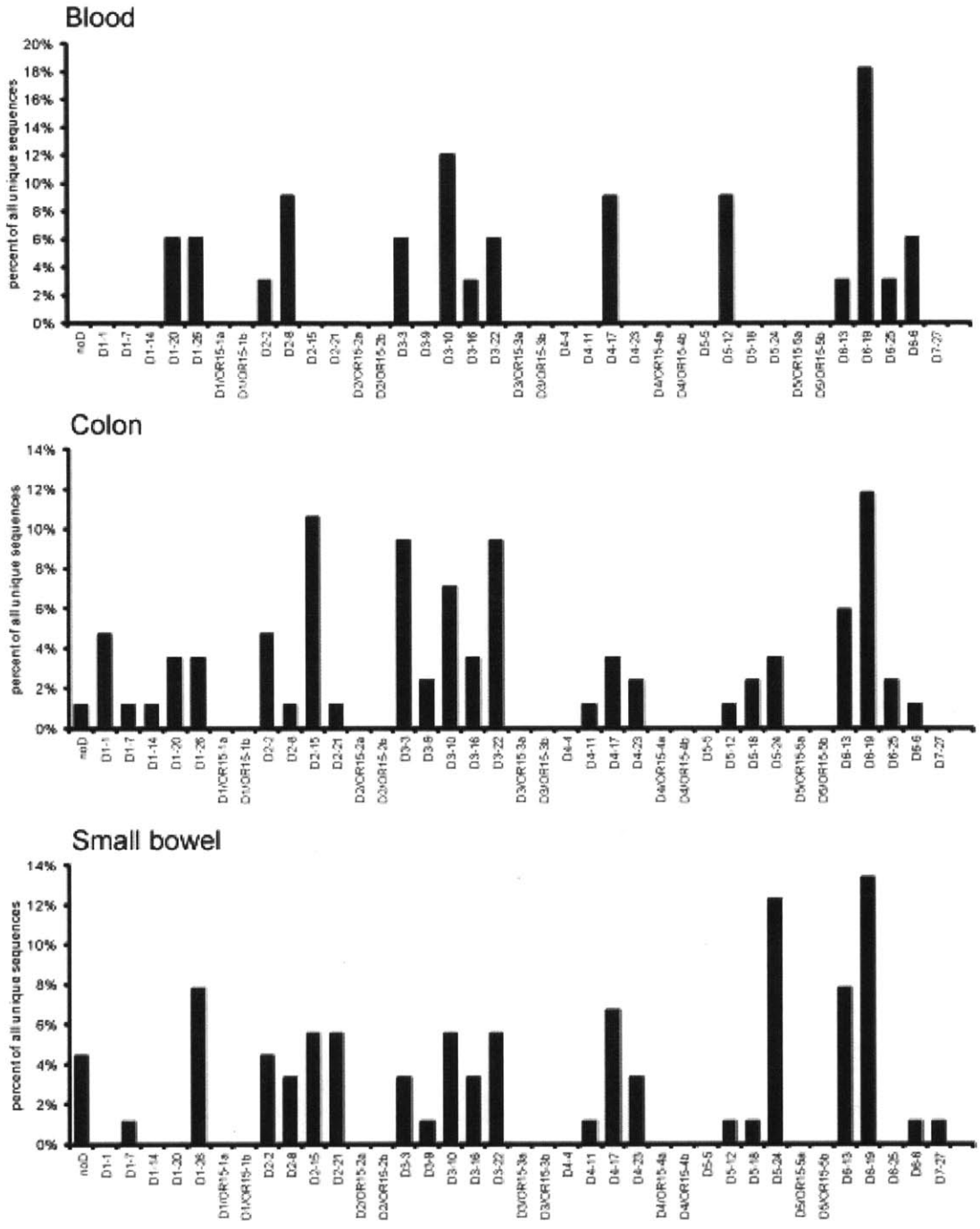

Figure A.6: Distribution of D_H genes in HIV-1 *Env*-specific clones in each compartment
Following the analysis of heavy chain sequences for *Env*-specific clones with IMGT/HighV-quest software, frequencies of the different D_H genes rearranged into antigen-specific antibodies were enumerated with IgAT software package. 33 unique clones were considered from the blood, 85 clones from the colon, and 90 clones from the small bowel.

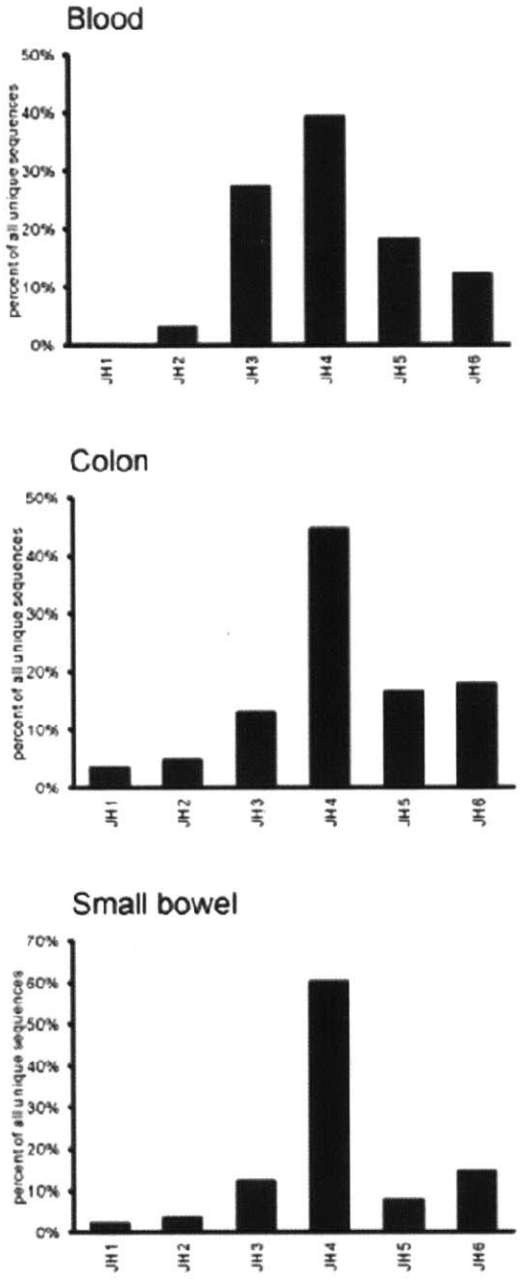

Figure A.7: Distribution of J_H genes in HIV-1 *Env*-specific clones in each compartment
Following the analysis of heavy chain sequences for *Env*-specific clones with IMGT/HighV-quest software, frequencies of the different J_H genes rearranged into antigen-specific antibodies were enumerated with IgAT software package. 33 unique clones were considered from the blood, 85 clones from the colon, and 90 clones from the small bowel.

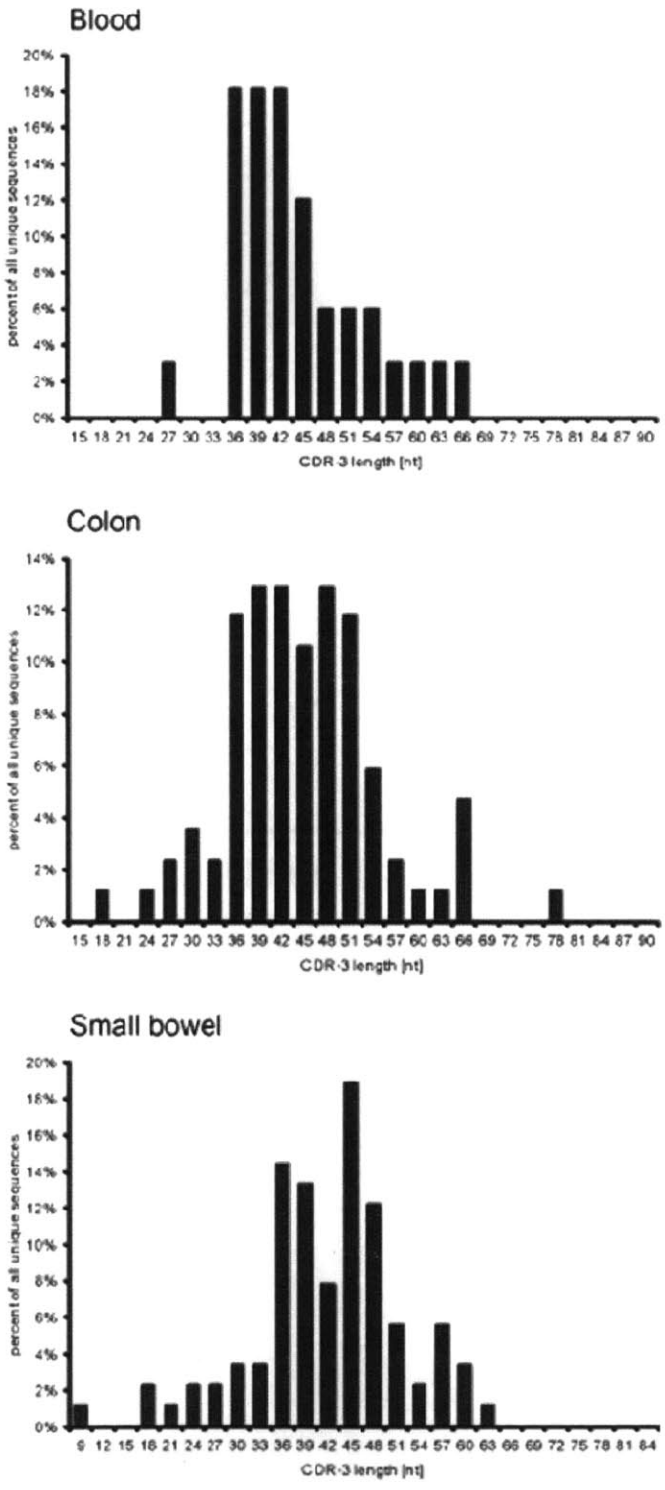

Figure A.8: Distribution of CDR3 lengths for heavy chains of HIV-1 *Env*-specific clones in each compartment

CDR3 lengths of heavy chains were compared for unique clones recovered from the blood and GALT of the HIV-infected subjects analyzed. The median lengths were determined to be 42, 45 and 42 nucleotides in the blood (n = 33), colon (n = 85) and small bowel (n = 90), respectively.

Table A.6: Neutralization IC_{50} (μg/mL) measurements for tested antibodies

TIER	1	2	1	1	1	2
CLADE	B	B	B	B	C	A
VIRUS	HxB2	JRCSF	SF162	89.6	93IN905	92RW020
MIT 34	1.476	NN	2.272	3.187	60	NN
MIT 41	1.473	NN	171	0.165	25	NN
MIT 44	NN	NN	NN	NN	NN	NN
MIT 45	NN	NN	NN	NN	NN	NN
2G12	0.108	0.348	2.664	0.138	NN	0.354

Table A.7: Summary of heavy and light chain gene usage for WNV E-specific clones

	total sequences	non functional sequences	functional sequences	unique sequences	clonotypes	diversity: clonotypes	diversity: unique functional
	39	3	36	32	30	0.9375	0.8889
heavy chain	19	0	19	19	18	0.9474	1.0000
lambda chain	4	1	3	3	3	1.0000	1.0000
kappa chain	16	2	14	10	9	0.9000	0.7143

no. of not imported sequences 1 (40)
(marked by IMGT as no result, or unknown)

V gene usage			D gene usage			J gene usage		
VH1	6	31.58%	No D	1	5.26%	JH1	1	5.26%
VH2	3	15.79%	D1	1	5.26%	JH2	1	5.26%
VH3	7	36.84%	D2	1	5.26%	JH3	1	5.26%
VH4	1	5.26%	D3	9	47.37%	JH4	6	31.58%
VH5	2	10.53%	D4	2	10.53%	JH5	5	26.32%
VH6	0	0.00%	D5	3	15.79%	JH6	5	26.32%
VH7	0	0.00%	D6	2	10.53%			
			D7	0	0.00%			

V gene usage			D gene usage			J gene usage		
VK1	6	60.00%	No D	10	100.00%	JK1	3	30.00%
VK2	0	0.00%				JK2	2	20.00%
VK3	4	40.00%				JK3	0	0.00%
VK4	0	0.00%				JK4	3	30.00%
VK5	0	0.00%				JK5	2	20.00%
VK6	0	0.00%						
VK7	0	0.00%						

V gene usage			D gene usage			J gene usage		
VL1	0	0.00%	No D	3	100.00%	JL1	0	0.00%
VL2	3	100.00%				JL2	2	66.67%
VL3	0	0.00%				JL3	1	33.33%
VL4	0	0.00%				JL4	0	0.00%
VL5	0	0.00%				JL5	0	0.00%
VL6	0	0.00%				JL6	0	0.00%
VL7	0	0.00%				JL7	0	0.00%
VL8	0	0.00%						
VL9	0	0.00%						
VL10	0	0.00%						
VL11	0	0.00%						

Table A.8: Germline gene usage of validated WNV E-specific clones

Clone No.	Patient ID	V Region	D Region	J Region	Mutation Rate (%)‡	CDR3	V Region	J Region	Mutation Rate (%)‡	CDR3
MIT 86	100041	IGHV2-26*01	IGHD3-22*01	IGHJ4*02	0.0	CARVNSSGYYFDYW	IGKV1D-33*01	IGKJ4*01	0.4	CQQYDNLPLTF
MIT 87	100041	IGHV4-59*01	IGHD3-22*01	IGHJ5*02	0.0	CARGYYDSTRDWFDPW	IGKV1-39*01	IGKJ1*01	0.6	CQQSYSTRTF
MIT 88	110038	IGHV3-64*05	IGHD3-3*01	IGHJ5*02	2.9	CVKDLTGAIFGVISELAVW	IGKV1D-12*01	IGKJ4*01	4.5	CQQAYSFPLTF
MIT 89	110038	IGHV1-2*02	IGHD3-10*02	IGHJ4*02	3.8	CARGRGVDVMSPLYDNW	IGLV2-23*03	IGLJ3*02	4.3	CCSFAGGGTWVF
MIT 90	110038	IGHV3-23*04	IGHD2-15*01	IGHJ5*02	4.3	CGKDPRRDCSDIKCNFGPNWFDPW	IGKV1-5*01	IGKJ2*01	2.1	CQQFNSYPNTF
MIT 91	100032	IGHV1-8*01	IGHD5-5*01	IGHJ5*02	0.0	CARGLVDTAMVTFDPW	IGKV1-9*01	IGKJ5*01	0.2	CQQLNSYLPITF
MIT 92	100032	IGHV5-51*03	IGHD3-3*01	IGHJ6*02	0.0	CARHFTQGYDFWSGYYTDYYGMDVW	IGKV4-1*01	IGKJ1*01	0.6	CQQYYSTPPTF
MIT 93	100032	IGHV5-51*03	IGHD3-3*01	IGHJ6*02	0.0	CARHFTQGYDFWSGYYTDYYGMDVW	IGKV1-39*01	IGKJ1*01	0.3	CQQSYSTRTF
MIT 94	100038	IGHV1-18*01	IGHD5-12*01	IGHJ5*02	7.7	CARLHYHLDQGWIDPW	IGKV3-20*01	IGKJ1*01	5.6	CQQYGSSPWTF
MIT 95	100038	IGHV3-33*01	IGHD5-24*01	IGHJ2*01	0.0	CARWGGRRDGYINWYFDLW	IGKV3-11*01	IGKJ5*01	0.3	CQQRSNWPPITF
MIT 96	100038	IGHV1-2*02	IGHD6-19*01	IGHJ6*02	0.3	CARGPPPYYYYGMDVW	IGLV9-49*01	IGLJ3*02	0.0	CGADHGSGSNFV*PE#VF

‡ Refers to mismatches in FWR1, CDR1, FWR2, CDR2 and FWR3

Antibodies highlighted in green were antigen specific.